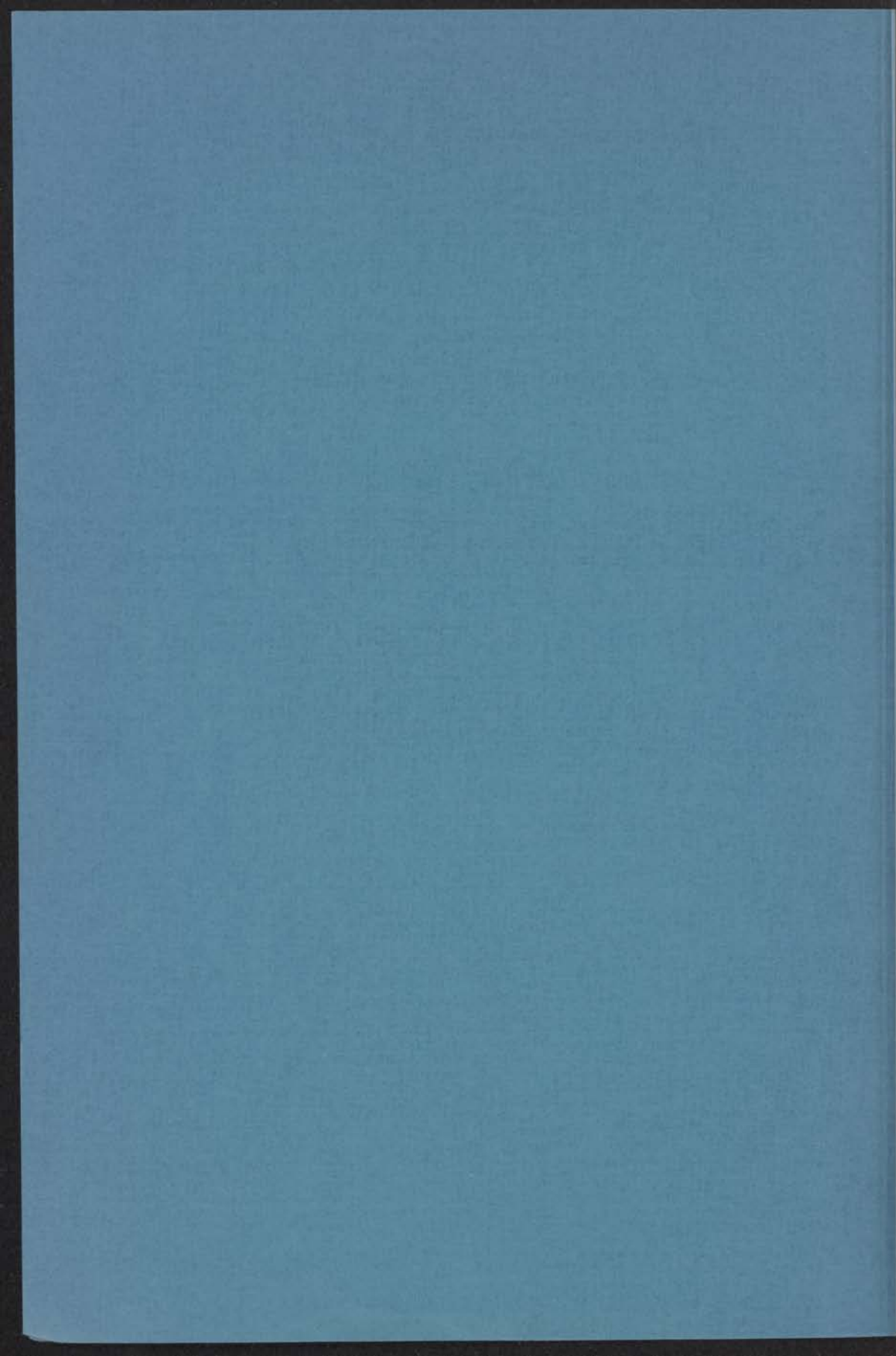


THERMAL CONDUCTIVITY  
OF  
TYPE - II SUPERCONDUCTORS

INSTITUUT LORENTZ  
voor theoretische natuurkunde  
Nieuwsteeg 16-Leliden-Nederland

P. H. KES



14 FEB. 1974

# THERMAL CONDUCTIVITY OF TYPE-II SUPERCONDUCTORS

PROEFSCHRIFT

TER VERKRIJGING VAN DE GRAAD VAN DOCTOR IN  
DE WISKUNDE EN NATUURWETENSCHAPPEN AAN DE  
RIJKSUNIVERSITEIT TE LEIDEN, OP GEZAG VAN DE  
RECTOR MAGNIFICUS DR. A.E. COHEN, HOGLERAAR  
IN DE FACULTEIT DER LETTEREN, VOLGENS  
BESLUIT VAN HET COLLEGE VAN DEKANEN TE  
VERDEDIGEN OP WOENSDAG 27 FEBRUARI 1974  
TE KLOKKE 15.15 UUR

**INSTITUUT-LORENTZ**  
voor theoretische natuurkunde  
Nieuwsteeg 18-Leiden-Nederland

door

Pieter Hendrik Kes  
geboren te Utrecht in 1944

Van Veen & Scheffers B.V. te Rotterdam

*kast dissertaties*

PROMOTOR: Dr. D. de Klerk

CONTENTS

Chapter 1	GENERAL INTRODUCTION	1
Chapter 2	PRODUCTION OF THE MODERN STATE	15
1	THE PRODUCTION OF MODERN STATE IN FRANCE	15
2	Centralization of power in the hands of the monarch	17
3	Centralization of power in the hands of the monarch	19
4	Centralization of power in the hands of the monarch	21
5	Centralization of power in the hands of the monarch	23
6	Centralization of power in the hands of the monarch	25
7	Centralization of power in the hands of the monarch	27
8	Centralization of power in the hands of the monarch	29
9	Centralization of power in the hands of the monarch	31
Chapter 3	PRODUCTION OF THE MODERN STATE	35
1	Introduction to the chapters of the production of the modern state	35
2	The production of the modern state in France	37
3	The production of the modern state in France	39
4	The production of the modern state in France	41
5	The production of the modern state in France	43
6	The production of the modern state in France	45
7	The production of the modern state in France	47
8	The production of the modern state in France	49
9	The production of the modern state in France	51
Chapter 4	THE PRODUCTION OF THE MODERN STATE	55
1	Introduction to the chapters of the production of the modern state	55
2	The production of the modern state in France	57
3	The production of the modern state in France	59
4	The production of the modern state in France	61
5	The production of the modern state in France	63
6	The production of the modern state in France	65
7	The production of the modern state in France	67
8	The production of the modern state in France	69
9	The production of the modern state in France	71

Aan mijn moeder  
Aan margriet

1877

1877

## CONTENTS

Chapter 1	GENERAL INTRODUCTION.	7
Chapter 2	THEORETICAL CONSIDERATIONS.	11
1.	Some Properties of Transport Theory in Metals.	11
2.	Thermal Conductivity of Normal Metals at Low Temperatures.	16
3.	Properties of Superconductors.	18
4.	Thermal Conductivity in Superconductors. Temperature Dependence.	25
5.	Thermal Conductivity in the Mixed State of Type-II Superconductors.	28
6.	Metal Properties of Niobium.	33
Chapter 3	DESCRIPTION OF THE EXPERIMENT.	38
1.	Introduction. The Magnitude of the Temperature Difference.	38
2.	The Experimental Set-Up and Measuring Procedure.	39
3.	The Thermometer Calibration. The Influence of a Magnetic Field.	49
Chapter 4	EXPERIMENTS IN THE PURELY SUPERCONDUCTING AND NORMAL STATE.	59
1.	Description of the Samples.	59
2.	Thermal Conductivity in the Normal State.	60
3.	Separation of the Phonon and Electron Contribution.	63
4.	Discussion of the Phonon Conductivity in the Normal State.	68
5.	Discussion of the Phonon Conductivity in the Superconducting State.	70
6.	The Phonon Conductivity in the Irradiated Sample.	73
Chapter 5.	THE FLUX DISTRIBUTION IN THE MIXED STATE.	76
1.	Introduction.	76
2.	The Reversible Magnetization Model.	77
3.	The Irreversible Magnetization Curves.	81
4.	Discussion of Some Critical State Models.	84

Chapter 6	THE THERMAL CONDUCTIVITY IN THE MIXED STATE.	89
1.	Introduction. Magnetization Measurements.	89
2.	The Average and Local Inductions for the Three Field Orientations.	91
3.	Some Experimental Results.	95
4.	Discussion of the Results at Small Inductions.	99
5.	Discussion of the Results near $H_{C2}$ .	106
Samenvatting		113
Studieoverzicht		115

## STELLINGEN

1. Bij zijn beschouwingen over de transporteigenschappen in supergeleiders met elkaar overlappende geleidingsbanden, sluit Kresin de mogelijkheid uit, dat bij lage temperaturen een elektron door wisselwerking met de roostertrillingen van het kristal tussen die energiebanden kan worden verstrooid. Dit betekent dat zijn theorie niet van toepassing is op niobium.  
V.Z. Kresin, J. Low Temp. Phys. 11, 519 (1973).
2. Het verband tussen weerstand en temperatuur voor germanium thermometers van het merk Cryocal wordt beneden 2 K gegeven door een eenvoudige formule uit de half-geleider theorie.
3. Het verdient aanbeveling susceptibiliteitsmetingen te verrichten aan irreversibele type-II supergeleiders in afnemende velden beneden  $H_{C1}$ .
4. De lijn in het (M,H)-diagram die volgens Aston, Dubeck en Rothwarf voor reversibele type-II supergeleiders met  $\kappa \approx \frac{1}{2}\sqrt{2}$  de overgang aangeeft tussen de intermediaire mengtoestand en de zuivere mengtoestand als functie van de demagnetisatie-coëfficiënt, is verkeerd getekend.  
— D.A. Aston, L.W. Dubeck en F. Rothwarf, Phys. Rev. B3, 2231 (1971).
5. Het feit dat Clement en Quinnell enerzijds en Zimmerman en Hoare anderzijds verschillende exponenten vinden voor de term  $(\log R)/T$  in hun, overigens identieke, aanpassingsformules voor Allen-Bradley koolthermometers, waarmee zij bovendien dezelfde nauwkeurigheid bereiken, is niet verwonderlijk.  
J.R. Clement en E.H. Quinnell, Rev. Sc. Instr. 23, 213 (1952).  
J.E. Zimmerman en F.E. Hoare, Phys. Chem. Solids 17, 52 (1960).  
Dit proefschrift, §3.3.
6. Bij de verklaring van het functioneren van p-n gelijkrichters wordt ten onrechte het gewone weerstandsgedrag van het halfgeleidende materiaal veelal buiten beschouwing gelaten.  
C. Kittel, Introduction to Solid State Physics (Wiley, New York, 1969).  
H. de Waard en D. Lazarus, Modern Electronics (Addison Wesley, London, 1966).

7. Om een beter inzicht te verkrijgen in de verschillende spin-rooster-relaxatieprocessen van  $\text{MnCl}_2 \cdot 4\text{H}_2\text{O}$  en  $\text{MnBr}_2 \cdot 4\text{H}_2\text{O}$ , is het gewenst metingen van de relaxatietijd uit te voeren in het temperatuurgebied tussen 20 K en 78 K als functie van zowel de temperatuur als van het magnetisch veld.
8. Het begrip levensduur van een energieniveau zoals Haupt dat gebruikt kan gemakkelijk aanleiding geven tot verwarring.  
J. Haupt, Z. Naturforsch. 26a, 1578 (1971).
9. De vaak gepubliceerde bewering dat kernfusie een „schone“ en veilige energiebron vormt, dient gerelativeerd te worden.
10. Om het zuinig rijden te bevorderen, zouden motorvoertuigen moeten worden uitgerust met een wijzerinstrument waarmee op elk moment het brandstofverbruik per kilometer is af te lezen. Een dergelijk apparaat is op eenvoudige wijze te konstrueren.

## CHAPTER 1

### GENERAL INTRODUCTION

In this thesis the thermal conductivity of type-II superconductors is studied in the purely superconducting, the mixed, and the normal states. The thermal conductivity is influenced in a more complicated way by the transition to the superconducting phase than the electrical conductivity. This is due to the fact that both the electrons and the phonons contribute to it, whereas both components are influenced by the appearance of a gap in the energy spectrum of the electrons around the Fermi energy.

The ratio of the thermal conductivities of superconductors in zero magnetic field (purely superconducting state) and fields well above  $H_{c2}$  (normal state) as a function of temperature is well described by the theory of Bardeen, Rickayzen, and Tewordt <sup>1)</sup>, and by that of Tewordt <sup>2)</sup>. It follows from these theories that the thermal conductivity of the electrons in the superconducting state, whether they are scattered by lattice defects or by the phonons, decreases below the normal state value. The conductivity of the phonons, to the contrary, increases nearly exponentially as the temperature is lowered. From the heat conductivity curves in the normal and (purely) superconducting states one can conclude whether the electron or the phonon conductivity is predominant, and which is the main scattering mechanism.

A rather complicated situation is encountered if a type-II superconductor is placed in a magnetic field. Below the first critical field  $H_{c1}$  the superconductor is in the Meissner state in which the magnetic field is excluded from the bulk of the sample. Above the second critical field  $H_{c2}$  it is in the normal state. In both field regions the thermal conductivity is independent of the field value. Between  $H_{c1}$  and  $H_{c2}$  a gradual transition from the Meissner to the normal state takes place. This situation is characterized by a triangular lattice of normal regions of cylindrical shape (flux vortices) embedded in purely superconducting material, and is therefore denoted as the "mixed state". In the simplest case the magnetic induction in the bulk is given by the Abrikosov curve <sup>3)</sup>. Crystal lattice defects and surface irregularities, however, disturb the idealized picture by pinning of the flux vortices, which can give rise to appreciable deviations from the Abrikosov curve and the occurrence of

hysteresis phenomena. Due to the recent work of Fietz and Webb<sup>4)</sup>, Labusch<sup>5)</sup>, and Kramer<sup>6)</sup> the mechanism of flux pinning is better understood than before, but nevertheless quite often the experimental circumstances are not ideal, so that the results can still be described more accurately by simple phenomenological models<sup>7,8)</sup> than by the more fundamental theoretical expressions.

The mixed state, whether reversible or irreversible, must obviously influence the thermal conductivity. In general the consequences are difficult to predict. In four special cases, however, the results of theoretical considerations are available.

1. For the dirty limit Caroli and Cyrot<sup>9)</sup> predicted a linear behaviour of the coefficient of thermal conductivity  $\lambda$  as a function of the magnetic induction near  $H_{c2}$ .
2. Maki<sup>10)</sup> demonstrated that for a pure superconductor  $\lambda$  should be proportional to  $(H_{c2} - B)^{\frac{1}{2}}$ , so that an infinite slope of the  $\lambda(B)$  and  $\lambda(H)$  curves must be found at  $H_{c2}$ . The coefficient of proportionality not only depends on temperature but also on the mutual angle between the field and the direction of heat flow.
3. Canel<sup>11)</sup> derived that in a pure superconductor a sharp decrease in  $\lambda$  should occur just above  $H_{c1}$  at low temperatures. For those temperatures we have predominantly phonon conductivity and the decrease is due to phonon-electron scattering in the normal cores of the flux vortices. Surprisingly, however, no direct increase of the conductivity of the electrons in the vortex cores can be expected due to their low group velocity.
4. Cleary<sup>12)</sup> pointed out that at temperatures near  $T_c$ , where the conductivity is predominantly electronic, a decrease in  $\lambda$  should be expected just above  $H_{c1}$  for pure superconductors. This decrease is due to scattering of the electronic excitations by the vortices.

In the above considerations "dirty" means that the mean free path of the electrons  $l$  is short as compared to the coherence length  $\xi_0$ , whereas "pure" means  $l \gg \xi_0$ .

All the investigations in this thesis were carried out on rectangular samples of niobium, an intrinsic type-II superconductor, of which the flux pinning properties are well understood<sup>8)</sup>. Its high critical temperature  $T_c$  (9.1 K) makes it possible to cover a wide temperature range by conventional cooling techniques. A serious difficulty is, however, the accurate calibration of the thermometers in the region between liquid helium and hydrogen.

In chapter 2 we give a more extensive survey of the theory of the thermal conductivity of metals at low temperatures in general, and of superconductors

particularly, both as a function of temperature and of magnetic field.

In chapter 3 a description is given of the measuring apparatus, the auxiliary equipment, and the experimental procedure, together with a detailed explanation of the calibration procedures and a discussion of the final experimental accuracy.

Chapter 4 deals with the experimental results and the discussion of the temperature dependence of the thermal conductivity of five niobium samples in the purely superconducting and normal states. The samples differ in crystalline defect structures due to different heat treatments and, in one case, subsequent neutron irradiation. By means of a precise analysis of the  $\lambda(T)$  curves in the normal and superconducting states it is possible to separate the electron and phonon contributions applying the theories of BRT <sup>1)</sup> and of Tewordt <sup>2)</sup>. The dependence of the phonon conductivity on the defect structure is discussed.

For a discussion of the thermal conductivity in the mixed state it is necessary to know more about the flux distribution in a sample. In chapter 5 this problem is elucidated. We introduce a mathematically simple expression for the description of the reversible magnetization curve, which fits the experimental data rather well <sup>7)</sup>. Next, the formulae for the irreversible magnetization curves between  $H_{c1}$  and  $H_{c2}$  are derived for a general flux pinning model. For the most reversible sample the model of Labusch <sup>5)</sup> turned out to give the best fit with the measurements. As a result the internal magnetic induction as a function of position inside the sample could be calculated.

The effect of an induction-free region just above  $H_{c1}$  in increasing field is clearly demonstrated by the irreversible behaviour of the thermal conductivity in the mixed state for small inductions. This, and the behaviour in the vicinity of  $H_{c2}$  are the subjects which are discussed in chapter 6. The field dependence of  $\lambda$  has been measured for three different orientations of the magnetic field with respect to the direction of the heat flow and the sample surface. The problem of demagnetization effects in the transversal and perpendicular field orientations is elucidated.

Although the purest sample can not be considered as a "pure" superconductor according to the definition given above, because  $\lambda \sim \xi_0$ , a reasonably good agreement was found for the results in the region just above  $H_{c1}$  with the theory for pure superconductors. For fields near  $H_{c2}$ , however, the conductivity turned out to be a linear function of the magnetic field, but with a slope which was an order of magnitude larger than what was theoretically predicted for "dirty" superconductors.

## References

1. J. Bardeen, G. Rickayzen, and L. Tewordt, Phys. Rev. 113, 982 (1959).
2. L. Tewordt, Phys. Rev. 129, 657 (1963).
3. A.A. Abrikosov, Zh. Eksperim. i Teor. Fiz. 32, 1442 (1957);  
[JETP 5, 1174 (1957)].
4. W.A. Fietz and W.W. Webb, Phys. Rev. 178, 657 (1969).
5. R. Labusch, Crystal Lattice Defects 1, 1 (1969).
6. E.J. Kramer, J. Appl. Phys. 44, 1360 (1973).
7. P.H. Kes, C.A.M. van der Klein, and D. de Klerk, J. of Low Temp. Phys.  
10, 759 (1973).
8. C.A.M. van der Klein, P.H. Kes, H. van Beelen, and D. de Klerk,  
J. Low Temp. Phys., in the press.
9. C. Caroli and M. Cyrot, Phys. Kond. Mat. 4, 285 (1965).
10. K. Maki, Phys. Kond. Mat. 8, 305 (1969).
11. E. Canel, Proc. Bat Sheva Seminar, HaTfa (1968), p. 587.
12. R.M. Cleary, Phys. Rev. B1, 169 (1970).

## CHAPTER 2

### THEORETICAL CONSIDERATIONS

#### *Introduction*

In this chapter a rather extensive survey is given of the theoretical background necessary to understand the phenomenon of thermal conductivity in the steady mixed state of a type-II superconductor. First of all one has to know something about transport theory in solid state physics, both in the semi-classical and in the pure quantum statistical mechanical limit, section 1. From the normal state thermal conductivity one can conclude which particles mainly contribute to the heat transport, and which is the main scattering phenomenon relaxing the transport current. The formulae underlying this procedure of separation will be discussed in section 2. Properties of superconductors (both type-I and type-II), concerning the temperature dependence as well as the magnetic field dependence, must be known before any interpretation of the thermal conductivity behaviour is possible. These topics are to be elucidated in section 3. After this has been done, one has the tools to tackle the problem of thermal conductivity in superconductors, firstly with respect to its temperature dependence (section 4), secondly concerning its behaviour in the mixed state (section 5). Finally, this chapter will be concluded (section 6) with some remarks about the specific solid state properties of the material (niobium) on which the experiments described in this thesis were carried out.

#### §2.1 *Some Properties of Transport Theory in Metals*

2.1.1 *Metals in Equilibrium. Quasi-Particles.* The properties of a metal are characterized by the properties of the free electrons and the quantized lattice waves, the phonons. A simple model for the electrons is that of the free electron gas with its well-known properties<sup>1</sup>). At temperatures well below the Fermi temperature the only electron states with physical importance are those lying in a range  $\pm k_B T$  around the Fermi level  $E_F$  ( $k_B$  is the Boltzmann constant). Their density of states is  $N(0)$ . The states of lower and higher energies are completely filled or empty. One may consider the occupied states

(electrons) above and the empty states (holes) below the Fermi level as independent quasi-particles with positive respectively negative energies, measured with respect to  $E_F$ . In this picture the technique of annihilation and creation operators (second quantization) fits quite well. The number of quasi-particles is not conserved, so in order to obtain thermodynamic quantities one has to use the grand ensemble average.

In reality the electrons in a metal are not free at all. Instead, they are continuously interacting with each other, with the phonons, and with impurities. In the quasi-particle language this means that an electron state can not exist forever, but will be destroyed by a scattering event; it has a finite lifetime and, because of the uncertainty principle, its energy is not exactly determined. It only is meaningful to speak about particles in a classical way if the uncertainty in energy is restricted to a narrow band around the energy state itself. This requires that one has to construct quasi-particles with only weak mutual interaction. This can be done by transforming the Hamiltonian in a suitable way, which for example has been done (Pines and Bohm <sup>2</sup>) for the strong Coulomb interaction between the electrons in a metal. The quasi-particle in this case is an electron with a "positive" cloud around it, corresponding to the effective exclusion of other electrons from its neighbourhood. The remaining interaction is only a weak screened-Coulomb interaction. The effect of the cloud can be incorporated in the effective mass of the quasi-particle. Another example is the complicated problem of the electron-phonon interaction, which has been dealt with by Fröhlich <sup>3</sup>), providing the key for a microscopic theory of superconductivity.

The same considerations can be given for the phonons, which themselves are already a kind of quasi-particle or, rather, collective excitations. The number of phonon modes of a certain frequency is given by a spectral density function, which can be rather complicated. As a first approximation the Debye spectrum is often used.

Of course, one can distinguish two kinds of quasi-particles: the fermions, obeying Fermi-Dirac statistics (their occupation number being given by the Fermi-Dirac distribution function), and the bosons, their occupation number is given by the Bose-Einstein distribution function.

2.1.2 *The Boltzmann Equation* <sup>4</sup>). In non-equilibrium conditions the distribution functions depend not only on momentum but also on position and time, say  $f(\vec{k}, \vec{r}, t)$ , considering only electrons in the first instance. This local distribution function can be changed by diffusion of particles from or into neighbouring

regions, by applying an external field, which gives rise to changes in the wave-vector  $\vec{k}$ , or by scattering of an electron out of or into the state  $\vec{k}$ . The Boltzmann equation follows from the steady state condition  $\frac{df}{dt} = 0$ , leading to:

$$\left(\frac{\partial f}{\partial t}\right)_{\text{scatt}} = \vec{v}_k \cdot \text{grad}_r f + \dot{\vec{k}} \cdot \text{grad}_k f \quad (2.1)$$

in which  $\vec{v}_k$  is the group velocity of the electrons, and  $\dot{\vec{k}} = \frac{e}{\hbar} \vec{E}$ , if we have only an electric field  $\vec{E}$ . The quantity to be determined from eq. (2.1) is the deviation from the local equilibrium distribution function  $f_k^0$ , viz:

$$g_k(\vec{r}) = f_k(\vec{r}) - f_k^0(T(\vec{r})) \quad (2.2)$$

The scattering term in (2.1) can be a complicated integral expression involving the matrix elements of the scattering mechanism, but can often be expressed in terms of a relaxation time  $\tau$  by the assumption:

$$\left(\frac{\partial f_k}{\partial t}\right)_{\text{scatt}} = \frac{\partial g_k}{\partial t} = -\frac{g_k}{\tau} \quad (2.3)$$

If the diffusion term is zero (no thermal gradient), and if  $g_k(\vec{r})$  is assumed to be small, eq. (2.1) is easily solved:

$$g_k(\vec{r}) = \left(-\frac{\partial f_k^0}{\partial \xi_k}\right) e \tau \vec{v}_k \cdot \vec{E} \quad (2.4)$$

where  $\xi_k = \frac{\hbar^2 k^2}{2m} - E_F$ . The electrical conductivity follows from the relation for the current density  $\vec{J} = \vec{\sigma} \cdot \vec{E} = 2 \int e \vec{v}_k g_k d\vec{k}$ . Substitution of eq. (2.4) gives

$$\vec{\sigma} = 2 \tau \int d\vec{k} \left(-\frac{\partial f_k^0}{\partial \xi_k}\right) e^2 \vec{v}_k \vec{v}_k \quad (2.5)$$

For a free electron gas eq. (2.5) becomes equal to the well-known expression

$$\sigma = \frac{1}{3} e^2 \tau v_F^2 N(0) = \frac{e^2 \tau n}{m} \quad (2.6)$$

where  $v_F$  is the Fermi velocity, in the electron mass, and  $n$  the number of electrons per unit volume.

If we only have a thermal gradient ( $\vec{E} = 0$ ) the solution of (2.1) is

$$g_k(\vec{r}) = - \left(-\frac{\partial f_k^0}{\partial \xi_k}\right) \left(\frac{\xi_k}{T}\right) \tau \vec{v}_k \cdot \text{grad } T \quad (2.7)$$

The heat flux is given by  $2 \int d\vec{k} g_k \xi_k \vec{v}_k$ . This is equal to  $-\vec{\lambda} \cdot \text{grad } T$ , which yields for the thermal conductivity

$$\vec{\lambda}_e = 2\tau \int d\vec{k} \left( -\frac{\partial f_k^0}{\partial \xi_k} \right) \left( \frac{\xi_k^2}{T} \right) \vec{v}_k \vec{v}_k \quad (2.8)$$

In the case of a free electron gas eq. (2.8) simplifies to a formula also known from kinetic gas theory:

$$\lambda_e = \frac{1}{3} C_e v_F^2 \tau = \frac{1}{3} C_e v_F \ell \quad (2.9)$$

In which  $C_e$  is the specific heat of the electrons per unit volume, and  $\ell$  their mean free path. Together with  $C_e = \frac{\pi^2}{3} k_B^2 T N(0)$ , eqs. (2.6) and (2.9) lead to the well-known Wiedemann-Franz law:

$$\lambda_e = \frac{\pi^2}{3} \frac{k_B^2}{e^2} T \sigma \equiv L_0 T \sigma \quad (2.10)$$

where  $L_0$  is the Lorenz number.

The expression for  $\tau$  depends on the scattering mechanism. If there are several simultaneous scattering mechanisms, acting independently, each with a specific relaxation time  $\tau_i$ , Matthiessen's rule yields:

$$\tau^{-1} = \sum_i \tau_i^{-1} \quad (2.11a)$$

A difficulty is that not always a relaxation time can be defined as was done in eq. (2.3). For example, Fröhlich<sup>5)</sup> pointed out that in the case of electrical conductivity  $\tau$  could not be defined at low temperatures if the electrons were scattered by phonons. However, it turned out to be possible to replace  $\tau$  by a transport lifetime  $\tau_{tr} = \tau_0 |\overline{\Delta k/k}|^{-1}$ , in which  $\tau_0$  is the mean time between two events of an electron (scattering lifetime), and  $|\overline{\Delta k/k}|$  the average relative change of momentum per scattering event. The latter factor is correlated to the effectiveness of the scattering mechanism. We can generalize this replacement by defining:

$$\tau_{tr} = \varepsilon^{-1} \tau_0 \quad (2.12)$$

In which  $\varepsilon$  is a parameter expressing the scattering effectiveness, depending on the mechanism and on the transport phenomenon being considered. Under these circumstances equation (2.11) has to be replaced by

$$\tau_{tr}^{-1} = \sum_i \tau_{tr i}^{-1} \quad (2.11b)$$

This procedure is certainly not correct from a purely theoretical point of view, but in practice it can be used in order to explain the temperature dependence of the transport coefficients.

For the phonon thermal conductivity one can also derive an expression from the Boltzmann equation in terms of a parameter  $\tau$ , but in this case it is always a function of the phonon wave-vector  $\vec{q}$ . The analogue of eq. (2.9) becomes

$$\lambda_p = \frac{1}{3} \int d\vec{q} v_s^2 c(\vec{q}) \tau(\vec{q}) \quad (2.13)$$

in which  $v_s$  is the velocity of sound and  $c(\vec{q})$  the phonon specific heat per unit volume for phonons with wave-vector  $\vec{q}$ .

Finally we want to conclude this section by remarking that a general restriction for using the Boltzmann equation is, that a distribution function can only be defined for the quasi-particles if they have well-defined energies.

2.1.3 *The Kubo Formalism*<sup>6</sup>). There are situations in which it is not possible to use the formalism of the preceding section. For example, in superconductors in the gapless region (see section 2.3) the energy of the electrons with momentum near the Fermi momentum can not be treated as a narrow band of energies. So the quasi-particle approximation breaks down. This kind of situation is only taken into account in a quite new set-up of the transport theory, the Kubo formalism.

It is not my intention to give a complete discussion of the Kubo formulae for the transport coefficients. Worth mentioning, however, is its general validity, as it has been derived from first principles of quantum statistical mechanics. Moreover, in solving the problem one always makes use of the advanced technique of modern many-body theory, the Green's function method. With this method both the energy spectrum and the lifetimes of the quasi-particles are treated simultaneously. Any kind of scattering mechanism can, in principle, be dealt with by means of diagrammatical series expansions, although the mathematics can be very complicated.

The Kubo formula, together with the Green's functions technique, makes it possible to calculate the coefficient of thermal conductivity in complicated physical situations, such as superconductors in the mixed state.

## §2.2 Thermal Conductivity of Normal Metals at Low Temperatures<sup>7)</sup>

In metals energy can be transported by electrons and phonons. It is commonly accepted, as a first approximation, to consider both mechanisms as operating separately, but parallel, so that their conductivities add together to

$$\lambda = \lambda_e + \lambda_p \quad (2.14)$$

Let us first give our attention to the electronic contribution, for it is by far the greatest in pure normal metals at low temperatures.

**2.2.1 Contribution of the Electrons.** Firstly we define a thermal resistivity,  $W_e$ , equal to  $\lambda_e^{-1}$ . As indicated by eq. (2.8),  $\lambda_e \propto \tau$  and therefore  $W_e \propto \tau^{-1}$ . In view of the eqs. (2.11a) and (2.11b) we obtain for several independent scattering mechanisms:

$$W_e = \sum_i W_{ei} \quad (2.15)$$

We distinguish:

$W_{ed}$ : Elastic scattering of the electrons by lattice defects. The effect is a change of the angle of the electron momentum with respect to the direction of the transport current; the magnitude (energy) does not change. This scattering mechanism will affect energy and charge transport in the same way, that is, both will have the same transport lifetime (see eq. (2.12)), and the Wiedemann-Franz law, eq. (2.10), will be obeyed:

$$W_{ed} = \rho_0 (L_0 T)^{-1} \quad (2.16)$$

where  $\rho_0$  is the residual resistivity.

$W_{ep}$ : The electrons are inelastically scattered by absorption or emission of phonons. The energy transfer is of the order of  $k_B T$ , which is about the mean phonon energy. Because this is of the same order of magnitude as the spread in the distribution function of the electrons, it can change a relatively hot electron into a cold one, and vice versa. That is, the effectiveness is almost one:  $\tau_{tr} = \tau_0$  for heat transport. For charge transport, however, the effectiveness is of the order of magnitude of the relative momentum change, which is more a change of angle than of magnitude. It will depend on temperature via the phonon momentum:  $\epsilon \propto T^2$ . The scattering lifetime is inversely proportional to the

phonon number, so that  $\tau_0 \propto T^{-3}$ . Therefore we have for the electrical conductivity  $\sigma_{ep} \propto T^{-5}$ , the well-known Bloch-Grüneisen law. For the thermal resistivity we obtain:

$$W_{ep} = bT^2 \quad (2.17)$$

b is a constant<sup>4)</sup>. The Wiedemann-Franz law is not obeyed.

Substituting the results, eqs. (2.16) and (2.17), into eq. (2.15) we obtain for the electronic heat resistivity at low temperatures

$$W_e = a/T + bT^2 \quad (2.18)$$

where  $a = \rho_0/L_0$ . This law has been verified by many experiments.

2.2.2 *Contribution of the Phonons.* Although the phonon conductivity in normal metals can usually be ignored, it plays an important part in superconductors well below the critical temperature. Therefore it will be discussed here. Again we have the impurities as an important scattering source, and, of course, also the electrons. Each kind of impurity now has its specific scattering cross section or inverse scattering time, depending on the phonon frequency  $\omega$ , as was calculated by Klemens<sup>8)</sup>. His results are presented in the following table: (phonon-phonon Umklapp processes do not contribute at low temperatures)

scattering mechanism	$\tau^{-1}$	temperature dependence in $\lambda_p$
dislocations	$\omega^1$	$T^2$
point defects	$\omega^4$	$T^{-1}$
external, grain boundaries	$\omega^0$	$T^3$
electrons	$\omega^1$	$T^2$

The temperature dependence of  $\lambda$  for one scattering mechanism follows directly from eq. (2.13) after substitution of a Debye spectrum and changing the variable of integration into  $x = \hbar\omega/k_B T$ . In the temperature range of our experiment and for the samples we investigated, only point defect, grain boundary, dislocation, and electron scattering are important. In that case we obtain for the phonon thermal conductivity (using Matthiessen's rule):

$$\lambda_p = \frac{k_B^4 T^3}{2\pi^2 \hbar^3 v_s} \int_0^{\theta_D/T} dx \frac{x^4 e^x (e^x - 1)^{-2}}{[Px^4 T^4 + B + ExT + DxT]} \quad (2.19)$$

$v_s$  is the velocity of sound. For details about the constants P (point defects), B (boundaries), D (dislocation), and E (electrons) we refer to Klemens' papers<sup>8</sup>. We see that it is not possible to separate the different terms contributing to the phonon resistivity, as could be done for the electrons. This obviously is due to the different frequency dependences of the  $\tau$ 's.

Now we can show why  $\lambda_p \ll \lambda_e$ . If only phonon-electron scattering is taken into account we can relate the resistivity belonging to this mechanism  $W_{pe}$  to  $W_{ep}$ . We obtain for Nb:  $W_{pe}/W_{ep} \approx 10^{-2} (\theta_D/T)^4$ . Moreover,  $W_{ep} = (bT^3/a)W_{ed}$ . Below 10 K it is correct to replace  $W_{ed}$  by  $W_e$  (depending on the sample purity  $0.5 W_e \leq W_{ed} \leq W_e$ ). Putting everything together we obtain:

$$\lambda_p \leq \lambda_e \frac{a \cdot 10^2}{bT^3} \left(\frac{T}{\theta_D}\right)^4 \quad (2.20)$$

For our Nb samples  $a/b \sim 10^{-5}$  and the Debye temperature  $\theta_D$  of Nb is 275 K<sup>9</sup>, thus we have  $\lambda_p \leq 10^{-3} T \lambda_e$ . The phonon contribution at temperatures below 10 K is smaller than one percent of the total thermal conductivity in the normal state. If the impurity increases (increasing a) the phonon contribution increases proportionally.

## §2.3 Properties of Superconductors

### 2.3.1 Weak-Coupling Superconductors in Zero Field.

The energy spectrum of the electrons in superconductors below the critical temperature  $T_c$  deviates from the normal state energy spectrum by the appearance of a temperature dependent energy gap just around the Fermi level and an infinite density of states at the gap edges. Bardeen, Cooper and Schrieffer<sup>10</sup> (hereafter referred to as BCS) provided the explanation of this peculiar phenomenon by showing that at  $T = 0$  under the influence of an attractive electron-phonon-electron interaction all the electrons near the Fermi level will lower their energy by the formation of Cooper pairs<sup>11</sup>, characterized by anti-parallel momentum and spin. The range of this pair correlation is given by the Pippard coherence length

$$\xi_0 = 0.18 \hbar v_F / k_B T_c \quad (2.21)$$

To create an excited state from the BCS ground state, whether this is a hole-like or electron-like quasi-particle, a minimum energy  $\Delta(T)$ , equal to the energy gap, is necessary. It is self-consistently given by the gap equation, which can be easily solved in the BCS approximation, in which the actual electron-phonon interaction is replaced by a constant potential  $V$ , defined in an energy band limited by the Debye frequency  $\hbar\omega_D$ . Moreover, it is assumed that the coupling constant  $N(0)\cdot V$  is smaller than 0.25 (weak coupling limit). Taking into account these assumptions the BCS theory predicts that all superconductors will exhibit a universal behaviour governed by the temperature dependence of  $\Delta_{BCS}$ , shown in fig. 2.1, with  $T_c$  as the only parameter. Some features of

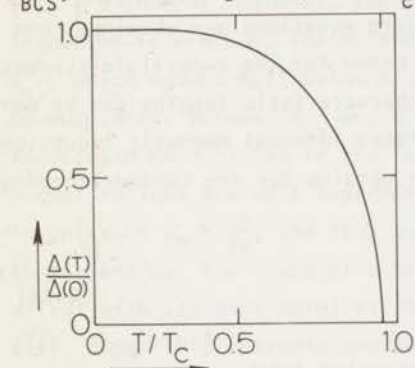


Fig. 2.1 *Reduced energy gap versus reduced temperature, according to the BCS theory.*

$\Delta_{BCS}$  are:

$$\Delta_{BCS}(0) = 1.76 k_B T_c \quad (2.22)$$

$$\Delta_{BCS}(T) = 3.06 k_B T_c (1 - T/T_c)^{1/2} \quad (2.23)$$

near  $T_c$ . In the weak coupling limit  $\Delta_{BCS}(0) = 2\hbar\omega_D \exp[-1/N(0)V]$ , which together with eq. (2.22) yields a simple relation between  $T_c$  and  $\theta_D$ :

$$T_c = 0.88 \theta_D \exp[-1/N(0)V] \quad (2.24)$$

from which  $N(0)V$  can be calculated.

2.3.2 *The Influence of a Magnetic Field. Phenomenological Theory.* Well before the development of the microscopic theory Ginzburg and Landau<sup>12)</sup> proposed in 1950 a phenomenological relation for the free energy of a superconductor in a magnetic field for temperatures close to  $T_c$ . It was a generalization of an original theory of Landau<sup>13)</sup> describing the ordered phase near a second order ferromagnetic phase transition. The idea is that the free energy near the transition can be expanded in powers of an internal order parameter  $\psi$ , which is

small in that region. Landau proved that the first and third order terms must be identically zero if the ordered and disordered phases were separated by a transition line in the phase diagram.

The extension of the theory to superconductivity consists of the introduction of a magnetic field term and a term accounting for spatial variations of  $\Psi(\vec{r})$ , which now also could be a complex quantity. It was interpreted as the wave function of the macroscopically occupied quantum state of the superconducting electrons, also proposed by Landau<sup>14)</sup>. Its squared amplitude is equal to the superfluid density of the Gorter-Casimir theory<sup>15)</sup>, its phase is related to phenomena like flux quantization and the Josephson effects. By minimizing the free energy expression the two Landau-Ginzburg equations are obtained, one giving a relation for the order parameter, the other for the superfluid currents in the superconductor. From these equations the characteristic lengths can be derived over which  $|\Psi|$  and the current (or associated internal magnetic induction) can vary from zero to their maximum values. One obtains for the Landau-Ginzburg coherence length

$$\xi(T) = 0.74 \xi_0 \left( \frac{T_c}{T_c - T} \right)^{\frac{1}{2}} \quad (2.25)$$

(in which  $\xi_0$  obeys (2.21)) and for the L-G penetration depth

$$\lambda(T) = \frac{1}{2}\sqrt{2} \lambda_L(0) \left( \frac{T_c}{T_c - T} \right)^{\frac{1}{2}} \quad (2.26)$$

in which  $\lambda_L(0)$  is the London penetration depth at zero temperature:

$$\lambda_L(0) = (4\pi |\Psi|^2 e^2 / mc^2)^{\frac{1}{2}} .$$

The ratio of  $\xi(T)$  and  $\lambda(T)$  is a constant called the Landau-Ginzburg parameter  $\kappa$ . GL already pointed out that this parameter determines to a great extent the surface energy of a normal-superconducting interface. It is negative for  $\kappa > \frac{1}{2}\sqrt{2}$ , indicating that, in a magnetic field, a mixed state of alternating superconducting and normal regions will be a more stable state than the homogeneous Meissner state with zero internal induction.

The existence of the mixed state was theoretically predicted by Abrikosov<sup>16)</sup> in 1957. He solved the L-G equations for small  $|\Psi|$  and strong magnetic fields. In decreasing field a spontaneous nucleation of superconducting regions will show up at a certain field  $H = H_{c2}$ , obeying the relation

$$H_{c2} = \kappa\sqrt{2} H_c \quad (2.27)$$

where  $H_c$  is the thermodynamic critical field. If  $\kappa < \frac{1}{2}\sqrt{2}$  no anomalous effect can be observed, because in that case  $H_{c2} < H_c$  and a transition into the Meissner state takes already place at  $H_c$ . The latter behaviour is called type-I superconductivity. If  $\kappa > \frac{1}{2}\sqrt{2}$ , or  $H_{c2} > H_c$ , the L-G equations have a solution  $\Psi \neq 0$  for fields well above  $H_c$ . Energetically most favourable is a triangular periodicity of the order parameter and of the magnetic induction<sup>17)</sup>. Where  $\Psi(\vec{r}) = 0$  (normal regions), the induction is maximum, where  $\Psi$  is maximum, the induction is minimum. The Meissner state will be realized only below a field  $H_{c1}$ , which occurs well below  $H_c$ . In this case we are dealing with type-II superconductivity. Between  $H_{c1}$  and  $H_c$  the triangular lattice is also the most favourable one<sup>18)</sup>, as in the region between  $H_c$  and  $H_{c2}$ . Just above  $H_{c1}$  the normal regions are well separated and the magnetic flux they carry is quantized in units of  $\phi_0 = \frac{ch}{2e}$ , the flux quantum. One quantum per normal region gives the lowest energy. The shape of a normal region, because of the symmetry, is cylindrical with its axes parallel to the external field; its radius is of the order  $\xi(T)$ . Superfluid currents around the normal core screen off the magnetic field of the core. They circulate over a characteristic distance  $\lambda(T)$  (obeying (2.26)) around the core. In analogy with superfluid helium the cylinders are called vortex lines, or vortices, or flux lines, because of the flux they carry.

The current of a vortex in the field of an other one causes a repulsive mutual interaction leading to the triangular lattice of the flux lines described above. Near  $H_{c1}$  the distance  $a_0$  between neighbouring vortices is related to the average internal induction  $B$  according to

$$a_0 = \left[ \frac{2}{\sqrt{3}} \frac{\phi_0}{B} \right]^{\frac{1}{2}} \quad (2.28)$$

A quite useful relation between  $H_{c2}$  and  $\xi(T)$  is

$$\xi(T) = \left[ \frac{\phi_0}{2\pi H_{c2}} \right]^{\frac{1}{2}} \quad (2.29)$$

This leads to:

$$\frac{a_0}{\xi(T)} = 2.7 \left[ \frac{H_{c2}}{B} \right]^{\frac{1}{2}} \quad (2.30)$$

If  $H$  approaches  $H_{c2}$ , the vortex cores begin to overlap, so that the maximum value of the order parameter between the vortices will be considerably reduced. In this field region one can hardly speak about vortices, merely about a small order parameter fluctuation with triangular periodicity. The spatial average  $\langle |\psi(\vec{r})|^2 \rangle$  will go to zero linearly with field, if  $H$  goes to  $H_{c2}$ , which means that the transition to the normal state is of second order for all temperatures below  $T_c$ . The magnetization, as Abrikosov showed, is proportional with  $\langle |\psi|^2 \rangle$ . He obtained for  $H \leq H_{c2}$ :

$$4\pi M = \frac{H - H_{c2}}{\beta_A (2\kappa^2 - 1)} = \frac{B - H_{c2}}{\beta_A (2\kappa^2 - 1) + 1} \quad (2.31)$$

$\beta_A$  is a constant which reaches its minimum for the triangular configuration:  $\beta_A = 1.16$ .

### 2.3.3 *Extension of the Microscopic Theory to Non-Homogeneous Situations.*

The BCS theory only deals with a homogeneous electron gas with attractive interaction. In order to describe the effect of a magnetic field or of impurities the theory had to be generalized. This has been done by Bogolubov<sup>19)</sup>, who eventually derived two coupled equations for the operators  $\hat{\psi}(\vec{r}, \alpha)$  and  $\hat{\psi}^\dagger(\vec{r}, \alpha)$  which annihilate or create a quasi-particle excitation from the BCS ground state at a position  $\vec{r}$  with spin  $\alpha$ , up ( $\uparrow$ ) or down ( $\downarrow$ ). These operators are functions of the pair potential  $\Delta(\vec{r})$  which - in the BCS approximation - is self-consistently given by the relation

$$\Delta(\vec{r}) = V \langle \hat{\psi}(\vec{r}, \uparrow) \hat{\psi}(\vec{r}, \downarrow) \rangle \quad (2.32)$$

$V$  is the BCS electron-phonon interaction. The average is taken over a grand ensemble, because the number of quasi-particles is not conserved, for terms with  $\Delta$  in the Hamiltonian create or annihilate two quasi-particles, so respectively annihilate or create a Cooper pair. In the absence of an applied field and without impurities,  $\Delta(\vec{r})$  is spatially constant and is equal to the BCS energy gap  $\Delta_{BCS}$ .

The Bogolubov equations - or, in a modified form, the Gorkov equations - together with the self-consistency equation (2.32) (which still can be generalized to strong coupling superconductors) are the starting point of modern superconductivity theory, of which we will present some important features here.

In 1964 Caroli, de Gennes, and Matricon<sup>20)</sup> solved the problem of the

spectrum of low energy excitations in the core of an isolated vortex in a pure type-II superconductor with  $\kappa \gg 1$  ( $\xi \ll \lambda$ ), (bound excitations). It was derived that there is a very small energy gap ( $\sim \Delta_{\text{BCS}}^2/E_F \approx 10^{-3} \Delta_{\text{BCS}}$ ) inside the core increasing to  $\Delta_{\text{BCS}}$  for  $r \gg \xi$ . The density of states is approximately equal to that of a normal metal cylinder of radius  $\xi$ . So the bound excitations behave like normal electrons. The high energy ( $> \Delta_{\text{BCS}}$ ) excitations, both in the core and far from the core (free excitations), behave like the ordinary quasi-particles of the BCS theory, although there remains a phase shift of the wave function in the core region due to the presence of a local magnetic field, superfluid currents and a variation of  $\Delta(\vec{r})$  <sup>21)</sup>. Bergk and Tewordt <sup>21)</sup> extended the calculations to low  $\kappa$ . The small gap now disappears, the density of states remains that of a normal metal cylinder with radius  $\xi$ .

For small  $\Delta(\vec{r})$  it is possible to expand the gap equation (2.32) in powers of  $\Delta$ . In this way Gorkov <sup>22)</sup> has made a link between the microscopic theory and the phenomenological Landau-Ginzburg theory. He showed that  $\Delta(\vec{r})$  is proportional to  $\Psi(\vec{r})$ , the order parameter of the L-G theory. For that reason  $\Delta(\vec{r})$  is often called order parameter as well. The Gorkov equation clarified theoretically the distinction between pure ( $\ell \gg \xi_0$ ) and dirty ( $\ell \ll \xi_0$ ) superconductors ( $\ell$  is the mean free path of the electrons). This was already known from experiment <sup>23)</sup> and then could be explained by the assumption that impurity scattering would destroy the ordering of the electrons and thus would result in a smaller effective coherence length. Pippard suggested

$$\frac{1}{\xi_{\text{eff}}} = \frac{1}{\xi_0} + \frac{1}{\ell} \quad (2.33)$$

which yields  $\xi_{\text{eff}} = \ell$  if  $\ell \ll \xi_0$ , as was later derived from microscopic theory. All kinds of parameters, like  $\kappa$  in eqs. (2.27) and (2.28), and characteristic lengths like  $\xi(T)$  and  $\lambda(T)$  in eqs. (2.25) and (2.26) turned out to be purity dependent, see for example de Gennes' book on superconductivity <sup>24)</sup>. Equations (2.25) and (2.26) are valid for  $\ell \gg \xi_0$ , eq. (2.27) becomes

$$H_{c2} = \kappa_1(T) \sqrt{2} H_c \quad (2.27a)$$

in which  $\kappa_1(T)$  is a purity dependent parameter which increases slowly with decreasing temperature <sup>25)</sup>. In eq. (2.31)  $\kappa$  has to be replaced by a different parameter, referred to as  $\kappa_2(T)$  <sup>26)</sup>.

Concerning the density of states there is a very interesting distinction between pure and dirty type-II superconductors in magnetic fields near  $H_{c2}$ .

For dirty superconductors<sup>27)</sup> the low energy excitation spectrum is that of a normal metal corrected with a small second order perturbation term proportional to  $\Delta^2(\vec{r})$ . There is no gap in the energy spectrum (gapless superconductivity), but there remains a certain amount of ordering due to a non-zero averaged order parameter. The high energy spectrum tends to the conventional BCS spectrum, which for those energies approaches that of a normal metal. The spatial average of the density of states is given by:

$$\frac{\langle N^s(\vec{r}) \rangle}{N^n(0)} - 1 \propto \langle |\Delta(\vec{r})|^2 \rangle \propto H_{c2} - H \quad (2.34)$$

(The superscripts s and n will be used throughout this thesis to refer to the superconducting and the normal state respectively). For the transport properties this means that they will decrease linearly in H with respect to the normal state values<sup>28)</sup>.

In pure superconductors near  $H_{c2}$ <sup>29)</sup> the energy spectrum is anisotropic, because quasi-particles moving along the field direction on the average will behave like BCS quasi-particle excitations, and experience a gap equal to  $\langle |\Delta|^2 \rangle^{\frac{1}{2}}$ , whereas quasi-particles moving perpendicular to the field direction on the average will experience no gap because of a strong oscillating phase of the order parameter along the path of the quasi-particles. A perturbation expansion like that in the dirty case now diverges due to the BCS like quasi-particles with a gap in their energy spectrum and an infinite density of states at the gap edge. The density of states thus depends not only on the energy but also on the propagation direction of the quasi-particles with respect to H. By making a conjecture for the spectral density function Maki<sup>30)</sup> could derive expressions for the ultrasonic attenuation and for the thermal conductivity. He derived a decrease of the transport quantities proportional to  $(H_{c2} - H)^{\frac{1}{2}}$ , in striking difference with eq. (2.34).

2.3.4 *Extension of the Microscopic Theory to Strong-Coupling Superconductors.* As follows from eq. (2.24) superconductive materials with relatively low  $\theta_D$  and high  $T_c$  will not satisfy the BCS weak-coupling assumption. Well-known exceptions are Pb and Hg with respectively  $N(0)V$  values of 0.39 and 0.35. Also Nb, with  $\theta_D = 270$  K and  $T_c = 9.2$  K, belongs to the class of strong-coupling superconductors:  $N(0)V = 0.32$ . In Nb this large value merely follows from the transition metal character, which accounts for a large density of states of the d-electrons and a nearly constant interaction potential<sup>31)</sup> (see section 2.6). This is in contrast with Pb or Hg, where the large coupling

constant follows from the strong electron-phonon interaction. In that case also the BCS approximation with a constant  $V$  can no longer be applied and one has to generalize the gap equation (2.32). This generalization has been given by Eliashberg<sup>32)</sup>. It forms the starting point of the strong coupling theory which was extensively reviewed by Scalapino<sup>33)</sup>.

We will only mention one result important for the following section of this chapter. In spite of the value of the coupling constant the reduced energy gap  $\Delta(T)/\Delta(0)$  as a function of  $T/T_c$  follows the same curve as was predicted by the BCS theory, fig. 2.1. Only the numerical constants in eqs. (2.22) and (2.23) have to be adapted to the specific material.

## §2.4 Thermal Conductivity in Superconductors. Temperature Dependence<sup>34)</sup>

The difference between the electron thermal conductivity in the superconducting and the normal state can be understood qualitatively in view of a simple two-fluid model. One kind of particles, the Cooper pairs, are unable to transport energy, the other kind, the normal excitations from the BCS ground state, can.

### 2.4.1 Contribution of the Electrons

2.4.1.1 *Defect Scattering.* Let us first pay attention to the electronic thermal conductivity in superconductors with dilute defect concentration. Elastic defect scattering does not break up the Cooper pairs. Therefore the only effect of entering into the superconducting state by lowering the temperature below  $T_c$  will be the appearance of the energy gap and from this the decrease in the number of normal excitations, roughly spoken proportional to  $\exp[-\Delta_{\text{BCS}}(T)/k_B T]$ . From fig. 2.1, showing  $\Delta_{\text{BCS}}(T)$ , it is clear that  $\lambda_{\text{ed}}^s/\lambda_{\text{ed}}^n$  will decrease below  $T_c$ ; at reduced temperature  $t(=T/T_c)$  of 0.2 it will be almost negligibly small.

The exact derivation of the formula was given by Geilikman<sup>35)</sup> and, independently, by Bardeen, Rickayzen, and Tewordt, referred to as BRT<sup>36)</sup>. These authors used a simple Boltzmann equation. Later derivations<sup>37)</sup> making use of the Kubo formalism and Green's functions technique confirmed the earlier result for arbitrary impurity concentrations. We restrict ourselves to the formula in the BRT form:

$$\frac{\lambda_{\text{ed}}^s}{\lambda_{\text{ed}}^n} = \frac{2F_1(-\gamma) + 2\gamma \ln(1 + e^{-\gamma}) + \gamma^2/(1 + e^{\gamma})}{2F_1(0)} \quad (2.35)$$

where  $\gamma = \frac{\Delta_{\text{BCS}}(T)}{\Delta_{\text{BCS}}(0)} \cdot \frac{\Delta_{\text{BCS}}(0)}{k_B T_c} \cdot \frac{T_c}{T}$  and  $F_n(-\gamma) = \int_0^\infty dz z^n (1 + e^{\gamma+z})^{-1}$ .

The functions  $F_n$  were tabulated by Rhodes<sup>38)</sup>, the values of  $\Delta_{\text{BCS}}(T)/\Delta_{\text{BCS}}(0)$  by Mühlischlegel<sup>39)</sup>. The only parameter in this equation is  $\Delta_{\text{BCS}}(0)/k_B T_c = \gamma_0$ . Therefore, with a suitable adaptation of this parameter, eq. (2.35) should hold for all coupling constants (see section 2.3.4). The graph of eq. (2.35) is shown in fig. 2.2 with the BCS value, eq. (2.22), substituted. The slope at  $T_c$  is zero.

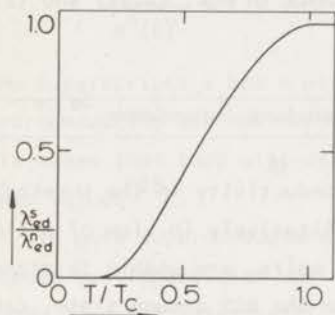


Fig. 2.2 Ratio of superconducting to normal state electronic thermal conductivity versus reduced temperature if defect scattering is predominant, according to BRT (eq. (2.35),  $\gamma_0 = 1.76$ )

**2.4.1.2 Phonon Scattering.** Next we will discuss the thermal conductivity of the electrons when scattering by phonons is predominant, which will occur in very pure superconductors near  $T_c$ . (It is the real electron-phonon interaction, which is considered here, not the virtual exchange of a phonon between the electrons of a Cooper pair.) This scattering is not elastic and can lead to pair breaking or pair creation. This effect accompanies the effect of the diminishing number of excitations with increasing gap, as was already discussed. In that case the mean free path of the normal excitations was the same both in superconducting and normal states, but in the case of phonon scattering there will be a difference in lifetime of the quasi-particles in the normal and superconducting state.

Again several authors tackled this problem. BRT<sup>36)</sup>, Kresin<sup>40)</sup>, and Geilikman and Kresin<sup>41)</sup> treated it by considering the Boltzmann equation. BRT used three trial functions which appeared to be much too simple as was shown by the Russian authors, who were able to derive an approximate solution near  $T_c$ . In fig. 2.3 it is shown as the dashed curve. Tewordt<sup>42)</sup> also used the BRT Boltzmann equation, but calculated the quasi-particle lifetime by means of Green's functions. He arrived at an expression depending on temperature through the parameter  $\gamma$  of eq. (2.35) and through the lifetime of the normal excitations. The results for two values of  $\gamma_0$  are shown in fig. 2.3 as well. The slope of the  $\lambda_{ep}^s/\lambda_{ep}^n$  curve at  $T_c$  has a value of about 1.6.

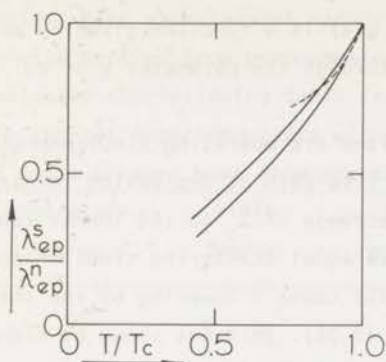


Fig. 2.3 Ratio of superconducting to normal state electronic thermal conductivity versus reduced temperature if phonon scattering is predominant. Broken curve, calculated by Geilikman and Kresin; continuous curves, calculated by Tewordt, upper one:  $\gamma_0 = 1.76$ , lower one:  $\gamma_0 = 2.0$ .

2.4.2 *Contribution of the Phonons.* The phonon contribution in the superconducting state will also be different from the normal state contribution. As we saw in section 2.2.2 the phonons contribute negligibly in the normal state due to the large phonon-electron scattering. But in the superconducting state, especially at temperatures well below  $T_c$ , the number of normal excitations is drastically reduced. In addition, phonons with energies  $< 2\Delta_{BCS}(T)$  can not annihilate Cooper pairs, so they are hardly scattered by them. On the other hand, phonons with energy  $> 2\Delta_{BCS}(T)$  will behave as in the normal state. However, their numbers and therefore their total contribution to the thermal conductivity is largely decreased at low temperatures. If we regard the electrons as the only phonon scatterers the result will be an exponentially increasing phonon conductivity with decreasing temperature.

The theoretical calculation has been carried out by Geilikman and Kresin<sup>43)</sup> and by BRT<sup>36)</sup>, leading to the curves in fig. 2.4. Again we only give the result of BRT:

$$\frac{\lambda_{pe}^s}{\lambda_{pe}^n} = \frac{\int_0^\infty dx x^4 e^x (e^x - 1)^{-2} [g(x) ExT]^{-1}}{\int_0^\infty dx x^4 e^x (e^x - 1)^{-2} [ExT]^{-1}} \quad (2.36)$$

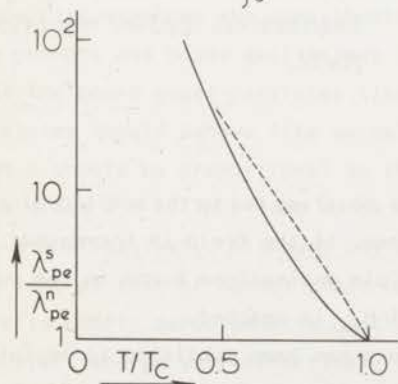


Fig. 2.4 Ratio of superconducting to normal state phonon conductivity versus reduced temperature, if electron scattering is predominant. Continuous curve, calculated by BRT; broken curve, calculated by Geilikman and Kresin.

(compare eq. (2.19)), in which  $x = \hbar\omega/k_B T$  and  $g(x)$  is a function given by an integral expression depending on temperature through the parameter  $y$  of eq. (2.35).

In reality more phonon scattering mechanisms are operating simultaneously, providing a limitation to the increasing mean free path at decreasing temperature. Eventually this leads to a power-like decrease of  $\lambda_p$  at the lowest temperatures. Although the different defects will have equal scattering times in the normal and superconducting states, it still will cause a lowering of the total phonon conductivity ratio with respect to eq. (2.36). This was shown by Klemens and Tewordt<sup>44)</sup> for point defects, but their formula is easily extended with the help of eq. (2.19) to include grain boundaries and dislocations as well:

$$\frac{\lambda_p^s}{\lambda_p^n} = \frac{\int_0^\infty dx x^4 e^x (e^x - 1)^{-2} [Px^4 T^4 + B + DxT + g(x)ExT]^{-1}}{\int_0^\infty dx x^4 e^x (e^x - 1)^{-2} [Px^4 T^4 + B + DxT + ExT]^{-1}} \quad (2.37)$$

However, it will not be easy to derive the contributions of the different mechanisms separately from the experimental results.

### §2.5 Thermal Conductivity in the Mixed State of Type-II Superconductors

A typical graph of the thermal conductivity of a type-II superconductor in a longitudinal magnetic field is shown in fig. 2.5. With the entrance of

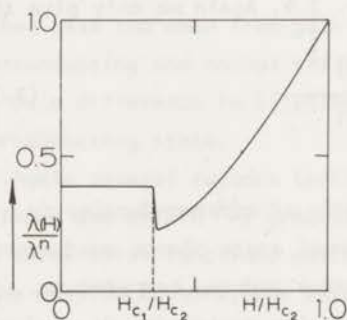


Fig. 2.5 Typical behaviour of the thermal conductivity of a type-II superconductor in a longitudinal applied magnetic field.

flux lines above  $H_{c1}$  a sharp decrease in  $\lambda$  is observed due to the additional scattering of the energy carriers by the flux lines. If the field is increased, the vortices begin to overlap and the quasi-particle excitations bound to the vortex cores begin to contribute more and more until  $H_{c2}$  is reached.

Rather little fundamental theoretical work has been published to explain these phenomena. This is not too surprising in view of the complexity of the

problem. Most experimental results will have to be compared with qualitative formulae derived from phenomenological models. To give an impression of this complexity the following table is presented, which deals only with the case of pure type-II superconductors without taking into account the anisotropy due to the angle between heat flow direction and magnetic field.

Temperature Region	Field Region	Principle Heat Carriers	Theory, Phenom. Models
$T \ll T_c$	$H \geq H_{c1}$	phonons	Canel <sup>45</sup> ); Vinen <sup>46</sup> ); Lowell <sup>47</sup> )
	$H_{c1} < H \ll H_{c2}$	both	Vinen et.al <sup>46</sup> )
	$H \leq H_{c2}$	electrons	Maki <sup>30</sup> )
$T \leq T_c$	$H \geq H_{c1}$	electrons	Cleary <sup>50</sup> )
	$H_{c1} < H < H_{c2}$	electrons	-
	$H \leq H_{c2}$	electrons	Maki <sup>51</sup> )

In the case of a dirty type-II superconductor the situation is even worse. We only have at our disposal the theory of Caroli and Cyrot dealing with the electronic thermal conductivity near  $H_{c2}$ .

In the following subsections we will elucidate in more detail the merits of the theories and models thus far available in the literature.

### 2.5.1 Pure Type-II Superconductors ( $\lambda \gg \xi_0$ )

2.5.1.1 At low temperatures and small inductions ( $T \ll T_c, H \geq H_{c1}$ ). For these circumstances the contribution to the thermal conductivity may come from the phonons and bound excitations (sections 2.3.3 and 2.4.1). One should expect that the bound quasi-particles (inside the vortex cores) with a normal density of states should behave like normal electrons in a cylinder with radius  $\xi$ , so that  $\lambda$  should be proportional to the number of (well-separated) vortices per unit area:  $\lambda \propto B$ . This idea turns out to be wrong as Canel<sup>45</sup>) was able to prove qualitatively. Although the scattering time of the bound excitations is the same as that of normal electrons, their group velocity along the vortex core is nearly zero. Canel's conclusion was that bound excitations can not transport energy very effectively and do not contribute to the thermal

conductivity. The only carriers of heat therefore will be the phonons:  $\lambda = \lambda_p$ .

The phonons will be scattered very effectively by the bound excitations in the vortex cores, as by electrons in the normal state (section 2.2.2). At least, if their wavelength is smaller than the core dimension, thus for temperatures  $T > \hbar v_s / k_B \xi$  ( $\approx 1$  K in niobium), and if the angle between wave vector and magnetic field exceeds:  $(v_s / v_F) \cdot (\Delta_{BCS}(0) / k_B T)$  ( $\approx 0.26$  rad at 1 K).

Based on Canel's conclusions Vinen, Forgan, Gough, and Hood<sup>46)</sup> proposed the following relation for the phonon mean free path if the field is perpendicular to the heat current, and if a random array of vortices is assumed:

$$\frac{1}{\lambda_p(B)} = \frac{1}{\lambda_p(0)} + \alpha \frac{B}{H_{c2}} \frac{1}{\lambda_p^n} \quad (2.38)$$

in which  $\alpha$  is a constant of order unity, and  $\lambda_p^n$  the phonon mean free path in the normal state. This yields for the thermal conductivity:

$$\frac{\lambda_p(0)}{\lambda_p(B)} - 1 = \alpha \frac{B}{H_{c2}} \frac{\lambda_p(0)}{\lambda_p^n} \quad (2.39)$$

which accounts for the fast decrease of  $\lambda$  beyond  $H_{c1}$ . Their measurement agreed with this relation quite well. Even in longitudinal fields the agreement was satisfactory for the lowest inductions. This justifies Canel's conclusion that the bound excitations have an anomalously low group velocity along the vortex core.

2.5.1.2 *At low temperatures and intermediate inductions ( $T \ll T_c$ ,*

*$H_{c1} < H \ll H_{c2}$ ). At intermediate perpendicular fields a deviation from eq. (2.39) shows up (Vinen et al.<sup>46)</sup>), which can be contributed to the tunneling of the bound excitations between neighbouring vortex cores. The eigenfunctions outside the core are roughly behaving like<sup>20)</sup>  $r^{-\frac{1}{2}} \exp(-\alpha r / \xi)$  ( $\alpha \approx \frac{1}{\pi}$ ) so that the electronic contribution to  $\lambda$  will be (see eqs. (2.28) - (2.30)):*

$$\lambda_e(B) \propto B^{\frac{1}{2}} \exp\{-\beta(H_{c2}/B)^{\frac{1}{2}}\} \quad (2.40)$$

with  $\beta \approx 1.7$ . This relation fits well with their experiments ( $\beta = 1.66$ ).

2.5.1.3 *At low temperatures near  $H_{c2}$  ( $T \ll T_c$ ,  $H \lesssim H_{c2}$ ). In section 2.3.3 we already mentioned the anomalous orientation dependence of the density of*

states in the pure limit, which urged Maki <sup>30)</sup> to make his conjecture. He proved that in first approximation  $\lambda$  should be proportional to  $\langle |\Delta|^2 \rangle^{\frac{1}{2}}$  and thus obtained the relation:

$$\lambda_e^n - \lambda_e(H) = C_p(T) (H_{c_2} - H)^{\frac{1}{2}} \quad (2.41)$$

The  $\lambda(H)$  curve should exhibit an infinite slope at  $H_{c_2}$ ! This expression can be directly compared with experimental results, because the phonon contribution can be neglected in this field region,  $\lambda = \lambda_e$ . Equation (2.41) was confirmed qualitatively by experiments of several authors <sup>46,47,48)</sup>. However, it turned out that the experimental values of  $C_p(T)$  were an order of magnitude larger than theoretically predicted, and, in addition, depended on the electron mean free path. In a later publication, together with Houghton, Maki <sup>49)</sup> could eliminate these discrepancies by making use of the BPT <sup>29)</sup> Green's function of a pure type-II superconductor, yielding an increasing coefficient with increasing mean free path.

2.5.1.4 *At high temperatures and small inductions ( $T \leq T_c$ ,  $H \geq H_{c_1}$ ).* At high temperatures the electron contribution to the thermal conductivity is predominant,  $\lambda = \lambda_e$ .

At small inductions only the free excitations will contribute to the conductivity. Far from the vortex cores  $r \gg \lambda$  (penetration depth) they behave like ordinary BCS excitations, but they are modified if they approach a flux line and interact with the superfluid current, magnetic field, and the modulation in  $|\Delta(\vec{r})|$  (section 2.3.3). Cleary <sup>50)</sup> treated this interaction and the elastic scattering involved in detail. Scattering by the modulation in the pair potential is predominant for the thermal resistivity, because it can scatter an electron-like quasi-particle into a hole-like quasi-particle, or vice versa. If this occurs the energy (with respect to  $E_F$ ) changes sign whereas the particle still moves in the same direction, so the contribution to the energy flow is reversed by the interaction.

The effective scattering diameter  $a$  of a flux line has been calculated by Cleary. It is of the order of  $300 \text{ \AA}$ , both if the field and the heat flow are perpendicular and if they are parallel; the first case being somewhat more effective. The thermal conductivity just above  $H_{c_1}$  will decrease like:

$$\frac{\lambda_e(0)}{\lambda_e(B)} - 1 = \frac{2aB}{\Phi_0} \quad (2.42)$$

2.5.1.5 At high temperatures near  $H_{c2}$  ( $T \leq T_c$ ,  $H \leq H_{c2}$ ). Near  $H_{c2}$  the conductivity will obey the same equation as at low temperatures near  $H_{c2}$ . It is given by eq. (2.41), but with a somewhat higher coefficient, if electron-phonon scattering is also taken into account<sup>51</sup>).

## 2.5.2 Dirty Type-II Superconductors ( $\ell \ll \xi_0$ )

2.5.2.1 At low temperatures and small inductions ( $T \ll T_c$ ,  $H \geq H_{c2}$ ). If the mean free path of the phonons is much smaller than  $\xi$ , we may consider the flux lines as conductors of normal metal parallel to the superconducting matrix. Then  $\lambda_p(B) = \lambda_p^S - c(\lambda_p^S - \lambda_p^N)B/H_{c2}$ ;  $c \approx 0.5$ .

2.5.2.2 For all temperatures near  $H_{c2}$  ( $0 \leq T \leq T_c$ ,  $H \leq H_{c2}$ ). The behaviour is quite different from that in the pure limit, because all quasi-particles in the dirty limit near  $H_{c2}$  are gapless, although the excitation energies are modified in second order by an amount proportional with  $\langle |\Delta(\vec{r})|^2 \rangle$  (section 2.3.3). Caroli and Cyrot<sup>52</sup>) proved that this property is reflected in the thermal conductivity if the main contribution comes from the electrons scattered by impurities.

$$\frac{\lambda_e(H)}{\lambda_e^N} = 1 - C_d(T) (H_{c2} - H) \quad (2.43)$$

so no infinite slope at  $H_{c2}$ .

The slope of the  $\lambda(H)$  curve at  $H_{c2}$  can be related to the slope of the reversible magnetization curve, which yields:

$$\left( \frac{d\lambda_e}{dH} \right)_{H_{c2}} = \frac{ck_B}{2|e|} \rho \left\{ 1 + \rho \frac{\Psi^{(2)}(\frac{1}{2} + \rho)}{\Psi^{(1)}(\frac{1}{2} + \rho)} \right\} \quad (2.44)$$

in which  $\rho$  is a temperature dependent parameter given by

$$\ln(T/T_c) = \Psi(\frac{1}{2} + \rho) - \Psi(\frac{1}{2}) \quad (2.45)$$

The functions  $\Psi(z)$ ,  $\Psi^{(1)}$  and  $\Psi^{(2)}$  are the di-gamma function and its first and second derivatives;  $e$  is the electron charge in CGS units,  $c$  the light velocity.

Equation (2.43) is in good agreement with experiments carried out on concentrated alloys, but discrepancies are found for dilute alloys. It turned out that for those cases  $C_d(T)$  was always larger than the theoretical prediction. Very interesting is the result of an experiment on an evaporated

$\text{In}_{0.95}\text{Pb}_{0.05}$  film carried out by Parks, Zumsteg, and Mochel<sup>53</sup>). The phonon conductivity is strongly reduced in such films. The measurements confirmed eq. (2.43), not only near  $H_{c2}$ , but in the whole field region between  $H_{c1}$  and  $H_{c2}$ . This might indicate that for such films even in fields down to  $H_{c1}$  the superconductor is essentially gapless.

## §2.6 Metal Properties of Niobium

Niobium is a transition metal with one electron in the 5s-state and four electrons in the incomplete 4d-shell. In the solid state configuration the electron states will split up into energy bands because of the spatial overlap of the electron wave functions of neighbouring ions. The s-electrons form a broad s-band not very different from the conduction band in ordinary metals. The d-electrons are localized inside the ion cores, so that the overlap is small, giving rise to a relatively narrow d-band. It must be capable to hold 10 electrons. Therefore, the density of states of the d-band is much larger than that of the s-band, resulting into a large effective mass, and a low group velocity of the d-electrons with respect to the s-electrons. The Fermi surface will consist of s- and d-regions.

2.6.1 *Transport Properties of Normal Niobium.* The properties mentioned above explain the relatively large electrical resistivity of the transition metals. The s-electrons will contribute predominantly to the current, but they have a considerable chance to be scattered into, and trapped by, the d-band, as was first suggested by Mott<sup>54</sup>).

In fact scattering of electrons can be divided into s-s or d-d *intraband* scattering, and s-d *interband* scattering. Typical transition metal effects will arise from the latter, which in very pure materials is mainly caused by electron-phonon scattering. Wilson<sup>55</sup>) extended Mott's idea, introducing a model in which two sheets of the Fermi surface, one with s-, the other with d-band character, are assumed to be spherical and very close in k space. In addition, it was assumed that interband scattering completely removes the momentum, so that the effectiveness of the scattering process is equal to one, and  $\tau_{tr} = \tau_0$  (see sections 2.1.2 and 2.2.1). If all phonons were able to give rise to s-d-band transitions, the electrical resistivity due to this process would be proportional to  $T^3$ . If not (at low temperatures a considerable number of phonons will not have large enough wave vectors), the resistivity would fall off exponentially. We notice that this kind of scattering process will not have

any influence on the thermal conductivity, because we already know that for heat transport  $\tau_{tr} = \tau_0$ .

In Nb a  $T^3$  dependence of  $\rho$  actually was measured in extremely pure mono-crystals by Webb<sup>56</sup>). This can be explained by the specific shape of the Fermi surface of Nb calculated by Mattheiss<sup>57</sup>). There turned out to be three sheets which touch each other at several points and intersect along some lines. The electrons lying near the touching regions will be involved in the interband electron-phonon scattering.

2.6.2 *Superconducting Properties of Transition Metals.* In 1959 Suhl, Matthias, and Walker<sup>58</sup>) suggested the existence of a second energy gap in transition metal superconductors. Experiments in pure Nb on the specific heat (Shen, Senozan, and Phillips<sup>59</sup>), thermal conductivity (Carlson and Satterthwait<sup>60</sup>), and tunneling (Hafström and MacVicar<sup>61</sup>) seemed to justify the two gap idea. There should be a large gap, associated with the d-band equal to the BCS gap, and a small one, associated with the s-band electrons:  $\Delta_s(0) \sim 0.1\Delta_d(0)$ . But later experiments on thermal conductivity and specific heat<sup>62,63</sup>) could explain the anomalies measured before, but did not support the two gap theory in Nb. If there were electrons with a small gap, it should only be a very small fraction,  $< 10^{-3}$ . A careful analysis of ultrasonic attenuation data at temperatures well below  $T_c$  by Almond, Lea, and Dobbs<sup>64</sup>) showed unambiguously that this fraction must even be smaller than  $10^{-4}$ .

At temperatures near  $T_c$  ultrasonic attenuation experiments in very pure Nb<sup>65,66,67</sup>) showed a large discrepancy with the BCS theory. A good fit to the experimental data could be obtained by assuming two energy gaps, one equal to the BCS gap (at  $T \ll T_c$ ), the other (near  $T_c$ ) being three times as large, which looks rather strange. Very recently, Forgan and Gough<sup>68</sup>) elucidated why the effective gap measured near  $T_c$  is much larger than the BCS gap. This has nothing to do with a second energy gap, but is rather due to an additional temperature dependent electron-phonon scattering becoming important if  $k_B T > \Delta_{BCS}(T)$ , near  $T_c$ .

We therefore finish this chapter with the conclusion that no special transition metal properties have to be taken into account in the discussion of our measurements.

## References

1. See for example J.M. Ziman, *Principles of the Theory of Solids* (Cambridge University Press, Cambridge 1969).
2. D. Pines and D. Bohm, *Phys. Rev.* 85, 338 (1952).
3. H. Fröhlich, *Proc. Roy. Soc. (London)* A215, 291 (1952).
4. J.M. Ziman, *Electrons and Phonons* (Oxford University Press, Oxford, 1960).
5. H. Fröhlich, *Elektronentheorie der Metalle* (Springer, Berlin, 1936), §14 and 15.
6. S. Fujita, *Introduction to Non-Equilibrium Quantum Statistical Mechanics* (Saunders, Philadelphia, 1966).
7. P.G. Klemens, *Handbuch der Physik* (Springer, Berlin, 1956), tome XIV, p. 266.
8. P.G. Klemens, *Sol. St. Phys.* 7 (1958) and *Proc. Phys. Soc. (London)* A68, 1113 (1955).
9. J. Ferreira da Silva, Thesis, Leiden, 1967.
10. J. Bardeen, L.N. Cooper, and J.A. Schrieffer, *Phys. Rev.* 108, 1175 (1957).
11. L.N. Cooper, *Phys. Rev.* 104, 1189 (1956).
12. V.L. Ginzburg and L.D. Landau, *Zh. Eksperim. i Teor. Fiz.* 20, 1064. (1950). English Transl. *Collected Papers of L.D. Landau*, ed. D. ter Haar (Gordon and Breach, New York, 1967), p. 546.
13. L.D. Landau and E.M. Lifschitz, *Statistical Physics* (Clarendon Press, Oxford, 1970), p. 204.
14. F. London, *Superfluids I* (John Wiley, New York, 1950), part E.
15. C.J. Gorter and H.B.G. Casimir, *Physica* 1, 306 (1934), *Phys. Z.* 35, 963 (1934), *Z. techn. Phys.* 15, 539 (1934).
16. A.A. Abrikosov, *Zh. Eksperim. i Teor. Fiz.* 32, 1442 (1957); [*JETP* 5, 1174 (1957)].
17. W.H. Kleiner, L.M. Roth, and S.W. Autler, *Phys. Rev.* 133A, 1226 (1964).
18. J. Matricon, *Phys. Letters* 9, 289 (1964).
19. N.N. Bogolubov, V.V. Tolmachev, and D.V. Schirkov, *A New Method in the Theory of Superconductivity* (Consultant Bureau, New York, 1959).
20. C. Caroli, P.G. de Gennes, and J. Matricon, *Phys. Letters* 9, 307 (1964) and C. Caroli and J. Matricon, *Phys. Konds. Mat.* 3, 380 (1965).
21. W. Bergk and L. Tewordt, *Z. Physik* 230, 178 (1970).
22. L.P. Gorkov, *Zh. Eksperim. i Teor. Fiz.* 36, 1918 and 37, 1407 (1959); [*JETP* 9, 1364 (1959) and 10, 998 (1960)].
23. A.B. Pippard, *Proc. Roy. Soc. (London)* A216, 547 (1953).

24. P.G. de Gennes, *Superconductivity of Metals and Alloys* (Benjamin, New York, 1966), p. 225.
25. Pure limit : L.P. Gorgov, *Zh. Eksperim. i Teor. Fiz.* 37, 833 (1959); [*JETP* 10, 593 (1960)].  
 Dirty limit: K. Maki, *Physics* 1, 21 (1964).  
                   P.G. de Gennes, *Phys. Konds. Mat.* 3, 79 (1965).  
 Arbitrary imp. concentration: E. Helfland and N.R. Wertheimer, *Phys. Rev.* 147, 288 (1966).  
   G. Eilenberger, *Phys. Rev.* 153, 584 (1967).
26. Pure limit : K. Maki and T. Tsuzuki, *Phys. Rev.* 139A, 868 (1965).  
 Dirty limit: C. Caroli, M. Cyrot, and P.G. de Gennes, *Solid St. Comm.* 4, 17 (1966).  
 Arbitrary imp. concentration: G. Eilenberger, ref. 25.
27. P.G. de Gennes, ref. 25.
28. C. Caroli and K. Maki, *Phys. Rev.* 164, 591 (1967); K. Maki, *J. Low Temp. Phys.* 1, 45 (1969).
29. U. Brandt, W. Pesch, and L. Tewordt, *Z. Physik* 201, 209 (1967).
30. K. Maki, *Phys. Rev.* 156, 437 (1967), and 158, 397 (1967).
31. D. Pines, *Phys. Rev.* 109, 280 (1958).
32. G.M. Eliashberg, *Zh. Eksperim. i Teor. Fiz.* 38, 966 (1960); [*JETP* 11, 696 (1960)].
33. D.J. Scalapino in "Superconductivity", ed. R.D. Parks (Dekker, New York, 1969), chapter 10.
34. A review on this subject recently has been given by  
                   B.T. Geilikman and V.Z. Kresin, *Usp. Fiz. Nauk.* 99, 51 (1969); [*Sov. Phys. Usp.* 12, 620 (1970)].
35. B.T. Geilikman, *Zh. Eksperim. i Teor. Fiz.* 34, 1042 (1958); [*JETP* 7, 721 (1958)].
36. J. Bardeen, G. Rickayzen, and L. Tewordt, *Phys. Rev.* 113, 982 (1959).
37. V.V. Andreyev and V.V. Slezov, *Fiz. Metal. Metalloved.* 17, 477 (1964); [*Phys. Met. Metall.* 17, 150 (1964)].  
                   L.P. Kadanoff, and P.C. Martin, *Phys. Rev.* 124, 670 (1961).
38. P. Rhodes, *Proc. Roy. Soc. (London)* A204, 396 (1950).
39. B. Mühlischlegel, *Z. Physik* 155, 313 (1959).
40. V.Z. Kresin, *Zh. Eksperim. i Teor. Fiz.* 36, 1947 (1959); [*JETP* 9, 1385 (1959)].
41. B.T. Geilikman and V.Z. Kresin, *Zh. Eksperim. i Teor. Fiz.* 41, 1142 (1961); [*JETP* 14, 816 (1962)].

42. L. Tewordt, Phys. Rev. 128, 12 (1962), and 129, 657 (1963).
43. B.T. Geilikman and V.Z. Kresin, Zh. Eksperim. i Teor. Fiz. 36, 959 (1959); [JETP 9, 677 (1959)].
44. P.G. Klemens and L. Tewordt, Rev. Mod. Phys. 36, 118 (1964).
45. E. Canel, Proc. Bat Sheva Seminar, HaTfa (1968), p. 587.
46. W.F. Vinen, E.M. Forgan, C.E. Gough, and M.J. Hood, Physica 55, 94 (1971).
47. J. Lowell and J.B. Sousa, J. Low Temp. Phys. 3, 65 (1970).
48. Y. Muto, K. Noto, and T. Fukuroi, J. Phys. Soc. Japan 23, 130 (1967).
49. A. Houghton and K. Maki, Phys. Rev. B4, 843 (1971).
50. R.M. Cleary, Phys. Rev. 175, 587 (1968), and B1, 169 (1970).
51. K. Maki, Phys. Kond. Mat. 8, 305 (1969).
52. C. Caroli and M. Cyrot, Phys. Kond. Mat. 4, 285 (1965).
53. R.D. Parks, F.C. Zumsteg, and J.M. Mochel, Phys. Rev. Letters 18, 47 (1967).
54. N.F. Mott, Proc. Roy. Soc. (London) A153, 699 (1935).
55. A.H. Wilson, Proc. Roy. Soc. (London) A167, 580 (1938).
56. G.W. Webb, Phys. Rev. 181, 1127 (1969).
57. L.F. Mattheis, Phys. Rev. B1, 373 (1970).
58. H. Suhl, B.T. Matthias, and L.R. Walker, Phys. Rev. Letters 3, 552 (1959).
59. L.J.T. Shen, N.M. Senozan, and N.E. Phillips, Phys. Rev. Letters 14, 1025 (1965).
60. J.A. Carlson and C.B. Satterthwaite, Phys. Rev. Letters 24, 461 (1970).
61. J.W. Hafström and M.L.A. MacVicar, Phys. Rev. B2, 4511 (1970).
62. A.C. Anderson, C.B. Satterthwaite, and S.C. Smith, Phys. Rev. B3, 3762 (1971).
63. G.J. Sellers, A.C. Anderson, H.K. Birnbaum, Phys. Letters 44A, 173 (1973).
64. D.P. Almond, M.J. Lea, and E.R. Dobbs, Phys. Rev. Letters 29, 764 (1972).
65. F. Carsey, R. Kagiwada, M. Levy, and K. Maki, Phys. Rev. B4, 854 (1971).
66. F. Carsey and M. Levy, Phys. Rev. B7, 4123 (1973).
67. L.L. Lacy and A.C. Daniel, Phys. Rev. Letters 27, 1128 (1971).
68. E.M. Forgan and C.E. Gough, J. Phys. F3, 1596 (1973).

## CHAPTER 3

### DESCRIPTION OF THE EXPERIMENT

#### §3.1 Introduction. The Magnitude of the Temperature Difference

The thermal conductivity measurements have been carried out on rectangular samples of niobium with typical dimensions 20 x 3 x 0.2 mm in a temperature range from 1 to 10 kelvin in magnetic fields up to 6 kOe (= 477 kA/m in MKSA units). A temperature difference  $\Delta T$  over a distance  $L$  along the longest side of the samples causes a heat flow through the samples parallel to this side. In stationary state the thermal conductivity  $\lambda$  is determined by the relation:

$$\lambda(\bar{T}) = J_Q \frac{L}{\Delta T} = \frac{\dot{Q}}{A} \frac{L}{\Delta T} \quad (3.1)$$

in which  $\bar{T}$  is the mean temperature of the sample,  $J_Q$  the heat flow per unit area of cross section,  $A$  the area of cross section, and  $\dot{Q}$  the total amount of heat passing per second through the sample. This formula will be used throughout this thesis for the determination of  $\lambda$  from measured quantities, although the exact definition of  $\lambda$  is given by:

$$J_Q = \frac{1}{L} \int_{T(0)}^{T(L)} dT \lambda(T) \quad (3.2)$$

The difference between eqs. (3.1) and (3.2) causes a systematic error  $\delta\lambda$ , which can be determined by expanding  $\lambda$  in a Taylor series around  $\bar{T}$ . The impare order terms vanish, the second order term yields:

$$\frac{\delta\lambda}{\lambda} = \frac{1}{24} \frac{\bar{T}^2}{\lambda} \frac{\partial^2 \lambda}{\partial T^2} \left(\frac{\Delta T}{\bar{T}}\right)^2 \quad (3.3)$$

Higher order terms can be neglected. If the relation between  $\lambda$  and  $T$  is known, and if we put  $\Delta T = 50$  mK, which is the maximum value we used throughout the experiments, it is possible to calculate the theoretical error  $\delta\lambda/\lambda$ . If  $\lambda \propto T^\nu$  with  $\nu$  equal to one or zero, it is easy to see that the error is zero. All the other integer values of  $\nu$ , which occur in practice, lay between -2 and +3. For these values the maximum error - occurring at the lowest temperatures -

turns out to be  $6 \times 10^{-4}$ . If  $\lambda$  follows a BRT-like relation (2.35) the maximum error is  $1.5 \times 10^{-3}$ , also for the lowest temperatures. Therefore our choice of  $\Delta T \approx 50$  mK is justified so far.

It may seem that at temperatures near  $T_c$  (which is  $\sim 9$  K for Nb), the temperature difference can be chosen much larger than 50 mK in order to guarantee more accurate measurements. However, the variation of  $H_{c1}$ ,  $H_{c2}$ , and  $\Delta_{BCS}(T)$  along the samples can become appreciable for those temperatures. For example at  $T = 8$  K they are respectively 3, 2.5, and 1.3 percent for  $\Delta T = 50$  mK, increasing fast for temperatures still closer to  $T_c$ . As to this it would be desirable to diminish  $\Delta T$ , but this will result into less accurate measurements. As a compromise we decided to use  $\Delta T = 50$  mK at all measuring temperatures.

Detailed accuracy considerations will be given in the following sections. In section 2 we give a description of the apparatus, the auxiliary equipment, and the measuring procedure. Here we include a discussion of the error sources and the corrections to be made. In section 3 we describe the calibration procedure of the thermometers and the corrections necessary for measurements in a magnetic field.

### §3.2 *The Experimental Set-Up and Measuring Procedure*

3.2.1 *The Apparatus.* The apparatus shown in fig. 3.1 was designed in such a way that the samples could be easily exchanged. Four platinum wires of 0.2 mm diameter were welded to the samples. Via copper leads, soldered to the platinum wires, thermal contact was established between sample, heater  $H_1$ , thermometers  $G_1$ ,  $G_2$ , and C, and the thermal anchor TA. A thin nylon thread, 0.11 mm diameter, supported heater  $H_1$  and thermometer  $G_1$ . It prevented them from vibrating, causing a possible eddy-current heating during measurements in a magnetic field. The thread was attached to a brass bar mounted on the thermal anchor, on which also a second heater  $H_2$  was soldered. The anchor, made of pure copper, was soldered to a copper bar which, in turn, was mounted on a massive copper flange F forming the top of the vacuum can. Several holes were drilled into it, one for the pumping tube and four for the electrical wire feedthroughs FT. Copper radiation shields RS in the pumping tube prevented the interior of the vacuum can from warming up. All the soldering was carried out with hard solder and tin, so that the final joint of the can with F could be made with Wood's metal.

A superconducting coil magnet could be connected to a flange FL supported by the pumping tube. In this way the vacuum can could not vibrate with respect to the coil, which would give rise to extra heating of the metallic parts in

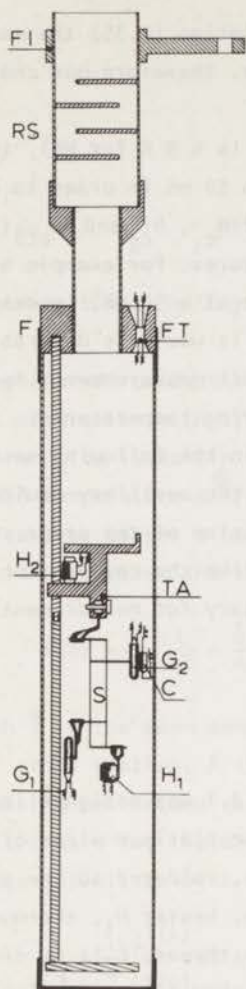


Fig. 3.1 Apparatus for measuring thermal conductivity. *S* = sample;  $G_1$ ,  $G_2$ , and *C* = germanium and carbon thermometers;  $H_1$ ,  $H_2$  = heaters; *TA* = thermal anchor; *F* = copper flange; *FT* = wire feedthroughs; *RS* = radiation shields; *FL* = supporting flange for superconducting coil magnet.

inhomogeneous field regions. The current leads of the coil were constructed from folded copper foil with a superconducting NbSn wire soldered to it. Each one ran through a glass tube functioning as a heat exchanger<sup>1</sup>). Vacuum can and superconducting coil were immersed in the same helium bath. For the measurements in a magnetic field perpendicular to the heat current we used an iron magnet after removing the superconducting coil magnet and replacing the helium and nitrogen dewars by finger dewars.

The vacuum was obtained by means of a mercury diffusion pump in series with a rotary pump. Before cooling the cryostat we first pumped the vacuum can during 24 hours at room temperature. The pressure could be measured with Penning and McLeod gauges. During the thermal conductivity measurements it was lower than  $3 \times 10^{-7}$  torr. It was possible to fill the vacuum can with He

exchange gas for calibration purposes.

3.2.2 *Magnetic Field.* A superconducting coil generated a magnetic field both parallel to the longest side of the samples and to the direction of the heat flow. We will call this field direction  $H_{//}$ . An iron magnet was used for the generation of a field perpendicular to the direction of the heat current. This field could be rotated with respect to the sample surface, we call it  $H_{\theta}$ , where  $\theta$  is the angle between field and sample surface. If  $\theta = 90^{\circ}$  we will talk about  $H_{\perp}$ , if  $\theta = 0^{\circ}$  about  $H_{\parallel}$  (see fig. 3.2).

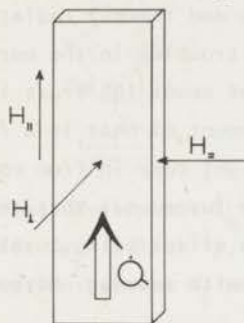


Fig. 3.2 *Definition of the magnetic field directions.*

The superconducting coil magnet, inner diameter 2.8 cm, length 13 cm, was wound from single core niobium-titanium wire covered with a copper layer and insulating material (Niomax S, 0.3 mm). It consisted of 19 layers of about 280 turns each and 5 layers of 44 turns each at both ends, the latter serving as correction coils to improve the homogeneity. Experimentally this turned out to be just as good as we had calculated: better than 0.1 per cent over a distance of 7 cm along the axis. The field to current ratio was measured in several ways at room temperature and at He temperatures. Within the measuring accuracy we did not find any temperature dependence. The  $H/I$ -value was  $582 \pm 3$  Oe/A. The current source was a Hewlett-Packard 6256B 10V/20A power supply.

The iron magnet showed an  $H$  versus  $I$  curve which was linear up to 7 kOe with a slope of  $199 \pm 1$  Oe/A. During cycling back to zero current we find a fieldshift of 25 Oe with respect to the increasing field curve. The remnant field was of the same order of magnitude. It could be shielded off by means of a cylinder consisting of two layers of  $\mu$ -metal (Allegheny Ludlum Moly Permalloy). After "shaking" with an ac field the remaining field at the sample site was weaker than 0.5 Oe. The magnet current was electronically stabilized and could be regulated continuously or in steps of 0.1 A.

3.2.3 *Spurious Heat Sources.* The thermal conductivity of niobium as a function of magnetic field far below  $T_c$  showed a fast decrease just above the first critical field  $H_{c1}$ . This effect, which will be extensively discussed in later chapters, results in a minimum value of the conductivity, which, at the lowest temperatures, is as low as a few  $\text{mW K}^{-1} \text{cm}^{-1}$ . The dimensions of the samples and the magnitude of the temperature difference required that under these conditions the heat production in heater  $H_1$  ( $= \dot{Q}_s$ ) should be smaller than 5 erg/s. This meant that we had to be aware of extra heating by spurious sources.

We already mentioned the effect of vibrations and thermal radiation. As for the latter, it proved to be the cause of many troubles in the early days of the experiments. We detected an extra heating of about 100 erg/s in spite of the presence of four radiation shields. This amount of heat is a fraction of  $10^{-3}$  of the black body radiation energy that might come in from room temperature down through the pumping tube. It finally turned out that the absorption of the radiation shields was rather poor, the effect being totally suppressed by painting black the tube and the shield with aquadag. Moreover, the carbon on the wall acted as a cryogenic pump.

R.f. radiation heating of metallic parts in the vacuum can was prevented by surrounding the can with copper foil. The shielding of the can itself (made of german silver) might not have been good enough: for 1 MHz the skin depth is 0.3 mm, whereas the wall thickness was 0.5 mm.

The electrical current in the thermometers was kept so low that the Joule heating always was less than  $10^{-3} \times \dot{Q}_s$ .

In order to get experimental evidence that no important extra heat sources were present we measured the temperature difference between  $G_1$  and  $G_2$  at  $\dot{Q}_s = 0$  before and after some He exchange gas was admitted into the vacuum can. We could not detect any change in  $\Delta T$ , which assured us that spurious heat production is certainly less than  $10^{-2}$  erg/s.

3.2.4 *Parallel Conduction.* A quite different source of systematic errors might be parallel conduction,  $\dot{Q}_p$ , through residual He gas, or along the measuring leads and supporting thread. Concerning the first possibility we can use the well-known formula<sup>2)</sup>:

$$\dot{Q}_p = \frac{1}{3} \times 2.8 \times \frac{P(\text{torr})}{10^{-7}} \times \frac{\Delta T(\text{mK})}{10^2} \times \frac{0(\text{cm}^2)}{1} \times 10^{-3} \text{ erg/s.}$$

Substituting  $P = 3 \times 10^{-7}$  torr,  $\Delta T = 50$  mK,  $0 = 2 \text{ cm}^2$  ( $\approx$  area of  $\frac{1}{2}S + H_1 + G_1$

of fig. 3.1) we arrive at  $\dot{Q}_p \approx 3 \times 10^{-3}$  erg/s, thus less than 0.1 per cent of the lowest value of  $\dot{Q}_s$ . The nylon thread gives no trouble either: for all temperatures  $\dot{Q}_p < 10^{-4} \times \dot{Q}_s$ .

To get an idea of the correction due to parallel conduction through the measuring leads we can use the following simplified picture, fig. 3.3. We call

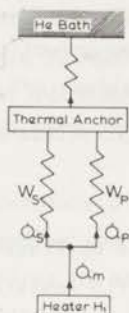


Fig. 3.3 Schematic picture of the heat flux through sample and measuring leads.

the total heat development  $\dot{Q}_m$ ;  $W_s$  and  $W_p$  are the heat resistances of the sample and the leads ( $W = (\lambda A/L)^{-1}$ ). The corresponding heat conductivities are  $\lambda_s$  and  $\lambda_p$ . The relation between  $\lambda_s$  and the measured conductivity  $\lambda_m$  is now given by:

$$\lambda_s = \lambda_m - \lambda_p \frac{A_p L_s}{A_s L_p} \equiv \lambda_m - \Delta\lambda \quad (3.5)$$

The leads were made of Nb-25%Zr strips (further referred to as NbZr), rolled from 0.28 mm Supercon wire. This shape provided a good thermal contact with the thermal anchor, on which they were glued by means of GE 7031 varnish. NbZr is a type-II superconductor with high  $T_c$  (10.8 K) and high upper critical field (at 4.2 K  $\approx 70$  kOe), so that there was no Joule heating in the leads. Further, the thermal conductivity is appreciably lower than that of pure niobium. From (3.5) one can see that the parallel conductivity  $\Delta\lambda$  also depends on the dimensional ratios of sample and leads. This yielded a factor of only 0.15, so it was necessary to measure the thermal conductivity of the NbZr strips.

We cut 32 parts of 1.5 cm length of NbZr strip and welded each 4 of them parallel to each other. The 8 samples obtained in this way were welded parallel to each other between two platinum wires at their ends. Then, two more platinum wires for the thermometer connections were welded in between at a mutual distance of 10 mm. This sample was mounted in the apparatus. Because now the same material was used for the sample and the measuring leads it was easy to estimate the correction for the parallel conduction:  $\Delta\lambda$  was about 4 per cent of  $\lambda_m$ . The final accuracy in  $\lambda_m$  was estimated to be about 5 per cent.

In fig. 3.4 the results of the measurements in zero magnetic field for

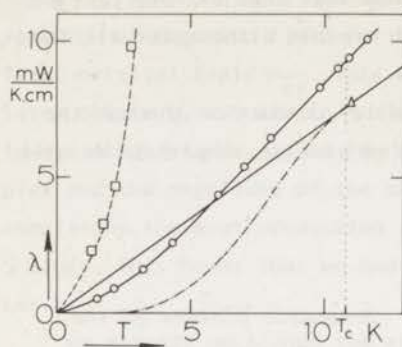


Fig. 3.4 Thermal conductivity of a rolled Nb-25%Zr sample versus temperature. ○, measured in zero field; △, obtained from Wiedemann-Franz law; heavily drawn line, electron thermal conductivity in the normal state; broken line, idem in superconducting state. Also shown are the typical minimum conductivities of the Nb samples: □.

different temperatures  $\lambda^s(T)$  are shown together with the estimated electron conductivity in the normal state  $\lambda_e^n$  - deduced from a specific resistance measurement and the Wiedemann-Franz law -, and the estimated electron conductivity in the superconducting state  $\lambda_e^s$ , using the BRT formula, eq. (2.35), together with the value 1.9 for the parameter  $\Delta(0)/k_B T_c$ . One reads from the figure that the phonons contribute appreciably to the thermal conductivity, so that we certainly have to correct our low temperature measurements for parallel conduction. To illustrate this we have also given in fig. 3.4 the low-temperature values of the typical minimum conductivities of our Nb samples. Moreover, table 3.1 shows the

T(K)	NbZr $\lambda^s$	Nb $\lambda_{\text{minimum}}$	$\Delta\lambda^{*})$	max.correction in per cent
1	0.3	1.6	0.05	3
2	0.8	4.1	0.12	3
3	1.3	13.3	0.22	2
4	2.3	30.6	0.35	1
5	3.2	60.7	0.49	0.8
6	4.3	102	0.66	0.7
7	5.4	149	0.83	0.6
8	6.4	202	0.98	0.5
9	7.5	297	1.15	0.4
9.5	8.0	315	1.23	0.4

\*) all  $\lambda$ 's in  $\text{mWK}^{-1}\text{cm}^{-1}$

Table 3.1 Thermal conductivity of Nb-25%Zr sample at several temperatures and the resulting parallel conduction.

measured NbZr conductivities, the typical minimum values of the Nb conductivities, the parallel conductivity, and the maximum correction we have to make for  $\lambda_m$ .

The correction can be as large as 3 percent, but it can easily be dealt with in the case of  $\lambda$  measurements versus magnetic field. It appeared that the field dependence of the NbZr sample was very small up to fields of 6 kOe, showing a slight decrease of at most 5 percent. This feature justifies a simple shift of the  $\lambda(H)$  curves of niobium over a distance  $\Delta\lambda$  as the only correction to be made.

In the following we will always work with corrected values of the thermal conductivity. The remaining error due to the uncertainty in the correction and due to spurious heat sources is estimated to be smaller than 0.2 percent.

3.2.5 *Temperature Stability.* Since the temperature difference between both ends of the samples was only 50 mK, much care was given to the control of the temperature. First of all the temperature of the He bath was kept constant within one millidegree. Above the  $\lambda$ -point a manostat gave satisfactory results. Below the  $\lambda$ -point, however, the pumping speed through this device was not sufficient; here we used an electronic stabilizer. The temperature was measured with an Allen-Bradley carbon resistor (0.1 W, 100  $\Omega$ ) in a dc Wheatstone bridge. The unbalance of the bridge, amplified by an Analog Device 180 B dc amplifier, regulated the current through a heater in the helium bath. The short term temperature constancy was much better than  $10^{-3}$  K, but due to dc drift a variation up to a few millidegrees might be generated in the long run.

A second temperature stabilizer directly regulated the temperature at the upper end of the sample. It followed the same principle, but had to be much more sensitive than the circuit we just described, because we had to use low bridge voltages ( $\sim$  mV) to avoid Joule heating of the thermometers. Therefore an ac method with phase sensitive detection was used, see fig. 3.5. The carbon

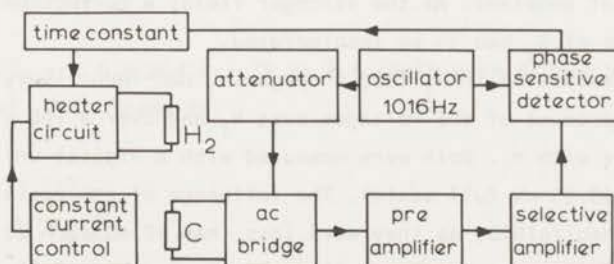


Fig. 3.5 Block diagram of the sample temperature stabilizer.

resistor C (again Allen-Bradley, 0.1 W, 100  $\Omega$ ) was mounted on the capsule of the germanium thermometer  $G_2$ , so that both had the same temperature. The current of the heater circuit ran through heater  $H_2$  (100  $\Omega$  constantan, non-inductively wound). The desired measuring temperature, which could vary from 0.1 to 6 K above the bath temperature, was established by adjusting the constant current control and stabilized by the output voltage of the phase sensitive detector.

The influence of the magnetic field on the stabilization could be ignored for the field values we used, since the magneto-resistance of Allen-Bradley resistors is very small. This has already been mentioned by Clement and Quinell in 1952<sup>3)</sup>, and has been confirmed by many authors<sup>4,5,6,7)</sup>. It shows a slight increase with decreasing temperatures, giving rise to a corresponding shift in temperature of at most 1 mK at 1.3 K in a field of 5 kOe. For this estimation we used the empirical formula of Belanger<sup>5)</sup>.

Apart from the magneto-resistance effect it turned out experimentally that the temperature stability of  $G_2$ , both in presence and in absence of heat flux through the sample, was always better than 1 mK. Therefore we may say that, roughly spoken,  $G_2$  was at constant temperature during the measurements.

**3.2.6 Measuring Procedure. Measured Quantities.** The measuring procedure was as follows. We started with a careful measurement of the resistances of  $G_1$  and  $G_2$  in zero field without heat production in  $H_1$ . This was repeated several times during the measurements. We assumed that both thermometers under these circumstances had the same temperature. Next the heater current was switched on and adjusted to a value that increased the temperature of  $G_1$  by 50 mK. The heat flow and  $G_1$  and  $G_2$  were measured. After that the magnetic field was cycled up. If this caused a change in conductivity we had to readjust the heater current in order to keep  $\Delta T$  constant. At the stronger fields a correction for the magneto-resistance of  $G_1$  had to be incorporated.

The power dissipation in  $H_1$  (100  $\Omega$  manganin, non-inductively wound) was derived from the product of the voltages over  $H_1$  and over a 100  $\Omega$  standard resistor in series with  $H_1$ . Both were measured with a digital voltmeter (Scheiner VT200, 99.99 mV full scale). The influence of the resistance of the feedthroughs was negligible, as they were less than 40 m $\Omega$  each at room temperature. Thermal emfs were certainly smaller than 5  $\mu$ V, which followed from current commutation. We may therefore conclude that the accuracy of  $\dot{Q}_s$  is better than 0.1 per cent.

The germanium resistors were manufactured by Cryocal Incorporation. The resistance at 4.2 K was about 1300  $\Omega$ . It was measured in a dc Wheatstone bridge

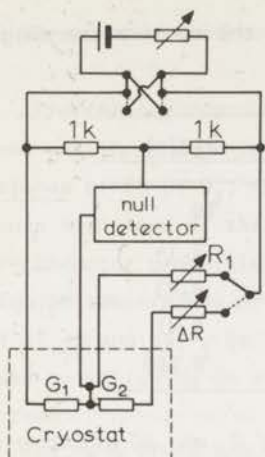


Fig. 3.6 Diagram of the Wheatstone bridge.

shown in fig. 3.6. Actually not  $G_1$  and  $G_2$  were measured, but  $G_1$  and  $\Delta G = G_1 - G_2$ . By connecting one end of the null-detector leads directly to  $G_1$  the influence of thermometer leads was greatly reduced. For the measurement of  $G_1$  and  $\Delta G$  two ESI 6 decade Decaboxes were used ( $R_1$  and  $\Delta R$ ) with an accuracy of 1 part in  $10^4$  and maximum value of 111 111.0  $\Omega$ . The zero setting of the Keithley 150B  $\mu V$  null-detector was established by varying  $R_1$  or  $\Delta R$  until commutation of the bridge current showed the smallest change. The amount of the change could easily be used to increase the sensitivity to 0.01  $\Omega$ , which is useful at temperatures above 4 K.

The reason for measuring  $G_1$  and  $\Delta G$  instead of  $G_1$  and  $G_2$  was the more direct relationship between  $\Delta G$  and the temperature difference  $\Delta T$ , which was the quantity we had to know in order to determine  $\lambda$ . Suppose that  $G_1$  and  $G_2$  obey the following simplified temperature dependence:

$$T_i = C_i (G_i)^{-\gamma_i} \quad (3.6)$$

with  $i = 1$  or  $2$ ,  $\gamma \approx 0.4$  and  $C \approx 70$  at 4 K (both were slowly varying functions of temperature). This leads to:

$$\frac{\partial \Delta T}{\partial \Delta G} = -\gamma_2 \frac{T_2}{G_2} \quad (3.7a)$$

$$\begin{aligned} \frac{\partial \Delta T}{\partial G_1} &= \gamma_2 \frac{T_2}{G_2} \times \frac{\Delta G + G_2(1 - \gamma_1 T_1 / \gamma_2 T_2)}{G_1} \\ &\leq \gamma_2 \frac{T_2}{G_2} \times \frac{1.5 \Delta G}{G_1} \end{aligned} \quad (3.7b)$$

The factor 1.5 in (3.7b) held for the resistors in the temperature range from 1 to 10 K.

T(K)	$G_1$ ( $\Omega$ )	$\Delta G/G_1$	$\delta G_1$ ( $\Omega$ )	$\delta \Delta G$ ( $\Omega$ )
1	32780	0.52	13	10
3	2831	0.21	0.45	0.14
5	946	0.13	0.17	0.03
7	438	0.07	0.12	0.01
9	244	0.03	0.12	0.006

Table 3.2 *The necessary measuring accuracy of  $G_1$  and  $\Delta G$  allowing an error of 0.1 mK in  $\Delta T$  for several temperatures.*

Since  $\Delta G/G_1 \ll 1$ , especially above 5 K (see table 3.2),  $\Delta T$  was much more sensitive to measuring errors in  $\Delta G$ , than to errors in  $G_1$ . This means that - in order to obtain the same partial error in  $\Delta T$  - only  $\Delta G$  has to be measured very accurately, whereas for  $G_1$  an accuracy, often a factor of 10 less, is already sufficient (table 3.2). If  $G_1$  and  $G_2$  were measured instead, both had to be measured as accurately as now only was necessary for  $\Delta G$ . A second advantage of the chosen procedure is that  $\Delta G$  was not so sensitive to bath temperature fluctuations, which made it easier to measure and increased the accuracy.

Even at the highest temperatures the scattering of the measuring points in the  $\lambda(H)$ -curves below  $H_{c1}$  and above  $H_{c2}$ , which should be straight horizontal lines, did not exceed 0.3 per cent. Therefore we considered this value as the maximum relative error of the measurements at any temperature.

Till now we ignored the error due to the uncertainty in the factor  $L/A$  of eq. (3.1), which is a systematic one, independent of temperature or magnetic field and therefore only important, if we want to compare the absolute data of different samples with each other. We estimated this error to be less than 1 per cent. Quite often, however, only relative data, like  $\lambda^5/\lambda^n$ , are compared, in which case the error in  $L/A$  is irrelevant. The other systematic errors we did not account for till now, are the uncertainty of the thermometer calibration and magneto-resistance correction, which certainly are temperature dependent. These will be discussed in the following section.

### §3.3 The Thermometer Calibration. The Influence of a Magnetic Field

3.3.1 *Preliminary Remarks.* The crucial quantity to be determined in our experiment was the change in temperature corresponding to the measured change in resistance of  $G_1$  or  $G_2$ , rather than the absolute temperature itself. Therefore it was the slope of the calibration curve (log R versus log T, because of the semi-conductor properties of the thermometers), which we wanted to know as a function of temperature or resistance.

Let  $\Delta T_{1,2}$  and  $\Delta G_{1,2}$  be the changes in temperature and resistance of  $G_1$  and  $G_2$ , caused by switching on a current through heater  $H_1$ . Their relationship follows from

$$\Delta T_i = S_i (T_i/G_i) \Delta G_i \quad (3.8a)$$

$$S_i = -d \log T_i / d \log G_i \quad (3.8b)$$

$i = 1$  or  $2$ . A miscalibration  $\delta S_i$  would cause an error in  $\Delta T_i$  of

$$\delta(\Delta T_i) = (\Delta T_i / S_i) \delta S_i \quad (3.9)$$

Since, owing to our experimental procedure,  $\Delta T_1 \geq 30\Delta T_2$ , it is clear that  $G_1$  would have to be calibrated with much higher precision than  $G_2$ .

A serious difficulty encountered with the calibration of germanium thermometers in the temperature region between liquid helium and hydrogen was, as can be seen from fig. 3.7, the irregularity in the slope of the calibration

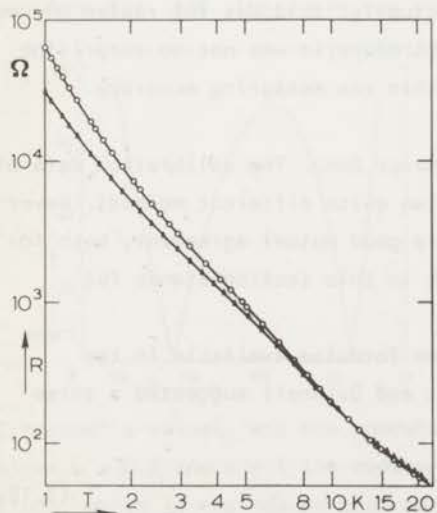


Fig. 3.7 Resistance of the germanium thermometers versus temperature.  $\circ$ ,  $G_1$ ;  $\triangle$ ,  $G_2$ .

curves in that region. Because such a phenomenon had never been observed with carbon resistors, we decided to use an Allen-Bradley resistor as a standard in this temperature range. Actually we did the calibration two times with two different A-B resistors of the same type (0.1 W, 100  $\Omega$ ). They will be referred to as AB<sub>I</sub> and AB<sub>II</sub>.

3.3.2 *The Calibration Procedure.* The three thermometers G<sub>1</sub>, G<sub>2</sub>, and AB<sub>I</sub> or AB<sub>II</sub> were sealed with GE 7031 varnish into three holes in a copper block which was, in turn, connected with copper foil to the thermal anchor. The wiring consisted of 0.1 mm manganin wires of equal lengths. They were thermally anchored in the copper foil. G<sub>1</sub> and the carbon resistor were measured in the dc Wheatstone bridge shown in fig. 3.6, G<sub>2</sub> in the ac bridge of the temperature stabilizer (fig. 3.5), which on this occasion did not function as such. Below 4.3 K and above 14 K the vacuum can was filled with He exchange gas. In the intermediate region the can was evacuated, and the temperature adjusted by means of a constant current through the heater H<sub>2</sub>. The cryostat was kept at liquid nitrogen temperatures between the calibration days to be sure of the reproducibility of the carbon resistor.

The temperatures below 4.3 K were deduced from the 1958 He<sup>4</sup> temperature scale<sup>8)</sup> and those in the liquid hydrogen region from the International Practical Temperature Scale of 1968<sup>9)</sup>. In order to deduce the slope S, we always took five calibration points in a small temperature range and adapted a straight line to the (log R, log T) data by means of a least squares procedure. It is well-known that the reproducibility of germanium thermometers is very good, much better than that of carbon thermometers; actually, this was the reason why we preferred to use germanium thermometers. Therefore it was not so surprising that also the slope reproduced at least within the measuring accuracy.

3.3.3 *Elaboration of the Carbon Thermometer Data.* The calibration data of the carbon resistors was elaborated using two quite different methods. Nevertheless the results turned out to be in very good mutual agreement, both for the log R(log T) curve and for the slope, which in this section stands for -d log R/d log T.

As for the first method we started from formulae available in the literature. In their original paper Clement and Quinnell suggested a three parameter formula<sup>3)</sup>:

$$\ln R + K/\ln R = A + B/T \quad (3.10a)$$

which can be written as

$$(\ln R)/T = a(\ln R)^2 + b \ln R + c \quad (3.10b)$$

The coefficients could be determined from a least squares fit to the calibration data. The authors claimed a precision of  $\pm 0.5$  per cent in  $T$  in the range from 2 K to 20 K.

A second empirical relation has been proposed by Zimmerman and Hoare<sup>10</sup>):

$$\left(\frac{\log R}{T}\right)^{\frac{1}{2}} = a(\log R)^2 + b \log R + c \quad (3.11)$$

where  $a$ ,  $b$ , and  $c$  are again adaptable parameters. The precision claimed by these authors was of the same order of magnitude, which is surprising because of the different powers in the left hand members of the formulae (3.10b) and (3.11). Therefore, we thought that a four parameter formula of the form:

$$\left(\frac{\log R}{T}\right)^{\alpha} = a(\log R)^2 + b \log R + c \quad (3.12)$$

might give a better agreement, if  $\alpha$  is properly chosen between 0.5 and 1.

We checked this idea on both  $AB_{\perp}$  and  $AB_{\parallel}$ , but we will only describe here in detail the results we obtained with  $AB_{\parallel}$ . For each chosen value of  $\alpha$  the parameters  $a$ ,  $b$ , and  $c$  of eq. (3.12) were adapted to the experimental data by means of a least squares fit procedure. It turned out that the root mean square of the  $\delta T$  ( $\delta T = T_{\text{meas}} - T_{\text{calc}}$ ) was a sharply varying function of  $\alpha$ , as can be seen from fig. 3.8. There are two pronounced minima, one somewhat above  $\alpha = 0.5$

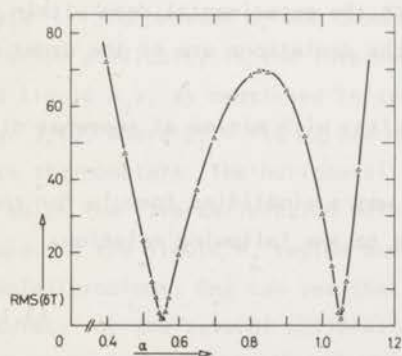


Fig. 3.8 *Root mean square of the temperature deviations versus the parameter  $\alpha$  of eq. (3.12).*

(Zimmerman's value), and one somewhere near  $\alpha = 1$  (Clement's value). For the values  $\alpha = 0.5$  and  $\alpha = 1$  the root mean squares are of the same order of magnitude, which is the reason that both authors found almost the same accuracy.

This can be more clearly illustrated in a graph of  $\delta T$  versus the measured temperature. In fig. 3.9 we show some of the  $\delta T$  values calculated in the helium

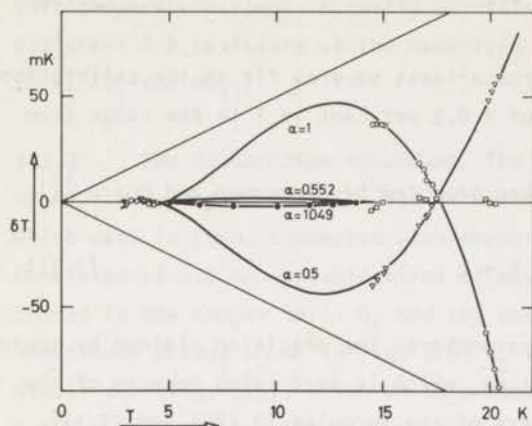


Fig. 3.9  
Deviation curves, ( $\delta T = T_{meas} - T_{calc}$ ).  
○, Clement's formula ( $\alpha = 1$ );  
▽, Zimmerman's formula ( $\alpha = 0.5$ );  
□, eq. (3.12) ( $\alpha = 0.552$  and  $\alpha = 1.049$ ); ●, semi-empirical formula, eq. (3.16).

and hydrogen regions for  $\alpha = 0.5$  and 1 and for  $\alpha = 0.552$  and 1.049, the values at which the minima occur. In the latter cases the points in the helium region have been omitted for clarity,  $\delta T$  here always being smaller than 0.5 mK; the points in the hydrogen region nearly coincide. In the intermediate region we only know the differences between calculated temperatures. The fact, that for  $\alpha = 0.552$  and 1.049 the deviations in the helium and hydrogen regions are negligible, and the fact that the mutual differences in the intermediate region never exceed 4 mK, give us some support for the assumption that the real temperature is equal to the average of the temperatures calculated from both  $\alpha$ 's within an accuracy of  $\pm 0.05$  per cent. The interpolations in fig. 3.9 are based on this assumption. Moreover, the room and liquid nitrogen temperatures derived from our formula are in agreement with the experimental data within two percent, whereas with eq. (3.10) or (3.11) the deviations are of the order of 20 per cent.

For  $AB_1$  we obtained almost the same results, with minima at somewhat different values of  $\alpha$ :  $\alpha = 0.593$  and  $\alpha = 0.915$ .

In the second method our starting point was a simplified formula for the conductivity of a semi-conductor<sup>11)</sup>, leading to the following relation:

$$R^{-1} = CT^{\gamma(T)} \exp(-E/k_B T) \quad (3.13)$$

in which  $C$  is a constant,  $E$  the main energy gap of the carriers (it appeared to be  $\sim 5 k_B T$ ), and  $\gamma(T)$  a slowly varying function of  $T$ , remaining between 0 and 3. The value of  $\gamma(T)$  depends on the scattering mechanism of the carriers.

It increases to a constant value at the lowest temperatures, where impurity scattering dominates. We could also write:

$$-\ln R = \ln C + \gamma(T) \times \ln T - E/k_B T \quad (3.14)$$

which yielded for the derivative:

$$-\frac{d \ln R}{d \ln T} = T \ln T \frac{d\gamma}{dT} + \gamma(T) + E/k_B T \quad (3.15)$$

A plot of experimentally derived  $-d \ln R/d \ln T$  values versus  $T^{-1}$  suggested that a good approximation for  $d(\gamma \ln T)/d \ln T$  between 2 and 20 K would be  $A \ln T + B$ ; A and B constants,  $\gamma(T)$  varying from 1.1 to 0.75 for  $T = 2$  K to 20 K respectively. This led to a simple four parameter formula, which I should like to call *semi-empirical* rather than eqs. (3.10), (3.11), and (3.12), viz.

$$\ln R = a(\ln T)^2 + b \ln T + c/T + d \quad (3.16)$$

with a, b, c, and d adaptable to the experimental data.

The calculated temperature in the intermediate temperature region coincided for  $AB_{11}$  exactly with those derived from eq. (3.12) with  $\alpha = 1.049$ . We concluded therefore, that the calibration of the temperature in the region between liquid helium and hydrogen by means of an Allen-Bradley carbon resistor was reliable with an accuracy of at least 0.05 per cent, and, what was even more important, the same was true for the logarithmic slope.

3.3.4 *Elaboration of the Germanium Thermometer Calibrations.* The interpolation difficulty in the intermediate temperature range (between liquid  $He^4$  and liquid  $H_2$ ), as mentioned in section 3.3.1, is very clearly illustrated in fig. 3.10, where  $S_i = -(d \log T/d \log G)_i$  was plotted against the resistance for both thermometers. The horizontal "error bars" represent the resistance regions in which the five calibration points had been taken in order to deduce the slope. In the liquid  $H_2$  region and in the  $He^4$  region above 2 K there were no special problems. One can see that the slope reproduced within the measuring accuracy for the several calibration runs we made over two years. The intermediate region could be handled with the help of the results discussed above.

Below 2 K the measuring accuracy becomes the worse the lower the temperature. Therefore we first made a double-logarithmic graph of resistance against temperature and deduced the slope graphically. In fig. 3.10 the points with

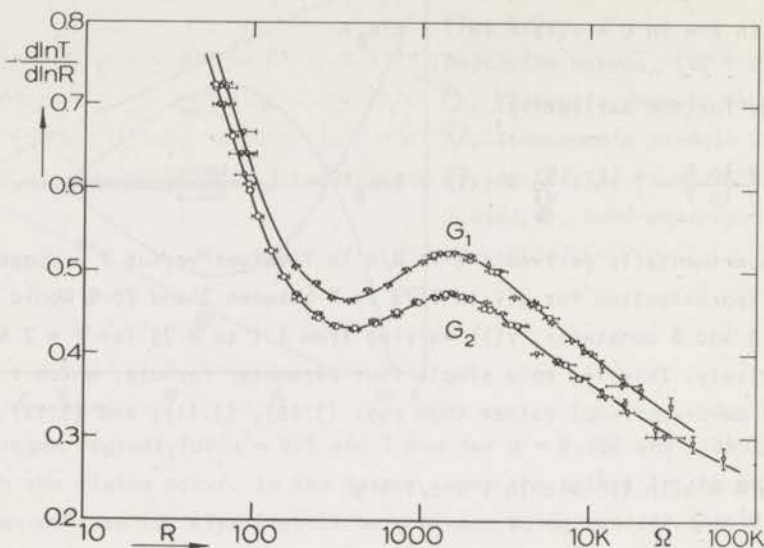


Fig. 3.10 Slopes of calibration curves (fig. 3.7) of the germanium thermometers versus resistance.

vertical error bars were derived by this method. A serious objection against this procedure is the uncertainty in the extrapolation from 1.2 K to 1 K. Therefore we started from the semi-empirical formula eq. (3.14). At these low temperatures  $\gamma(T)$  will be a constant, which means that in eq. (3.16) the parameter  $a$  is equal to zero. So a least squares fit of eq. (3.16) to the calibration data below 2 K was carried out with  $a = 0$ . The result was very promising: all the deviations between calculated and measured temperatures were smaller than 0.5 mK. The curves in fig. 3.10 below 2 K were derived in this way.

In the region above 2 K the drawn curves were obtained from least squares fits of orthogonal polynomials<sup>12)</sup> to the calibration data<sup>\*</sup>). In the liquid helium region good agreement was obtained by means of a fifth degree polynomial, at the higher temperatures a seventh degree polynomial was necessary.

After reading a sufficient number of points from fig. 3.10 we made a

<sup>\*</sup>) I would like to thank the thermometry group of the Kamerlingh Onnes Laboratory for putting their computer program at my disposal.

polynomial fit in order to obtain the coefficients of the series expansion:

$$-\left(\frac{d \ln T}{d \ln G}\right)_i = \sum_{j=0}^{13} c_{ji} \{\ln(G_i/100)\}^j \quad (3.17)$$

( $i = 1, 2$ ) which agreed with the curves of fig. 3.10 within 0.15 percent. Eq. (3.17) could be easily integrated, yielding the temperature belonging to a certain measured resistance. The constants of integration were determined by measuring  $G_1$  and  $G_2$  in the absence of heat flux through the sample.

3.3.5 *Magneto-Resistance.* For the experiments carried out in a magnetic field the resistance of the germanium thermometers had to be corrected for a positive magneto-resistance, which turned out to be dependent on the orientation of the field. For the field strengths we had to deal with (lower than 6 kOe) the increase in resistance depended quadratically on the field, which was also found by several other authors<sup>13,14</sup>). In addition, a strong temperature dependence was measured.

The results for  $G_1$  are shown in fig. 3.11 in a double-logarithmic plot

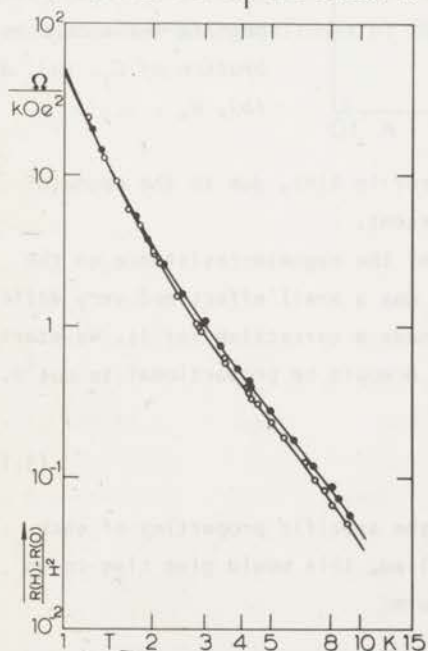


Fig. 3.11 Magneto-resistance of  $G_1$  versus temperature. Open dots,  $H_{//}$ ; black dots,  $H_{\perp}$

against the temperature. As is clear from the figure, the magneto-resistances in  $H_{//}$  and  $H_{\perp}$  were not equal, which could be expected because the thermometers were cut from mono-crystals. Theory, even if based on a simplified semi-conductor model, did not provide a simple relation between magneto-resistance and

temperature or resistance. Therefore we tried to adapt several ad-hoc formulae to the experimental data, unfortunately not successfully. Finally we chose a polynomial adaptation of the form:

$$\ln \left( \frac{G_i(H) - G_i(0)}{H^2} \right) = \sum_{j=0}^7 b_{ji} (\ln T)^j \quad (3.18)$$

( $i = 1, 2$ ) which yielded an agreement with the curves better than 0.5 per cent.

The maximum accuracy we needed to keep the inaccuracy in  $\Delta T$  below a certain limit could be calculated from the maximum field required at a given temperature and the relation between  $\{T(H) - T(0)\}/H^2$  and  $T(0)$ ;  $T(H)$  is the temperature corresponding to  $R(H)$ , without correction. It is shown, for a precision better than one per cent by the shaded area in fig. 3.12. From the scattering of the

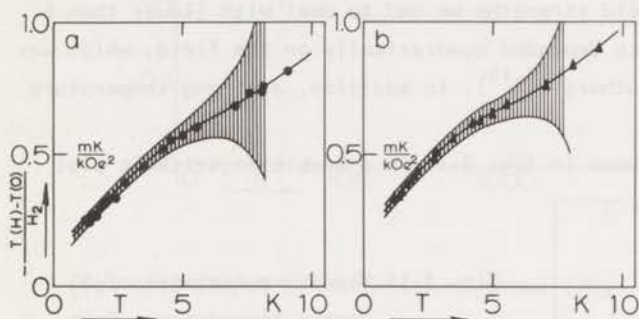


Fig. 3.12  
Area of one per cent accuracy in  $\Delta T$  due to possible errors in the magneto-resistance calibration of  $G_1$ . (a),  $H_{//}$ ; (b),  $H_{\perp}$ .

experimental data we concluded that the error in  $\lambda(H)$ , due to the magneto-resistance, always was smaller than 0.5 per cent.

One problem remained: the dependence of the magneto-resistance on the orientation angle  $\theta$  of the iron magnet. It was a small effect and very difficult to measure, but still there could be made a correction for it. We started from the assumption that the dependence on  $\theta$  would be proportional to  $\cos^2\theta$ , leading to

$$\delta MR_i(\theta) = \mu_i \cos^2(\theta - \phi_i) \quad (3.19)$$

where  $\mu$  and  $\phi$  are constants, depending on the specific properties of each thermometer. If no correction would be applied, this would give rise to an error in the thermal conductivity of the form:

$$\delta \lambda(\theta, H) \propto H^2 \{ \sin 2(\theta - \theta_0) - \sin 2(\theta_{MR} - \theta_0) \} \quad (3.20)$$

where  $\theta_{MR}$  is the orientation angle of the magnet at which the original determination of the magneto-resistance was carried out;  $\theta_0$  is defined in fig. 3.13.

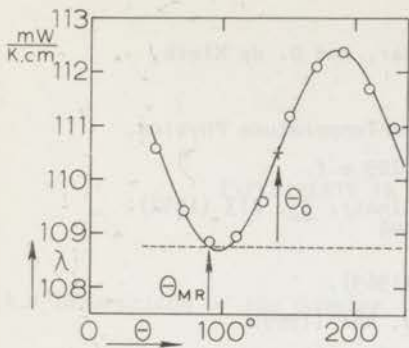


Fig. 3.13 Thermal conductivity variation well above  $H_{c2}$  versus orientation angle of iron magnet due to orientation dependency of magneto-resistance. Broken line, true value; O, experiment; drawn line, best fit of eq. (3.20) to experimental data.

Fig. 3.13 shows an experiment carried out well above  $H_{c2}$ , where the orientation of the magnet could not influence the thermal conductivity. The broken horizontal line corresponds to  $\theta = \theta_{MR}$ , so this was the true conductivity of the sample. The drawn line follows from eq. (3.20), in very good agreement with the experimental data. The proportionality constant in eq. (3.20) could be obtained from the figure, and enabled us to determine the true thermal conductivity for all orientations and all magnitudes of the magnetic field.

## References

1. J.W. Metselaar, H.A. Jordaan, J.W. Schutter, and D. de Klerk, *Cryogenics* 10, 220 (1970).
2. J.K. White, *Experimental Techniques in Low-Temperature Physics*, (Clarendon Press, Oxford, 1968), p. 209 e.f.
3. J.R. Clement and E.H. Quinell, *Rev. Sc. Instr.* 23, 213 (1952).
4. T. Amundson, *Cryogenics* 7, 368 (1967).
5. B.C. Belanger, *Rev. Sc. Instr.* 40, 1082 (1969).
6. D.L. Decker and H.L. Laguer, *Cryogenics* 9, 481 (1969).
7. L.J. Neuringer and Y. Shapira, *Rev. Sc. Instr.* 40, 1314 (1969).
8. F.G. Brickwedde, H. Van Dijk, M. Durieux, J.R. Clement, and J.K. Logan, *J. Res. N.B.S.* 64A, 1, (1960).
9. International Practical Temperature Scale of 1968, *Metrologica* 5, 35 (1969).
10. J.E. Zimmerman and F.E. Hoare, *Phys. Chem. Solids* 17, 52 (1960).
11. J.M. Ziman, *Principles of the Theory of Solids*, (Cambridge University Press, Cambridge, 1969), p. 122, 188, 194.
12. G.E. Forsythe, *J. Soc. Ind. Appl. Math.* 5, 74 (1957).
13. J.S. Blakemore, J.W. Schultz, and J.G. Myers, *Rev. Sc. Instr.* 33, 545, (1962).
14. L.J. Neuringer, A.J. Perlman, L.G. Rubin, and Y. Shapira, *Rev. Sc. Instr.* 42, 9 (1971).
15. See reference 11, page 216.

## CHAPTER 4

### EXPERIMENTS IN THE PURELY SUPERCONDUCTING AND NORMAL STATE

#### §4.1 Description of the Samples

The metallurgical character of the niobium samples on which we carried out our thermal conductivity measurements was, or will be, discussed in some papers by Van der Klein et al. <sup>1,2,3</sup>). We will shortly review the most important features.

Two of the samples were prepared from a rod of high-purity niobium obtained from Semi Elements Inc. The material was cold rolled into foil of 0.15 mm thickness. The three other samples were cut from a niobium foil (thickness 0.20 mm) of triple zone refined material (Marz grade) obtained from Materials Research Corp. They were annealed during one hour in a vacuum better than  $10^{-7}$  torr, one at 1400 °C, the others at 1600 °C, referred to respectively as P<sub>1400</sub>, P<sub>1600</sub> (the SEI samples), and N-0 (the MRC samples). From one of the samples N-0 the surface layer was chemically removed, after which it was heat treated for one minute in an oxygen atmosphere at 400 °C. This surface oxidation greatly removes the effect of pinning of flux vortices at the sample surface (see section 6.1). It will be further denoted by N0-0. The third sample N-0 was irradiated at about 60 °C with a dose of  $3.6 \times 10^{19}$  fast neutrons per  $\text{cm}^2$ ; it will be referred to as N-319.

The chemical purity of the samples did not differ very much, tantalum being the largest amount of impurity (about 200 ppm). The defect structures of P<sub>1600</sub>, N-0, and N0-0 were almost the same. The grain size was determined from light microscopy, the dislocation density from electron microscopy (see table 4.1). For P<sub>1400</sub> the grain size was about 4 times smaller, the dislocation density about 10 times larger than for the other samples.

The influence of neutron irradiation was discussed by Elen et al. <sup>4</sup>). Interstitials are created which cluster together in order to minimize the deformation energy. They form dislocation loops which can clearly be seen on electron microscope pictures <sup>2,3</sup>). Their average size in N-319 is about 100 Å, their spacing about 350 Å. Another result of the irradiation is the trapping of

Table 4.1

Sample	Grain size ( $\mu\text{m}$ )	Dislocation density	$\frac{\rho_{300}}{\rho_{4.2}}$	$T_c$ (K)
P <sub>1400</sub>	90	$6 \times 10^8 \text{ cm}^{-2}$	15.6	9.14
P <sub>1600</sub>	350	$< 5 \times 10^7 \text{ cm}^{-2}$	24.3	9.12
N-0, NO-0	400	$< 4 \times 10^7 \text{ cm}^{-2}$	21.1	9.12
N-319	400	*) $1 \times 10^{16} \text{ cm}^{-3}$	16.2	9.17

\*) Cluster density.

interstitials by the original dislocations and grain boundaries. Moreover, the background thermal neutron flux of  $1.4 \times 10^{20}$  neutrons/cm<sup>2</sup> is responsible for the creation of a large amount of point defects with deviating nuclear masses.

The specific resistances at room and liquid helium temperatures were measured. This yielded the resistance ratios shown in table 4.1. From the resistance measurements we could determine  $T_c$  with an accuracy of at least 5 mK, which means that the variations of  $T_c$  are not due to the measuring inaccuracy.

#### §4.2 Thermal Conductivity in the Normal State

The thermal conductivity as a function of temperature in zero magnetic field and fields well above  $H_{c2}$  of the samples P<sub>1400</sub>, P<sub>1600</sub>, N-0 and NO-0, and N-319 are shown in the figs. 4.1a, b, c, and d. The data of NO-0 coincide with that measured for N-0, as one should expect because the bulk properties remained unchanged after the surface oxidation.

The lower temperature measurements on N-319 had to be corrected for a secondary heating process due to  $\beta$ -radioactivity of the sample, caused by the neutron irradiation. The predominant contribution came from Ta<sup>182</sup>, but also the effects of Nb<sup>94</sup> and Nb<sup>95</sup> were non-negligible. It follows from  $\gamma$ -ray spectroscopy \*) that the radioactivity of the three isotopes was 38, 2.7, and 1.4  $\mu\text{C}$  respectively. This gives rise to a calculated  $\beta$ -heating of 0.7 erg/s, which can account for 90 per cent of the secondary heating we could detect in the thermal conductivity device by measuring the temperature difference with zero

\*) We want to thank Dr. L. Niessen for carrying out this experiment.

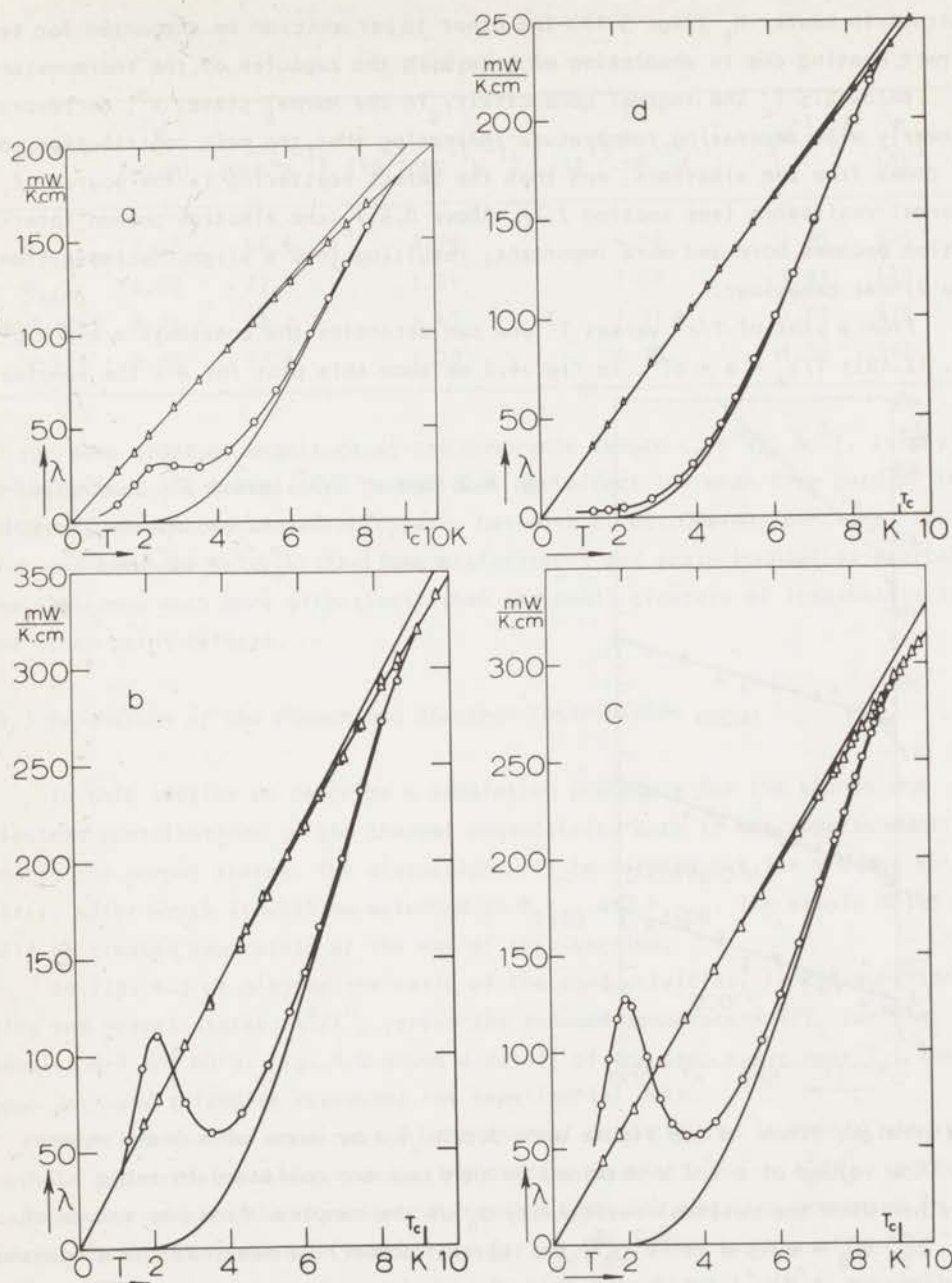


Fig. 4.1 Thermal conductivity of  $P_{1400}$  (a),  $P_{1600}$  (b),  $N-0$  and  $NO-0$  (c), and  $N-139$  (d) in the normal state,  $\Delta$ , and superconducting state at zero field,  $\circ$ . Also shown is the electronic thermal conductivity in the superconducting state.

current in heater  $H_1$  (fig. 3.1). The other 10 per cent can be accounted for by direct heating due to absorption of  $\gamma$ -rays in the capsules of the thermometers.

Below  $0.5 T_c$  the thermal conductivity in the normal state,  $\lambda^n$ , decreases linearly with decreasing temperature indicating that the main contribution to  $\lambda^n$  comes from the electrons, and that the defect scattering is the source of thermal resistance (see section 2.2). Above  $0.5 T_c$  the electron-phonon interaction becomes more and more important, resulting into a slight decrease from the linear behaviour.

From a plot of  $T/\lambda^n$  versus  $T^3$  one can determine the constants  $a$  and  $b$  of eq. (2.18):  $T/\lambda_e^n = a + bT^3$ . In fig. 4.2 we show this plot for all the samples.

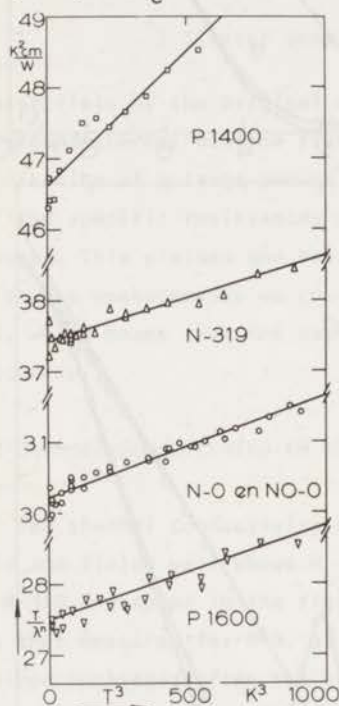


Fig. 4.2 Plot of  $T/\lambda^n$  versus  $T^3$ . A straight-line fit determines the coefficients  $a$  and  $b$  in  $(\lambda_e^n)^{-1} = aT^{-1} + bT^2$ .

The straight lines in the figure were determined by means of a least squares fit. The values of  $a$  and  $b$  obtained in this way are collected in table 4.2, together with the residual resistivity  $\rho_0$  of the samples. From the values of  $\rho_0 a^{-1} L_0^{-1}$  ( $L_0 = 2.45 \times 10^{-8} \text{V}^2/\text{K}^2$ , the Lorenz number) we see that the Wiedemann-Franz law is fairly well obeyed.

One can determine the mean free path of the electrons,  $\ell_e$ , (at least below  $0.5 T_c$ , but above this temperature it will not be very much different) from eq. (2.6):  $\rho_0^{-1} = \frac{1}{3} e^2 v_F \ell_e N(0)$ . We substituted  $v_F = 3 \times 10^7 \text{cm/s}$  and  $N(0) = 5.6 \times 10^{34} \text{states cm}^{-3} \text{erg}^{-1}$ . For all the samples  $\ell_e$  turns out to be

Table 4.2

Sample	$\rho_0$ ( $\mu\Omega\text{cm}$ )	a ( $\text{cmK}^2\text{W}^{-1}$ )	b ( $10^{-3}\text{cmK}^{-1}\text{W}^{-1}$ )	b' ( $10^{-3}\text{cmK}^{-1}\text{W}^{-1}$ )	$\rho_0 a^{-1} L_0^{-1}$	$\lambda_e$ ( $\text{\AA}$ )
P <sub>1400</sub>	1.08	46.6	3.78	4.10	0.95	305
P <sub>1600</sub>	0.68	27.5	1.34	1.50	1.01	520
N-0, NO-0	0.74	30.2	1.43	1.71	1.00	470
N-319	0.95	37.4	1.20	1.39	1.04	380

of the same order of magnitude as the coherence length  $\xi_0 = 430 \text{ \AA}$ <sup>5</sup>). It may be noted that the irradiation damage does not affect the mean free path of the electrons very much, annealing clearly has more effect. We may conclude, then, that the extended defects like line dislocations and grain boundaries scatter the electrons much more effectively than the small clusters of interstitials and other point defects.

#### §4.3 Separation of the Phonon and Electron Contribution

In this section we describe a separation procedure for the phonon and electron contributions to the thermal conductivity both in the superconducting and in the normal states. The discussion will be carried out for N-0 and NO-0 first, after which it will be extended to P<sub>1400</sub> and P<sub>1600</sub>. The sample N-319 will be treated separately at the end of this section.

In fig. 4.3 we plotted the ratio of the conductivities, in the superconducting and normal states,  $\lambda^S/\lambda^N$ , versus the reduced temperature  $T/T_c$  for the samples N-0 and NO-0. Fig. 4.4 shows a detail of the same curve near  $T_c$ , the open dots and triangles represent the experimental data.

We first assumed that near  $T_c$  the thermal conductivity is mainly electronic, both in the normal and superconducting states, so that  $\lambda^S/\lambda^N = \lambda_e^S/\lambda_e^N$ . In that case we can compare the experimental results with the theories presented in section 2.4. BRT derived an expression for  $\lambda_{ed}^S/\lambda_{ed}^N$ , that is, the effect of elastic scattering by lattice defects. Tewordt calculated  $\lambda_{ep}^S/\lambda_{ep}^N$ , the influence of electron-phonon scattering.

We can easily demonstrate that the latter contribution is small as compared with the first one, even close to  $T_c$ . Starting from

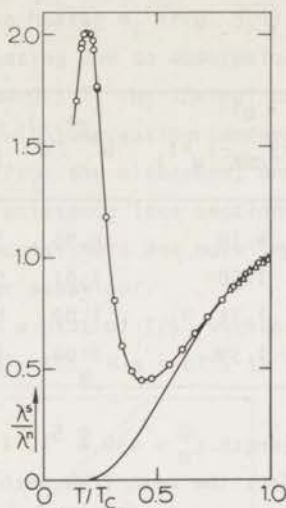


Fig. 4.3 Ratio of the superconducting and normal state thermal conductivity versus reduced temperature,  $\circ, \Delta$ : experimental data of N-0 and NO-0 respectively; lower curve, electronic part owing to eq. (4.1) with  $\Delta(0)/k_{B^T_c} = 1.90$ .

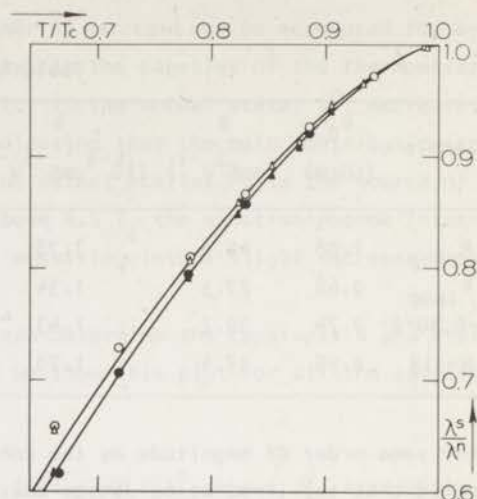


Fig. 4.4 Detail of fig. 4.3. Upper curve, eq. (4.1) with  $\Delta(0)/k_{B^T_c} = 1.90$ ; lower curve, eq. (4.1) with  $\Delta(0)/k_{B^T_c} = 1.95$ .  $\bullet, \blacktriangle$ :  $(\lambda^s - \lambda_p^s)/(\lambda^n - \lambda_p^n)$ .

$$\lambda_e^s = \{(\lambda_{ed}^s)^{-1} + (\lambda_{ep}^s)^{-1}\}^{-1}$$

$$= \{(f_{BRT} \lambda_{ed}^n)^{-1} + (f_{Tew} \lambda_{ep}^n)^{-1}\}^{-1}$$

with

$$f_{BRT} = \lambda_{ed}^s / \lambda_{ed}^n \text{ and } \lambda_{ed}^n = T/a$$

$$f_{Tew} = \lambda_{ep}^s / \lambda_{ep}^n \text{ and } \lambda_{ep}^n = (bT^2)^{-1}$$

we arrive at

$$\frac{\lambda_e^s}{\lambda_e^n} = \frac{f_{BRT}}{1 + \lambda_e^n b T^2 (f_{BRT} / f_{Tew} - 1)} \quad (4.1)$$

The correction to the BRT theory for our samples is at most 0.6 per cent at

$T/T_c = 0.85$ , below  $T = 0.6 T_c$  it becomes negligible. Therefore we can, as a first step, neglect the electron-phonon interaction and estimate the value of the parameter  $\Delta(0)/k_B T_c$  from a direct comparison of the experiment with the BRT theory. This yields for N-0 and N0-0 the value 1.90, from which the upper curve in fig. 4.4 and the lower one in fig. 4.3 were calculated by means of eq. (4.1). There is a good agreement for  $T/T_c > 0.78$ . At the lower temperatures, however, the experimental data is much higher than the theoretical values of  $\lambda_e^s/\lambda_e^n$ . This must be due to the increasing phonon conductivity in the superconducting state,  $\lambda_p^s$ , with decreasing temperatures, as was discussed in section 2.4.2.

Still assuming that  $\lambda_e^n = \lambda^n$  we can calculate  $\lambda_e^s$  and then obtain  $\lambda_p^s = \lambda^s - \lambda_e^s$  from the experimental data. The open circles in fig. 4.5 represent

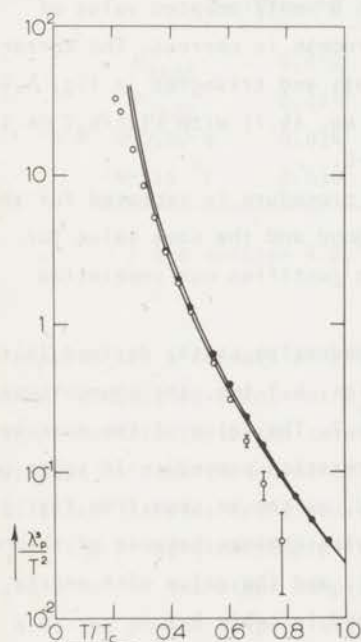


Fig. 4.5 Plot of  $\lambda_p^s/T^2$  versus  $T/T_c$ .  
 O, uncorrected experimental data; ●, corrected data.  
 Lower curve, eq. (2.36) with  $\Delta(0)/k_B T_c = 1.90$ ; upper curve, eq. (2.36) with  $\Delta(0)/k_B T_c = 1.95$ . The value at  $T = T_c$  yields the constant A in  $\lambda_p^n = AT^2$ .

$\lambda_p^s/T^2$ , obtained in this way, versus  $T/T_c$  on a semi-logarithmic scale (for N-0 only). It is clear that the accuracy at the higher temperatures must become rather poor, since here  $\lambda_p^s$  is the small difference of two large terms. This is illustrated by the vertical error bars, assuming an error of 0.5 per cent in  $\lambda^s$  and  $\lambda_e^s$ .

Under the plausible assumption that for this rather pure sample the scattering mechanism for the phonons is predominantly phonon-electron interaction we may compare  $\lambda_p^s/T^2$  with eq. (2.36), in which the function  $g(x)$  has to

be calculated for the value  $\Delta(0)/k_B T_c = 1.90$ . The result is represented by the lower curve of fig. 4.5. In spite of the large inaccuracy in the experimental points a clear discrepancy is observed at the higher temperatures. This must be due to the neglect of the phonon conductivity in the normal state, which must obey  $\lambda_p^n = AT^2$  (see section 2.2.2). From the value of the theoretical curve at  $T/T_c = 1$  we obtain  $A = 0.024 \text{ mWK}^{-3} \text{ cm}^{-1}$ . This leads to a correction in  $\lambda_e^n$  at the highest temperatures of about 1 per cent and to a small modification of the values a and b of table 4.2. The difference in "a" proves to be negligible, but the change in b can amount to up to 20 per cent. The new values (for all our samples) have been collected in table 4.2 as b'.

At the higher temperatures we now can recalculate  $\lambda_p^s$  from eq. (2.36) and determine  $\lambda_e^s = \lambda^s - \lambda_p^s$  as well. If now the values obtained in this way for  $\lambda_e^s/\lambda_e^n$  coincide with the curve of eq. (4.1) with a newly adapted value of  $\Delta(0)/k_B T_c$  we may conclude that our iteration process is correct. The corrected values of  $\lambda_e^s/\lambda_e^n$  are represented by the black dots and triangles in fig. 4.4 and the curve through these points is given by eq. (4.1) with  $\Delta(0)/k_B T_c = 1.95$ . The agreement is very good both for N=0 and N0=0.

It turns out, moreover, that if the whole procedure is repeated for the samples P<sub>1400</sub> and P<sub>1600</sub> the result is equally good and the same value for  $\Delta(0)/k_B T_c$  is found. We believe that this result justifies our separation procedure.

The electronic contribution in the superconducting state, derived in this way, is shown for each of the samples in the figs. 4.1 too, the phonon contribution has been plotted versus T in the figs. 4.7. The value of the constant A in  $\lambda_p^n = AT^2$  does not change very much by the iteration procedure in spite of the fact that the  $\lambda_p^s$  values have been increased, as can be seen from fig. 4.5 (black dots). The theoretical curve, however, also changes because of the new value  $\Delta(0)/k_B T_c$  (the upper curve in the figure), and the value of A nearly remains constant. The final results are collected in table 4.3.

A check on the reliability of the value of A can be obtained by considering the product of A and b'. On the one hand the ratio of  $\lambda_{pe}^n$  and  $\lambda_{ep}^n$  can be written as <sup>10)</sup>:

$$\frac{\lambda_{pe}^n}{\lambda_{ep}^n} = \frac{313}{n_a^{4/3}} \left(\frac{T}{\theta_D}\right)^4 \quad (4.2)$$

where  $n_a$  is the effective number of conduction electrons per atom. On the other hand we have

$$\frac{\lambda_{pe}^n}{\lambda_{ep}^n} = Ab'T^4 \quad (4.3)$$

so that the product of A and b' should be a constant for all the niobium samples. Table 4.3 shows that this requirement is reasonably well fulfilled in spite of the fact that the A value of P<sub>1400</sub> is a factor of two smaller than for P<sub>1600</sub>, N-0, and N0-0.

Table 4.3

Sample	A (mWK <sup>-3</sup> cm <sup>-1</sup> )	Ab' (10 <sup>-8</sup> K <sup>-4</sup> )	n <sub>a</sub>	E (10 <sup>9</sup> K <sup>-1</sup> s <sup>-1</sup> )
P <sub>1400</sub>	0.012	4.7	1.1	3.2
P <sub>1600</sub>	0.025 <sup>5</sup>	3.8	1.3	1.5
N-0, N0-0	0.024	4.1	1.2	1.6
N-319 <sup>*</sup> )	0.030	4.2		1.3

<sup>\*</sup>) See section 4.6.

Niobium has 5 conduction electrons per atom. Nevertheless the effective number of conduction electrons n<sub>a</sub> may well be smaller, because only the s-electrons contribute to the conductivity. In fact we can now calculate n<sub>a</sub> from the product Ab' and the value of Θ<sub>D</sub>, which is 275 K for niobium. The values for the different samples are given in table 4.3.

For the irradiated sample it is not possible to follow the same separation procedure as for the other samples. As is clearly seen from fig. 4.1d and from fig. 4.6, the phonon conductivity in the superconducting state does not show a very large increase with falling temperature. This suggests that due to the irradiation damage other scattering mechanisms than the phonon-electron interaction must play an important part. Therefore we can not use eq. (2.36) in order to determine λ<sub>p</sub><sup>n</sup>. For this reason we assumed that for N-319 the parameter Δ(0)/k<sub>B</sub>T<sub>c</sub> has the same value as for the other samples, 1.95. In this way we calculated the λ<sub>e</sub><sup>s</sup>/λ<sub>e</sub><sup>n</sup> curve in fig. 4.6, the λ<sub>e</sub><sup>s</sup> curve in fig. 4.1d and the λ<sub>p</sub><sup>s</sup> points in fig. 4.7d. The experimental points in fig. 4.6 even at temperatures near T<sub>c</sub> lie slightly higher than the theoretical curve, indicating that no

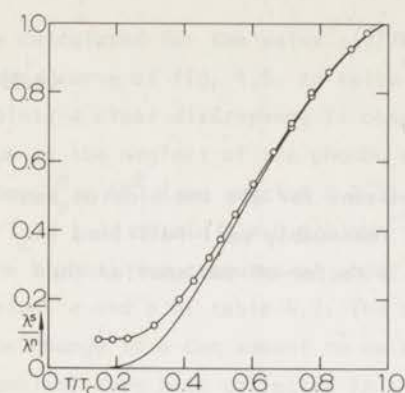


Fig. 4.6 Plot of  $\lambda^s/\lambda^n$  versus  $T/T_c$  for N-319. O, experimental data; lower curve,  $\lambda_e^s/\lambda_e^n$  owing to eq. (4.1) with  $\Delta(0)/k_B T_c = 1.95$ .

correction has yet been made for the phonon contribution.

In the following sections we will discuss the  $\lambda_p^n$  and  $\lambda_p^s$  behaviour in more detail, but we want to stress already now that the curve in fig. 4.7d is a theoretical fit, which enables us to calculate  $\lambda_p^n$  too. By subtracting it from the normal state thermal conductivity data we obtained  $\lambda_e^n$  and from that  $\lambda_e^s/\lambda_e^n$ , which coincided within the measuring accuracy with the theoretical curve in fig. 4.6. This gave us the confidence that the assumption was right.

The value 1.95 we derived for  $\Delta(0)/k_B T_c$  is in reasonable agreement with the value 1.92 recently determined by Lea and Dobbs <sup>7)</sup> from their ultrasonic attenuation measurements at low temperatures on a very pure niobium single crystal (resistance ratio  $\sim 5200$ ). A careful analysis of Forgan and Gough <sup>8)</sup> of similar measurements yields a value of 1.95 for  $T > 5$  K. At lower temperatures their measurements scale with a theoretical curve determined by an energy gap  $\Delta(0) = 1.55 k_B T_c$ , close to the BCS value. The same effect was found in ultrasonic absorption experiments on Nb by Carsey et al. <sup>9)</sup> and is not well understood <sup>8)</sup>.

#### §4.4 Discussion of the Phonon Conductivity in the Normal State

The phonon conductivity in the normal state at temperatures well below  $\Theta_D$  may be described by the relation (eq. (2.19)):

$$\lambda_p^n = \frac{k_B^4 T^3}{2\pi^2 \hbar^3 v_s} \int_0^\infty dx \frac{x^4 e^x (e^x - 1)^{-2}}{[B + DxT + ExT + Px^4 T^4]}$$

with  $x = \hbar\omega/k_B T$ . The denominator represents the sum of the inverse relaxation times of the four most probable scattering mechanisms: grain boundaries,

dislocations, electrons, and point defects. With  $v_s = 3 \times 10^5$  cm/s the constant  $k_B^4 (2\pi^2 n^3 v_s)^{-1}$  is equal to  $5.3 \times 10^6 \text{ mW K}^{-4} \text{ cm}^{-1} \text{ s}^{-1}$ . For the sample P<sub>1400</sub>, P<sub>1600</sub>, and N-0 we can calculate the magnitude of E from the values of A in table 4.3 and from  $\int_0^\infty dx x^3 e^x (e^x - 1)^{-2} = 7.2$ . The values for the different samples are given in table 4.3 as well.

It is not clear why the electron-phonon interaction is so much stronger in P<sub>1400</sub> than in the other samples. There will be a correlation between the electron and phonon mean free paths, as was suggested by Pippard<sup>11</sup>), but his formula can at most account for a factor 1.2. Nevertheless we believe that  $2 \times 10^9 \text{ K}^{-1} \text{ s}^{-1}$  is a good order of magnitude for the constant E, so that now we can check whether the other terms in the denominator of eq. (2.19) are important with respect to the inverse phonon-electron relaxation time.

The grain boundary scattering relaxation time is given by an expression derived by Klemens<sup>10</sup>):

$$\frac{1}{\tau_B} = B = 3.10^{-2} \gamma^2 \alpha^2 v_s N_g \quad (4.4)$$

where  $\gamma$  is the Grüneisenconstant ( $\gamma = 1.4$  for Nb<sup>12</sup>),  $\alpha$  is the angle of tilt of the crystal lattices separated by the boundary (clearly  $\alpha < \pi/4$ ), and  $N_g$  is the number of grain boundaries crossing a line of unit length.  $N_g$  is the largest for P<sub>1400</sub> ( $1.1 \times 10^2 \text{ cm}^{-1}$ ), but even then B is smaller than  $2 \times 10^6 \text{ s}^{-1}$ , which must be compared with  $E x_m T = 8 \times 10^9 \text{ Ts}^{-1}$ , and consequently can be neglected above 1 K ( $x_m$  is the value of  $x$  for which  $x^4 e^x (e^x - 1)^{-2}$  is maximum,  $x_m = 3.83$ ).

The same author also obtained an expression for the scattering by the strain field of a line dislocation:

$$\frac{1}{\tau_D} = D x T = 33.10^{-3} \gamma^2 b^2 N_d \omega \quad (4.5)$$

in which  $b$  is the Burgers vector ( $3.3 \times 10^{-8}$  cm in Nb), and  $N_d$  is the number of dislocation lines per unit area. We obtain

$$D = 93.10^{-7} N_d \text{ K}^{-1} \text{ s}^{-1}$$

which, even for P<sub>1400</sub> ( $N_d = 6 \times 10^8 \text{ cm}^{-2}$ ), given rise to a negligible term, both with respect to  $E x T$  and B.

For point defects with a concentration  $n_p$  Klemens derived:

$$\frac{1}{\tau_p} = P x^4 T^4 = \frac{3a^3 n_p}{\pi v_s^3} S^2 \omega^4 \quad (4.6)$$

where  $a^3$  is the volume per atom ( $1.8 \times 10^{-23} \text{ cm}^3$  for Nb), and  $S$  is the scattering amplitude of the point defects. It consists of two contributions:

$$S_1^2 = (\Delta M/M)^2/12, \text{ due to the difference in mass of the impurities,}$$

$$S_2^2 = 3\gamma^2 (\Delta R/R)^2, \text{ due to the lattice distortion by the impurities.}$$

$R$  is the lattice spacing. We obtain:

$$P = 19.10^4 n_p S^2 K^{-4} s^{-1}$$

If we think of Ta as the impurity atom, we have  $n_p = 2 \times 10^{-4}$ ,  $S_1^2 = 0.075$ , and  $S_2^2 = 0.098$  (here we assumed  $\Delta R/R \sim (R_{Ta} - R_{Nb})/R_{Nb}$ ). This yields  $P = 6.6 K^4 s^{-1}$ , which only gives rise to a comparable form if  $T \geq 175 K$ .

The conclusion is that in the normal state and at the temperatures of our experiments, the phonon-electron interaction is the only effective scattering mechanism. The low lying curves in the figs. 4.7 show  $\lambda_p^n$  as a function of  $T$ . The mean free path of the phonons can be determined from  $\lambda_p = v_s / (ExT) 10^8 \text{ \AA}$ . If we insert for  $x$  the value at which the maximum in the phonon spectrum is adopted ( $\tilde{x} = 1.6$ ), we obtain  $\tilde{\lambda}_p = 0.94 \times 10^4 T^{-1} \text{ \AA} \approx T^{-1} \mu\text{m}$  ( $T$  in K).

#### §4.5 Discussion of the Phonon Conductivity in the Superconducting State

In the superconducting state at the lowest temperatures the situation is quite different. The average phonon energy is much smaller than the energy gap in the electron spectrum, so that the phonon-electron scattering probability becomes very small. BRT expressed this by inserting a factor  $g(x,T)$  in front of the  $ExT$  term in eq. (2.19), giving rise to:

$$\lambda_p^s = \frac{k_B^4 T^3}{2\pi^2 \hbar^3 v_s} \int_0^\infty dx \frac{x^4 e^x (e^x - 1)^{-2}}{[B + DxT + g(x,T)ExT + Px^4 T^4]}$$

where  $g(x,T)$  is a monotonously decreasing function of  $x$ ;  $g(x_m, T)$  is not much smaller than  $g(0, T) = 2(e^y - 1)^{-1}$ , in which  $y = \Delta(T)/k_B T$ . In fig. 4.8  $g(0, T)E$  and  $g(0, T)Ex_m T$  are shown in a semi-logarithmic plot as functions of temperature,

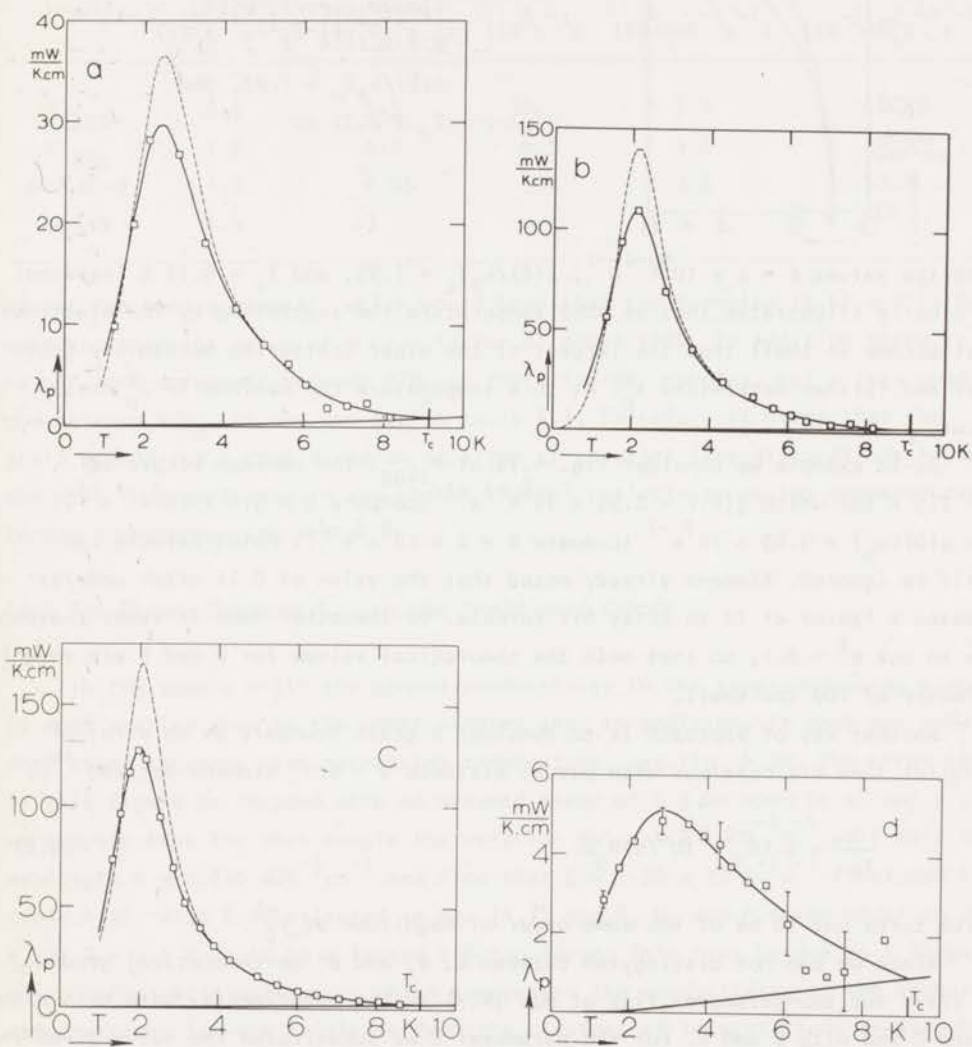


Fig. 4.7 Phonon thermal conductivity of  $P_{1400}$  (a),  $P_{1600}$  (b),  $N-0$  (c), and  $N-319$  (d).  $\square$ , experimental data of  $\lambda_p^s$ . Upper curves,  $\lambda_p^s$ , theoretical fit of eq. (4.7), drawn: dislocation term, broken: boundary term. Lower curves,  $\lambda_p^n$ .

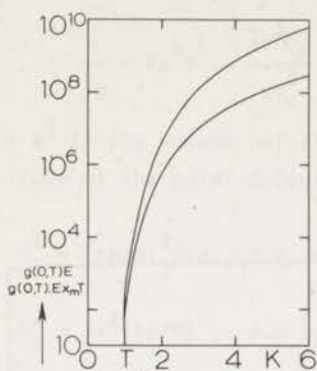


Fig. 4.8 Plot of  $g(0,T)Ex_m T$  versus  $T$  (upper curve), and of  $g(0,T)E$  versus  $T$  (lower curve), with  $E = 2 \cdot 10^9 K^{-1} s^{-1}$ ,  $\Delta(0)/k_B T_c = 1.95$ , and  $T_c = 9.12$  K.

with the values  $E = 2 \times 10^9 K^{-1} s^{-1}$ ,  $\Delta(0)/k_B T_c = 1.95$ , and  $T_c = 9.12$  K inserted. It clearly illustrates that at some temperature the scattering by the electrons must become so small that the largest of the other scattering mechanisms takes over and further determines  $\lambda_p^S$ . At this temperature the maximum in  $\lambda_p^S$  must occur.

As an example we consider fig. 4.7a of  $P_{1400}$ . The maximum occurs at  $T \sim 2.5$  K for which  $g(0)E = 2.95 \times 10^6 K^{-1} s^{-1}$  (compare  $D = 5.6 \times 10^3 K^{-1} s^{-1}$ ), and  $g(0)Ex_m T = 3.09 \times 10^7 s^{-1}$  (compare  $B = 2 \times 10^6 \alpha^2 s^{-1}$ ). Point defects can still be ignored. Klemens already noted that the value of  $D$  is often underestimated a factor of 10 to 20 by his formula. On the other hand it seems reasonable to put  $\alpha^2 \sim 0.1$ , so that both the theoretical values for  $D$  and  $B$  are roughly a factor of 100 too small.

Another way of approach is to consider a grain boundary as an array of parallel line dislocations with mutual distance  $d \sim b/\alpha$ . Klemens derived <sup>10)</sup>:

$$\frac{1}{\tau_{B'}} = 6 \cdot 10^{-2} \gamma^2 (b^2/d) N_g \omega \quad (4.8)$$

which turns out to be of the same order of magnitude as  $\tau_D^{-1}$ .

Since we can not distinguish between  $D$ ,  $B$ , and  $B'$  on theoretical grounds, we tried two two-parameter fits of eq. (4.7) to the experimental data both with  $E$  and  $D$  and with  $E$  and  $B$ . For the parameter  $E$  we substituted the value given in table 4.3, for the other parameter we inserted the value determined from the experimental curve at  $T = 1.50$  K, where the  $g(x,T)ExT$  term can be neglected as clearly follows from fig. 4.8. This did not give the best fit at the higher temperatures, but better results were readily obtained at  $E$  values (denoted by  $E_{fit}$  in table 4.4) that only differ a few per cent from the earlier values. The drawn curves in the figs. 4.7a, b, and c resulted from the  $D, E$  fit, the broken curves from the  $B, E$  fit. It is clear that the dislocation scattering term gives

Table 4.4

Sample	$E_{fit}$ ( $10^9 K^{-1} s^{-1}$ )	D ( $10^6 K^{-1} s^{-1}$ )	B ( $10^6 s^{-1}$ )	$D/N_g$ ( $10^4 cmK^{-1} s^{-1}$ )	$D/N_d$ ( $10^{-2} cm^2 K^{-1} s^{-1}$ )
P <sub>1400</sub>	3.1	5.5	30	5.0	0.92
P <sub>1600</sub>	1.6	1.2	6.5	4.2	>2.4
N-0,NO-0	1.7	0.95	5.1	3.8	>2.4
N-319	1.4	17			

by far the best agreement, which would mean that the formulae (4.5) and (4.8) underestimate the value of D by a factor of about 1000. In addition there is a rather good agreement between  $D/N_g$  of the different samples, but a less good one between  $D/N_d$ , as one can see in table 4.4. Therefore it seems that the grain boundaries - considered as an array of parallel line dislocations - play the most important part in the phonon thermal resistivity at low temperatures in the superconducting state.

#### §4.6 The Phonon Conductivity in the Irradiated Sample

In the sample N-319 the phonon conductivity in the superconducting state is much smaller than in the other samples and, in addition, it does not show a very sharp increase with decreasing temperature, see fig. 4.7d. The error bars in this figure correspond with an assumed error of 0.5 per cent in  $\lambda^S$  and  $\lambda^N$ . If we suppose that for this sample the relation  $Ab' = 4.2 \times 10^{-8} K^{-4}$  will hold too, we obtain  $A = 0.030 mWK^{-3} cm^{-1}$  and from that  $E = 1.26 \times 10^9 K^{-1} s^{-1}$  (included in table 4.3). With E substituted in eq. (4.7) and B, D, and P taken equal to zero,  $\lambda_p^S$  at  $T = 5.5$  K would be a factor 2.5 too large. This must be due to a large point defect scattering term which suppresses the conductivity at the higher temperatures. It must originate from the clusters of interstitials created by the fast neutron irradiation, rather than the mass defects created by the thermal neutrons, because the latter only have a very small scattering amplitude. Klemens<sup>10</sup> pointed out that, if the dimensions of a cluster are small as compared with the phonon wavelength (a few hundred angströms), the scattering probability is reinforced and varies as the square of the number of defects in the cluster, but it still has the same  $\omega^4$  dependence. Therefore:

$$\frac{1}{\tau_p} = P_X T^4 = \frac{3a^3}{\pi v_s^3} n_{cl} N_i^2 S_2^2 \omega^4 \quad (4.9)$$

where  $n_{cl}$  is the concentration of clusters ( $\approx 10^{16} a^3 = 1.8 \times 10^{-7}$ ), and  $N_i$  the average number of interstitials per cluster.

Suppose there is one interstitial per  $q$  ions of the original lattice. The average dimension of a cluster is  $100 \text{ \AA}$ , so that the number of ions per cluster is  $7 \times 10^3$ , and the number of interstitials per cluster is  $N_i = 7 \times 10^3 / q$ . The relative change in the lattice spacing is  $\Delta R/R \sim (q+1)^{-1/3}$ , which gives  $S_2^2 \sim 6(q+1)^{-2/3}$ . The final result is:

$$P = \frac{9.7 \times 10^6}{q^2 (q+1)^{2/3}} K^{-4} s^{-1} \quad (4.10)$$

With  $q = 10$  the term  $P_X T^3$  is already comparable with  $E$  at  $T = 9 \text{ K}$ , so that point defect scattering will certainly play an important part in the superconducting state.

Dislocation scattering must be responsible again for the decrease of  $\lambda_p^S$  at low temperatures. Unfortunately, one can not obtain  $D$  directly from the experimental curve at  $1.5 \text{ K}$ , because point defect scattering can not yet be neglected. It turns out that the best fit over the whole temperature range is obtained for  $D = 17 \times 10^6 K^{-1} s^{-1}$ ,  $E = 1.4 \times 10^9 K^{-1} s^{-1}$ , and  $P = 8.1 \times 10^4 K^{-4} s^{-1}$ . These values give rise to the upper curve in fig. 4.7d. The value of  $P$  can be obtained by inserting  $q = 6$  in eq. (4.10), correspondingly in a cluster there should be one interstitial per 6 ions of the lattice.

It is not quite clear which phenomenon is responsible for the increase in  $D$  (compare  $N=0$ :  $D = 1 \times 10^6 K^{-1} s^{-1}$ ). Perhaps the trapped interstitials in the grain boundaries and line dislocations give rise to the increase of the scattering amplitude of these defects.

The lower curve in fig. 4.7d represents  $\lambda_p^N$  calculated by means of eq. (2.19) with the same values of  $D$ ,  $E$ , and  $P$  substituted. It contributes less than 0.4 per cent to  $\lambda_p^N$ , which is of the same order of magnitude as the measuring accuracy.

## References

1. C.A.M. van der Klein, J.D. Elen, R. Wolf, and D. de Klerk, *Physica* 49 98, (1970).
2. C.A.M. van der Klein, P.H. Kes, and D. de Klerk, *Phil. Mag.* (in the press).
3. C.A.M. van der Klein, P.H. Kes, H. van Beelen, and D. de Klerk, *J. Low Temp. Phys.* (in the press).
4. J.D. Elen, G. Hamburg, and A. Mastenbroek, *J. Nucl. Mat.* 39, 194 (1971).
5. D.H. Finnemore, T.F. Stromberg, and C.A. Swenson, *Phys. Rev.* 149, 231 (1966).
6. B.J.C. van der Hoeven and P.H. Keesom, *Phys. Rev.* 134, A 1320 (1964).
7. M.J. Lea and E.R. Dobbs, *Phys. Letters* 45A, 39 (1973).
8. E.M. Forgan and G.E. Gough, *J. Phys.* F3, 1596 (1973).
9. F. Carsey, A. Kagiwada, M. Levy, and K. Maki, *Phys. Rev.* B4, 854 (1971).
10. P.G. Klemens, *Solid State Phys.* 7, 1 (1958).
11. A.B. Pippard, *J. Phys. Chem. Solids* 3, 175 (1957).
12. G.K. White, *Cryogenics* 2, 292 (1962).

## CHAPTER 5

### THE FLUX DISTRIBUTION IN THE MIXED STATE

#### §5.1 Introduction

In this chapter we will discuss the magnetic behaviour of reversible and irreversible low- $\kappa$  type-II superconductors in the mixed state <sup>1)</sup> (see also section 2.3). In irreversible type-II superconductors the free movement of the flux line lattice is counteracted by the interaction of the vortices with the imperfections of the crystal lattice (pinning centres), causing a gradient in the flux density  $\partial B/\partial x$ . The critical state can be described by an equation in which the driving force is in equilibrium with the pinning force.

An expression for the driving force  $F_d$  per unit volume has been given by Friedel et al. <sup>2)</sup>, who derived, from thermodynamic considerations, the relation between  $F_d$  and  $\partial B/\partial x$  in the one-dimensional case:

$$F_d = - \frac{B}{4\pi} \left( \frac{\partial B}{\partial H} \right)_{\text{rev}}^{-1} \frac{\partial B}{\partial x} \quad (5.1a)$$

in which  $\left( \frac{\partial B}{\partial H} \right)_{\text{rev}} = 1 + \left( \frac{\partial 4\pi M}{\partial H} \right)_{\text{rev}}$  can be derived from the slope of the reversible magnetization (Abrikosov) curve;  $B(x)$  is the local induction. A more general expression was derived by Evetts et al. <sup>3)</sup>:

$$\vec{F}_d = - \frac{\vec{B}(\vec{r})}{4\pi} \times \vec{\nabla} \times \vec{H}(\vec{r}) \quad (5.1b)$$

of which (5.1a) is a special case.

A much more complicated problem is the derivation of an adequate expression for the pinning force per unit volume  $F_p$ . Because the mutual interaction of the vortices is strong, resulting into a rather rigid vortex lattice (section 5.4), a statistical average has to be made up over all the interaction forces experienced by this rigid lattice <sup>4)</sup>. This cooperative effect gives rise to a less effective pinning than results from a linear superposition of the contributions of all the effective pinning centres, such as the models of Goedemoed et al. <sup>5)</sup> for point defects, and of Campbell et al. <sup>6)</sup> for line defects perpendicular to the vortices. The problem was for the first time formulated in

this general way by Fietz and Webb <sup>4)</sup> and somewhat later confirmed theoretically for some special cases by Labusch <sup>7)</sup> and by Good and Kramer <sup>8)</sup>.

Equalizing  $F_d$  and  $F_p$  we obtain the critical state equation from which, in principle, one should be able to calculate the local flux distribution  $B(x)$ , and, by means of integration, the irreversible magnetization curve in increasing and decreasing fields. However, this can only be carried out in practice if the reversible relation between  $B$  and  $H$  is known. The approximation  $B = H$ , which is often encountered in the literature on critical state studies <sup>9)</sup>, is only justified for high- $\kappa$  type-II superconductors in fields well above  $H_{c1}$ . The assumption is certainly not correct, however, for the much more interesting intrinsic type-II superconductors niobium and vanadium, which have a low kappa,  $\kappa \sim 0.8$ .

Theoretical expressions have only been given in some limiting cases. E.H. Brandt <sup>10)</sup> solved the Landau-Ginzburg equations near  $T_c$ , but it is evident from a comparison with experimental results that his final equation does not describe the Abrikosov curve very well at temperatures below the Landau-Ginzburg region. U. Brandt <sup>11)</sup> solved the Gorkov equations in the low temperature limit in fields well above  $H_{c1}$ , but unfortunately his result is only implicitly given by an equation which is too complicated for the numerical calculations. We succeeded to find a mathematically simple expression for  $B_{rev}(H)$ , which makes it possible to carry out calculations of the flux distribution  $B(x)$  and the irreversible magnetization curves for various critical state models.

In section 5.2 we will discuss our choice for the  $B_{rev}(H)$  relation and check its validity by comparing it with experimental results. In section 5.3 a derivation is given of the formulae for the irreversible magnetization curves for a general critical state equation. In addition, we will describe a method to determine the parameters which occur in the theory from the experimental curves. Finally, in section 5.4, a more detailed discussion will be given of some critical state models.

## §5.2 The Reversible Magnetization Model

In the following we will use the reduced quantities:

$$4\pi m = (4\pi M + H_{c1})/H_{c2} \quad (5.2a)$$

$$h_a = (H_a - H_{c1})/H_{c2} \quad (5.2b)$$

$$b = B/H_{c2} \quad (5.2c)$$

$$h_1 = H_{c1}/H_{c2} \quad (5.2d)$$

$$h_2 = (H_{c2} - H_{c1})/H_{c2} \quad (5.2e)$$

where  $H_a$  is the externally applied magnetic field.

Reversible magnetization curves of pure niobium<sup>12,13)</sup> and vanadium<sup>14)</sup> show a strikingly sharp decrease of  $-4\pi M$  just above  $H_{c1}$ , followed by a much more gradual decrease to zero. This shape is so very similar to a power function that we decided to represent the magnetization between  $H_{c1}$  and  $H_{c2}$  by

$$4\pi m = \alpha h_a^\beta \quad (5.3)$$

in which  $\alpha$  and  $\beta$  are constants for constant temperature. We want to emphasize that this relation is just an ad hoc hypothesis, which is not based upon any solution of the Gorkov equations.

The constants  $\alpha$  and  $\beta$  can be derived from the boundary conditions at  $H_{c2}$ :

$$4\pi M(H_{c2}) = 0 \quad ; \quad 4\pi m(h_2) = h_1 \quad (5.4a)$$

$$\left(\frac{d4\pi M}{dH}\right)_{H_{c2}} = \left(\frac{d4\pi m}{dh}\right) = 4\pi\chi_{c2} \quad (5.4b)$$

Hence

$$\alpha = h_1/h_2^\beta \quad (5.5a)$$

$$\beta = 4\pi\chi_{c2} \cdot h_2/h_1 \quad (5.5b)$$

In non-reduced quantities this corresponds to:

$$B = H_a + 4\pi M(H_a) = H_a - H_{c1} + H_{c1} \left(\frac{H_a - H_{c1}}{H_{c2} - H_{c1}}\right)^\beta \quad (5.6a)$$

and

$$\beta = 4\pi\chi_{c2} (H_{c2} - H_{c1})/H_{c1} \quad (5.6b)$$

The constant  $\beta$  may be deduced from the experimental Abrikosov curve in two different ways:

- (i) one can measure the values of  $H_{c1}$ ,  $H_{c2}$  and  $4\pi\chi_{c2}$ , then  $\beta$  follows from (5.6b)
- (ii) one can measure  $H_{c1}$  and  $H_{c2}$  and take one arbitrary point of the Abrikosov

curve; now  $\beta$  follows from (5.6a). In the ideal case both methods should give the same result. The magnitude of  $\beta$  depends on temperature and is of the order 0.3.

Two features of relation (5.6a) are the infinite slope at  $H_{c1}$ , since  $\beta < 1$ , and the linear character near  $H_{c2}$ , since a Taylor series expansion converges very rapidly in this field region.

In fig. 5.1 relation (5.6a) has been checked for the experimental curve

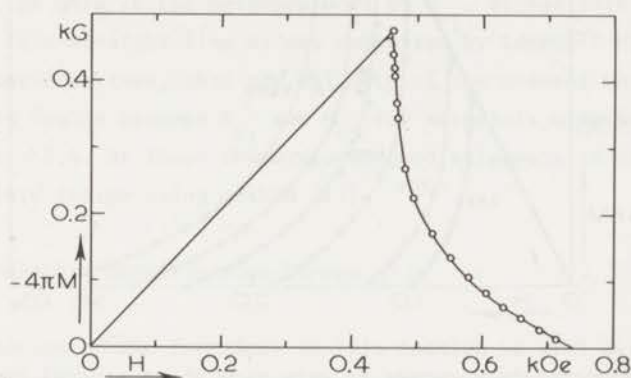


Fig. 5.1 Magnetization curve of very pure V at  $T = 4.207$  K ( $t = 0.775$ ), measured by Sekula and Kernohan. Continuous curve: experimental results; O, present model.

measured by Sekula and Kernohan<sup>14)</sup> on very pure vanadium ( $\kappa = 0.82$ ) at a reduced temperature  $T/T_c = t = 0.775$ . The fully drawn line represents the experimental result, the points indicate our calculations using Sekula's values of  $4\pi\chi_{c2} = [1.16(2\kappa^2 - 1)]^{-1}$ ,  $H_{c1}$  and  $H_{c2}$  (a correction for the demagnetization factor of 0.0264 has been made). It turns out that our model fits the experimental data surprisingly well.

Subsequently we wanted to check our model at lower reduced temperatures. For this purpose we used Freyhardt's data on pure niobium ( $\kappa = 0.83$ )<sup>13)</sup>. The results are shown in fig. 5.2, in which the drawn lines represent the experimental data. The circles are calculated from our model (again a correction for the demagnetization coefficient of 0.025 had to be made), using the values given in table 2 of ref. 13. The agreement is good for  $t > 0.65$  and still within a few per cent for  $t > 0.45$ . For lower  $t$ , however, the agreement becomes worse. The same trend can be seen in fig. 5.3 for Nb, measured by Finnemore et al.<sup>12)</sup>. At  $t = 0.835$  the agreement is very good (circles in fig. 5.3), at  $t = 0.26$  there is a disagreement of 25 per cent at  $H \sim 0.5 H_{c2}$ .

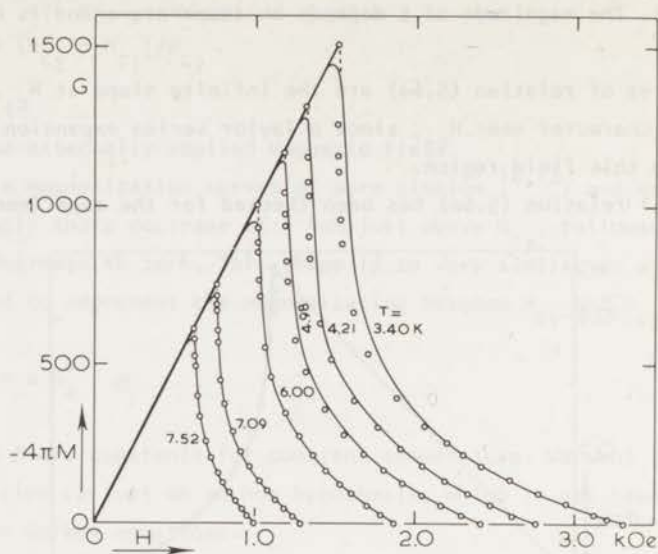


Fig. 5.2 Magnetization curves of very pure Nb at several temperatures ( $T_c = 9.2$  K), measured by Freyhardt. Continuous curves: experimental results;  $\circ$ , present model.

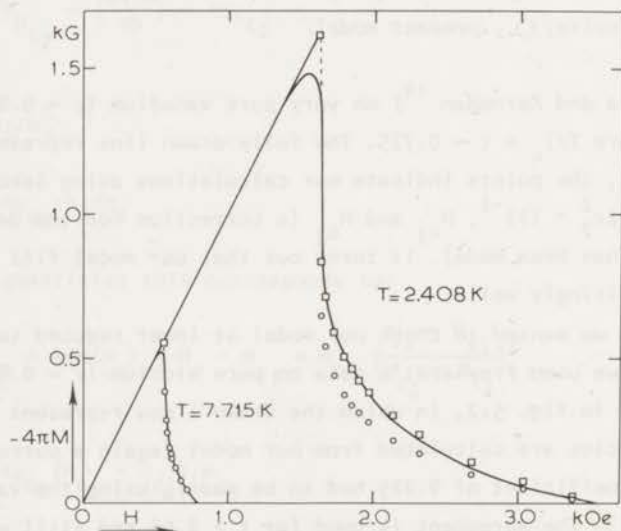


Fig. 5.3 Magnetization curves of very pure Nb ( $T_c = 9.25$  K), measured by Finnemore, Stromberg and Swenson. Continuous curves: experimental results;  $\circ$ , present model, method (i);  $\square$ , present model, method (ii), adaptation at 1900 Oe.

In the above calculations only method (i) was used to determine  $\beta$ . In the case of Finmore's data at  $t = 0.26$  we also used method (ii) making the adaptation at  $H = 1900$  Oe. Now there is a good agreement for fields between  $H_{c1}$  and 2000 Oe, but above this field region the calculated points (squares in fig. 5.3) lay about 15 per cent too high. The difference between the two  $\beta$ 's and thus between the slopes at  $H_{c2}$  is about 30 per cent.

Data on reversible material with  $\kappa \gg 1$  does not agree anymore with the present model, or only in the neighbourhood of  $H_{c1}$ . Beyond this region the best approximation is a straight line as was suggested by Campbell et al. <sup>15)</sup>.

We may conclude, then, that the validity of the present model is good over the total field region between  $H_{c1}$  and  $H_{c2}$  for materials with low  $\kappa$  at reduced temperatures  $t > 0.4$ . At lower temperatures good agreement is only obtained in part of the field region using method (ii).

### §5.3 The Irreversible Magnetization Curves

5.3.1 *Deduction of the Formulae.* In this section we will derive expressions for the irreversible magnetization curves in the first and second field quadrants between  $H_{c1}$  and  $H_{c2}$ . Only the case of a rectangular sample will be considered with the field  $H_a$  applied parallel to the longest side. The thickness  $2d$  is assumed to be much smaller than the other dimensions, so that demagnetization effects may be neglected.

The critical state equation for this one-dimensional case can generally be written as:

$$\left(\frac{\partial H}{\partial B}\right)_{\text{rev}} \cdot \frac{\partial B}{\partial x} = \gamma F(B, H) \cdot (H_{c2} - B) \quad (5.7)$$

in which  $\gamma$  is a parameter of the pinning model (in decreasing field it has to be replaced by  $-\gamma$ ), and  $F(B, H)$  is some function determined by the pinning model being considered. It generally depends on the local induction  $B(x)$  and the local field  $H(x)$ , which are related to each other, according to eq. (5.6a), by:

$$B(x) = H(x) - H_{c1} + H_{c1} \left( \frac{H(x) - H_{c1}}{H_{c2} - H_{c1}} \right)^\beta \quad (5.8)$$

Using this relation it is possible to write eq. (5.7) as a differential equation for  $H(x)$ . Introducing  $\xi = x/d$  and the reduced quantities defined in eqs. (5.4a) - (5.4c) it passes into

$$\frac{\partial h}{\partial \xi} = \gamma' d f[b(h), h] \cdot (1 - b) = \gamma' d f(h) \cdot (1 - h - \alpha h^\beta) \quad (5.9)$$

The solution is implicitly given by

$$\gamma' d(1 - \xi) = \int_{h(\xi)}^h dh [f(h) \cdot (1 - h - \alpha h^\beta)]^{-1} \quad (5.10)$$

from which  $b(\xi)$  follows as well.

In order to obtain an expression for the irreversible magnetization curves we have to calculate the average induction over the sample. However, it is not necessary to know  $b(\xi)$  explicitly. We just rewrite eq. (5.9), obtaining

$$b(\xi) = 1 - [\gamma' d f(h)]^{-1} \frac{\partial h}{\partial \xi} \quad (5.11)$$

which can be substituted into the expression for the irreversible magnetization in reduced quantities

$$4\pi m = \int_0^1 d\xi b(\xi) - h_a \quad (5.12)$$

For increasing field we have to distinguish two field regions.

(A) For the fields just above  $H_{c1}$  the flux has not yet reached the central plane of the sample:  $b(\xi) = 0$  for  $0 \leq \xi \leq \xi_0$ .

(B) For the higher fields,  $b(\xi)$  is non-zero throughout the whole sample.

In decreasing field only case (B) exists.

Performing the integration of eq. (5.12) we arrive at:

$$(A) \quad 4\pi m = (1 - \xi_0) - \int_0^{h_a} dh [\gamma' d f(h)]^{-1} - h_a \quad (5.13a)$$

$$(B) \quad 4\pi m = 1 - \int_{h_0}^{h_a} dh [\gamma' d f(h)]^{-1} - h_a \quad (5.13b)$$

in which  $h_0$  stands for  $h(\xi = 0)$ . The quantities  $\xi_0$  and  $h_0$  can be derived from eq. (5.10), inserting the proper limits:

$$(A) \quad \gamma' d(1 - \xi_0) = \int_0^{h_a} dh [f(h) (1 - h - \alpha h^\beta)]^{-1} \quad (5.14a)$$

$$(B) \quad \gamma' d = \int_{h_0}^{h_a} dh [f(h) (1 - h - \alpha h^\beta)]^{-1} \quad (5.14b)$$

The field for which (A) passes into (B) is found by substituting  $\xi_0 = 0$  in (5.14a); we call it  $h_a^*$  or, in non-reduced units,  $H_a^*$ .

With the help of a computer it is easy to solve eqs. (5.10) and (5.13a) - (5.14b) numerically. This has been carried out on the IBM computer of the Centraal Reken Instituut of the University of Leiden.

5.3.2 *Application of the Formulae.* In reference 1 we described a method to determine the parameter  $\gamma$  of the critical state model from the slopes,  $4\pi\chi_1$  and  $4\pi\chi_2$ , of the irreversible magnetization curves at  $H_{c2}$  in increasing and decreasing fields. The parameter  $\beta$  can be deduced, using method (i), from the slope of the Abrikosov curve which one should expect to measure in the absence of flux pinning. This slope is in very good approximation equal to  $(4\pi\chi_1 + 4\pi\chi_2)/2$ .

Quite often, however, the peak effect just below  $H_{c2}$ <sup>16)</sup> makes it impossible to use this procedure. Moreover, the inaccuracy in the slopes can be considerable. A much better and more general method (in some way analogous with method (ii) for the determination of  $\beta$ ) can be obtained from a series expansion of  $B(x)$  to second order in  $(d-x)$ , as was already discussed on page 774 of ref. 1. We derived for an external field  $H_a$  obeying  $H_a^* < H_a < H_{c2}$ :

$$4\pi M_{\text{rev}}(H_a) = \frac{1}{2}\{4\pi M_1(H_a) + 4\pi M_2(H_a)\} - \frac{1}{6}\left(\frac{\partial^2 B}{\partial \xi^2}\right)_{H_a} \quad (5.15)$$

$$\left(\frac{\partial B}{\partial \xi}\right)_{H_a} = -\Delta(4\pi M) = -\{4\pi M_1(H_a) - 4\pi M_2(H_a)\} \quad (5.16)$$

where the subscripts 1 and 2 refer to increasing and decreasing fields.

From the experimental curves  $4\pi M_1$  and  $4\pi M_2$  can be determined at  $H_a$ . Then, using an iteration procedure, the ultimate values of  $\beta$  and  $\gamma$  can be deduced from the eqs. (5.15), (5.16), and (5.7). It is not necessary to correct  $(\partial B/\partial \xi)_{H_a}$  for the third order term of the series expansion of the value of  $H_a$  is chosen sufficiently much larger than  $H_a^*$ , say  $H_a \geq H_a^* + 0.1(H_{c2} - H_a^*)$  which can be checked afterwards.

This method has the advantage of being applicable at temperatures below  $0.4 T_c$  too. Moreover, it turned out to be much more reliable than the former procedure. The reversible model expressed by eq. (5.6a) and the equations derived in this section for the irreversible magnetization curves turned out to be quite useful for comparison of some critical state models with the experimental results obtained for several niobium samples with different defect structure

introduced by neutron irradiation or by annealing at different temperatures (1,16,18).

#### §5.4 Discussion of Some Critical State Models

The flux lines form a two-dimensional array with a hexagonal unit cell. For such an isotropic system three independent elastic moduli can be defined. They have been derived by Labusch<sup>17a)</sup> in the case of well-separated vortices, i.e.  $H \ll H_{c2}$ :

$$C_{11} = C_{66} + \frac{B^2}{4\pi} \left( \frac{\partial H}{\partial B} \right)_{\text{rev}} \quad (5.17a)$$

$$C_{44} = \frac{BH_{\text{rev}}(B)}{4\pi} \quad (5.17b)$$

$$C_{66, H_{c1}} = \frac{B^2}{8\pi} \left( \frac{\partial H}{\partial B} \right)_{\text{rev}} - \frac{1}{4\pi} \int_{H_{c1}}^H B_{\text{rev}}(H') dH' \quad (5.17c)$$

$C_{11}-C_{66}$  is the compression modulus of the vortex lattice,  $C_{44}$  is a measure of the tilting of a flux line from its equilibrium position, and  $C_{66}$  is the shear modulus. In a subsequent paper<sup>17b)</sup> Labusch pointed out that the expressions for  $C_{11}-C_{66}$  and  $C_{44}$  hold for the entire field region between  $H_{c1}$  and  $H_{c2}$ . In addition, he proved that near  $H_{c2}$   $C_{66}$  goes to zero obeying the relation:

$$C_{66, H_{c2}} = \frac{0.475}{8\pi} \frac{(2\kappa_2^2 - 1)}{\{1 + 1.16(2\kappa_2^2 - 1)\}^2} (H_{c2} - B)^2 \quad (5.17d)$$

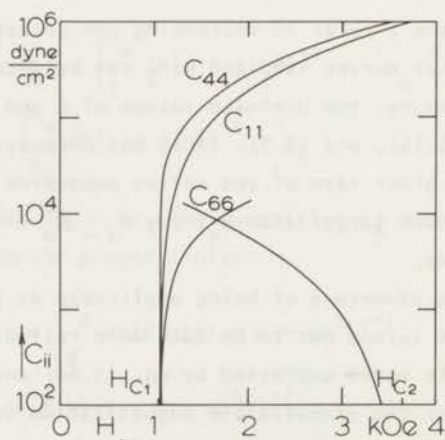


Fig. 5.4 Elastic moduli of the vortex lattice of Nb-O at  $T = 4.3$  K.

In fig. 5.4 the elastic moduli of the sample N0-0 at  $T = 4.3$  K are shown as functions of  $H$  using eqs. (5.6a) and (5.17a) - (5.17d). The curve for  $C_{66}$  consists of two parts corresponding with eqs. (5.17c) and (5.17d). Although  $C_{66}$  is not well-defined for the intermediate fields it seems reasonable to suppose that it is much smaller than the other moduli over the whole field region.

A rough criterion for flux pinning follows from the way in which the stored deformation energy is released during the movement of a flux line through a pinning centre. If the pinning force  $f_p$  decreases too fast at the edge of the pinning potential well, the elastic reaction force  $f_\ell$  of the vortex lattice experienced by the distorted flux line, is no longer in equilibrium with the pinning force. In that case the stored energy is not released reversibly. This will occur if  $df_p/dx > df_\ell/du$  in which  $u$  is the distortion of the flux line from its equilibrium position in the lattice.

If  $\delta$  is the width of the pinning potential and  $f_m$  is the maximum pinning force still in equilibrium with  $f_\ell$ , then  $df_p/dx \sim f_m/\delta$ . On the other hand  $u \propto f_\ell$ , so that the maximum distortion, apart from a numerical constant, is given by

$$u_m = \frac{1}{a} \frac{f_m}{C_{\text{eff}}} \quad (5.18)$$

where  $C_{\text{eff}}$  is the effective elastic modulus of the flux line lattice and  $a$  is a characteristic length, both still depending on the shape of the pinning centres being considered and their arrangement with respect to the vortex lattice. Then, the criterion for pinning can be expressed by a parameter  $\varepsilon = u_m/\delta$ , which should be roughly larger than one for pinning to become effective.

The resulting pinning force per unit volume is the statistical sum of all the effective pinning forces:

$$F_p = \left(N \frac{B}{\Phi_0} \delta\right) \varepsilon f_m \propto N \frac{B}{\Phi_0} \frac{1}{a} \frac{f_m^2}{C_{\text{eff}}} \quad (5.19)$$

in the case of  $N$  cm of small dislocation lines per unit volume,  $B/\Phi_0$  is the number of vortices per unit area.

The effective modulus  $C_{\text{eff}}$  which appears in the eqs. (5.18) and (5.19) can be expressed in terms of the moduli  $C_{ii}$ . Without going into detail we can already argue that the pinning is more effective if  $C_{66}$  enters into the expression of  $C_{\text{eff}}$  than if it does not.

If the pinning centres are small dislocations (i.e. small as compared to

$\xi$ ) and if they have a spacing larger than the vortex spacing  $a_0 = 1.07 (\phi_0/B)^{1/2}$ , Labusch <sup>7)</sup> derived for the maximum distortion

$$u_m = \frac{1.07}{4\sqrt{\pi}} \frac{f_m}{a_0} \{ (C_{44}C_{66})^{-1/2} + (C_{11}C_{66})^{-1/2} \} \quad (5.20)$$

If the pinning centres are dislocation lines with spacing  $\gg a_0$ , which are parallel to the vortices and much longer than  $\xi$ , Good and Kramer <sup>8)</sup> derived:

$$u_m = \frac{5C_{11} + C_{66}}{16\pi C_{11}C_{66}} \frac{f_m}{\Lambda} \ln(R/a_0) \quad (5.21)$$

in which  $f_m/\Lambda$  is the maximum pinning force per unit length, and  $R$  is an outer cut off distance of the order of half the dislocation spacing. Clearly, the result is not very sensitive for the exact definition of  $R$ .

If the pinning centres are long dislocation lines perpendicular to the vortices, Campbell and Evetts <sup>9)</sup> derived an expression for  $u_m$  which only contains  $C_{11}$ . This result is incorrect, because they ignored the possibility that the flux lattice might be tilted. From energy considerations we arrived at an estimation for the effective modulus  $C_{\text{eff}} = (C_{11} - C_{66}) + 2C_{44}/a_0$ , where  $2$  is the average spacing of the dislocation lines. Anyhow, both Campbell's result and our derivation yield moduli which are much larger than those of eqs. (5.20) and (5.21). Therefore this configuration of dislocation and vortex lines will not contribute very considerably to the volume pinning force, whereas the parallel configuration gives rise to a very effective pinning. Especially near  $H_{c2}$  the pinning can become very strong because  $C_{66}$  goes to zero as  $(H_{c2} - B)^2$ . Perhaps very close to  $H_{c1}$  the pinning is also somewhat more effective, but  $C_{66}$ , as all the moduli, rises very fast in this field region (fig. 5.4), because of the sharp increase of  $B$  as a function of  $(H - H_{c1})$  (figs. 6.1, 2, and 3). The Labusch theory is an intermediate case.

In the sample NO-0 the dislocation structure is very dilute except at the grain boundaries, but there the most probable configuration is the perpendicular one (if  $H_a$  is parallel to the longest side of the sample) with very weak pinning. Therefore we used the Labusch model in order to describe the irreversibility of the magnetization in this sample. The critical state equation for this case is

$$\frac{B}{4\pi} \left( \frac{\partial H}{\partial B} \right)_{\text{rev}} \frac{\partial B}{\partial x} = \frac{N}{8\sqrt{\pi}} \left( \frac{B}{\phi_0} \right)^{3/2} f_m^2 \{ (C_{44}C_{66})^{-1/2} + (C_{44}C_{11})^{-1/2} \} \quad (5.22)$$

For  $H \leq H_{c2}$  it is allowed to neglect the second term of the effective elastic modulus ( $C_{66} \ll C_{11}$ ), but for lower fields the exact equation should be

solved. This is a (computer) time consuming procedure and the question rises if this has any sense because the exact expression of  $C_{66}$  and therefore also of  $C_{11}$  is not known between the limiting field regions of eqs. (5.17c) and (5.17d). Therefore van der Klein et al. <sup>18)</sup> postulated a relation for the effective modulus

$$C_{\text{eff}} = \left\{ \frac{H - H_{c1}}{H_{c2} - H_{c1}} \frac{H_{c2}}{H} C_{44} C_{66, H_{c2}} \right\}^{\frac{1}{2}} \quad (5.23)$$

This modulus is shown in fig. 5.5 for N0-0 at  $T = 4.3$  K as the broken curve, whereas the continuous curve represents the modulus of the Labusch theory. The agreement is satisfactory over the whole field region.

Substitution into eq. (5.19) leads to the following critical state equation:

$$\left( \frac{\partial H}{\partial B} \right)_{\text{rev}} \frac{\partial B}{\partial x} = \gamma \frac{H_{c2} - B}{\sqrt{H - H_{c1}}} \quad (5.24)$$

in which  $f_m \propto (H_{c2} - B)$  has been inserted too <sup>9)</sup>. This equation will be used in chapter 6 to describe the experimental magnetization curves of N0-0 with a very satisfactory result.

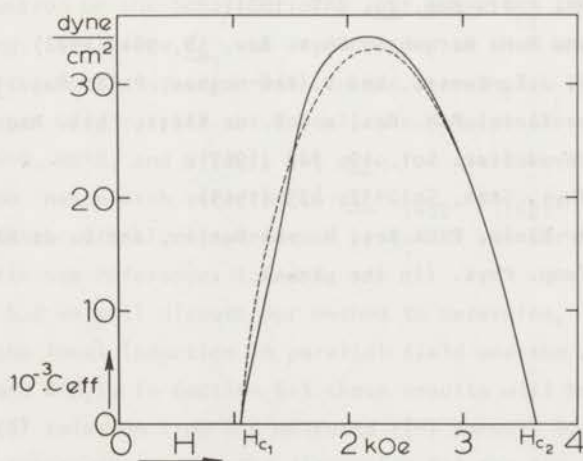


Fig. 5.5 Comparison of the effective elastic modulus of the Labusch theory (continuous curve) and the relation postulated by van der Klein et al. (broken curve).

## References

1. Many of the features of this chapter have already been discussed by:  
P.H. Kes, C.A.M. van der Klein, and D. de Klerk, *J. Low Temp. Phys.* 10, 759 (1973).
2. J. Friedel, P.G. de Gennes, and J. Matricon, *Appl. Phys. Letters* 2, 119 (1963).
3. J.E. Evetts, A.M. Campbell, and D. Dew-Hughes, *J. Phys.* C1, 715 (1968).
4. W.A. Fietz and W.W. Webb, *Phys. Rev.* 178, 657 (1969).
5. S.H. Goedemoed, P.H. Kes, F.Th.A. Jacobs, and D. de Klerk, *Physica* 35, 273 (1967).
6. A.M. Campbell, J.E. Evetts, and D. Dew-Hughes, *Phil. Mag.* 18, 313 (1968).
7. R. Labusch, *Crystal Lattice Defects* 1, 1 (1969).
8. J.E. Good and E.J. Kramer, *Phil. Mag.* 22, 329 (1970).
9. A.M. Campbell and J.E. Evetts, *Adv. Phys.* 21, 199 (1972).
10. E.H. Brandt, *Phys. Stat. Sol.* 51, 345 (1972).
11. U. Brandt, *Phys. Letters* 29A, 568 (1969).
12. D.H. Finnemore, T.F. Stromberg, and C.A. Swenson, *Phys. Rev.* 149, 231 (1966).
13. H.C. Freyhardt, *Phil. Mag.* 23, 345 (1971).
14. S.T. Sekula and R.H. Kernohan, *Phys. Rev.* 5B, 904 (1972).
15. A.M. Campbell, J.E. Evetts, and D. Dew-Hughes, *Phil. Mag.* 10, 333 (1964).
16. C.A.M. van der Klein, P.H. Kes, and D. de Klerk, *Phil. Mag.* (in the press).
- 17a. R. Labusch, *Phys. Stat. Sol.* 19, 715 (1967).
- 17b. R. Labusch, *Phys. Stat. Sol.* 32, 439 (1969).
18. C.A.M. van der Klein, P.H. Kes, H. van Beelen, and D. de Klerk, *J. Low Temp. Phys.* (in the press).

## CHAPTER 6

### THE THERMAL CONDUCTIVITY IN THE MIXED STATE

#### §6.1 Introduction. Magnetization Measurements

In this chapter the results of the thermal conductivity experiments in the mixed state will be compared with the theories discussed in section 2.5. The measurements have been carried out for three orientations of the magnetic field with respect to the sample surface and the direction of heat flow:  $H_{//}$ ,  $H_{\perp}$  and  $H_{\perp}$  (fig. 3.2), respectively referred to as "parallel", "transverse", and "perpendicular" field. We will give special attention to three temperatures: 2.13 K, where the phonon conductivity in zero field is predominant; 4.31 K, where the phonon and electron conductivities are both of the same order of magnitude; and 6.04 K, where the electron conductivity is the main contributor to the thermal conductivity.

For a discussion of the behaviour of  $\lambda$  just above  $H_{c1}$  in increasing field, and in decreasing field below  $H_{c1}$ , it is necessary to know the average magnetic induction  $B$  and the local induction  $B(x)$  inside the sample. Therefore magnetization measurements were carried out for all the samples discussed so far ( $P_{1400}$ ,  $P_{1600}$ ,  $N-0$ ,  $N0-0$ , and  $N-319$ ), but also for the same samples after surface oxidation, henceforth referred to as  $PO_{1400}$ ,  $PO_{1600}$ , and  $N0-319$ . Most of these experiments were kindly performed by C.A.M. van der Klein. For experimental details see references 1 and 2.

In section 6.2 we will discuss our method to determine, from the magnetization curves, the local induction in parallel field and the average inductions  $B(H_{//})$ ,  $B(H_{\perp})$ , and  $B(H_{\perp})$ . In section 6.3 these results will be applied to determine the  $\lambda(B)$  relation from the measured  $\lambda(H)$  curves. Some other general features are discussed there too. The discussion for the low induction range will be given in section 6.4 but, for several reasons mentioned below, only for the sample  $N0-0$ . The behaviour of the thermal conductivity in the vicinity of  $H_{c2}$  will finally be discussed in section 6.5 for all our samples, because no restricting difficulties arise in this case.

One reason to discuss the low induction behaviour only for  $N0-0$  and not for  $P_{1600}$  is that the physical properties of both samples are almost the same,

so that we do not expect greatly different results. The reason that also  $P_{1400}$  and N-319 were left out of the discussion is that even the small magnetic irreversibility of NO-0 makes a reliable discussion rather cumbersome. The much more pronounced irreversibility of the other samples leads to unsurmountable difficulties.

The irreversibility can be determined from the magnetization curves shown in fig. 6.1. The large difference in the irreversibility before and after the surface oxidation can be ascribed to a strong surface pinning removed by this treatment. The shift in the maxima of the curves in increasing and decreasing fields is an indication for this phenomenon<sup>3</sup>). The explanation may be found in a larger concentration of oxygen in the surface layer (niobium is a very

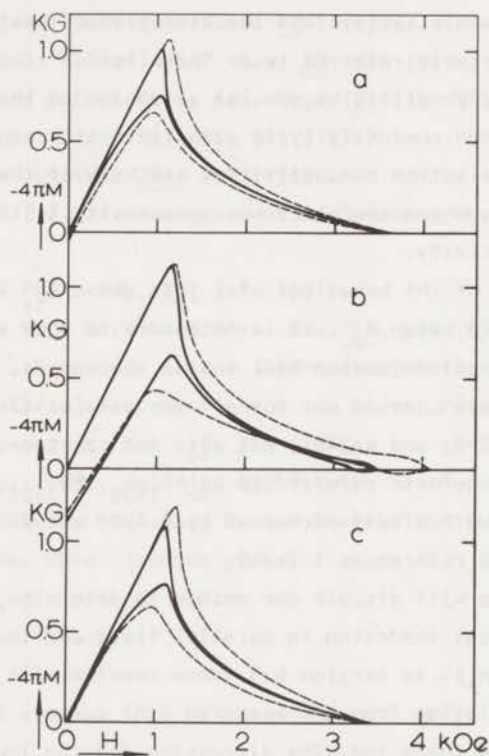


Fig. 6.1 Magnetization curves at 4.3 K; a. N-0 and NO-0; b. N-319 and NO-319; c.  $P_{1400}$  and  $PO_{1400}$ . The broken curves represent the samples before the surface treatment, the continuous curves after the oxidation.

good oxygen getter), resulting into a larger density of pinning centres near the surface. In addition, the pinning centres near the surface are more effective than in the bulk, because the shear modulus  $C_{66}$  of the flux lattice (section 5.4) is much smaller here<sup>4)</sup>. All this results into a strong surface pinning. Chemical removal of the surface layer, immediately followed by oxidation at 400 °C, gives rise to a very thin  $NbO_2$ -layer which protects the bulk of the sample<sup>5)</sup>. Only the pinning of the bulk remains, which for N0-0, as follows from fig. 6.1a, is very weak, because only just above  $H_{c1}$  the difference in the magnetization in increasing and decreasing fields is larger than the measuring accuracy of a few Oerstedes. It is clearly seen from the figures 6.1b and c that the irreversibility of P0<sub>1400</sub> and N0-319 turns out to be much larger. This gives rise to strong flux density gradients which prohibit a reliable discussion of the thermal conductivity results at low inductions.

## §6.2 The Average and Local Inductions for the Three Field Orientations

6.2.1 *The Magnetic Behaviour in Parallel Fields.* The magnetization curves of N0-0 between  $H_{c1}$  and  $H_{c2}$  could be well described by the critical state equation of Labusch with the effective modulus of Van der Klein et al.<sup>3)</sup> inserted (eq. (5.24)). In fig. 6.2 the calculated points are compared with the experimental curves at three temperatures. For the calculations we used method (ii) described in section 5.3.2 with the adaptations made at  $H = 800, 1210,$  and  $1500$  Oe respectively for  $T = 6.04, 4.31,$  and  $2.13$  K. The slight misfit at the lower temperatures and the higher fields is due to the difference between the Abrikosov curve and the mathematical expression we proposed in section 5.2, eq. (5.6a).

The local induction as calculated at  $T = 4.31$  K for several external field values in the vicinity of  $H_{c1}$  is shown in fig. 6.3. Below the field  $H^*$  the flux has not yet reached the central plane of the sample in increasing field, so that there remains a zone of zero induction referred to as the "Meissner zone". Above  $H^*$  it is obvious that for each increasing field we can find a decreasing field with the same average induction value. The local induction distributions for both fields are, turned inside out, but further identical, so that the thermal conductivities should be equal as well.

In decreasing field below  $H_{c1}$  the critical state theory predicts a field-independent induction, but from fig. 6.2 it is clear that there still leaks flux out of the sample. This is even more obvious from fig. 6.4 in which we show  $B(H_{//})$  (continuous curves) determined from the experimental magnetization curves

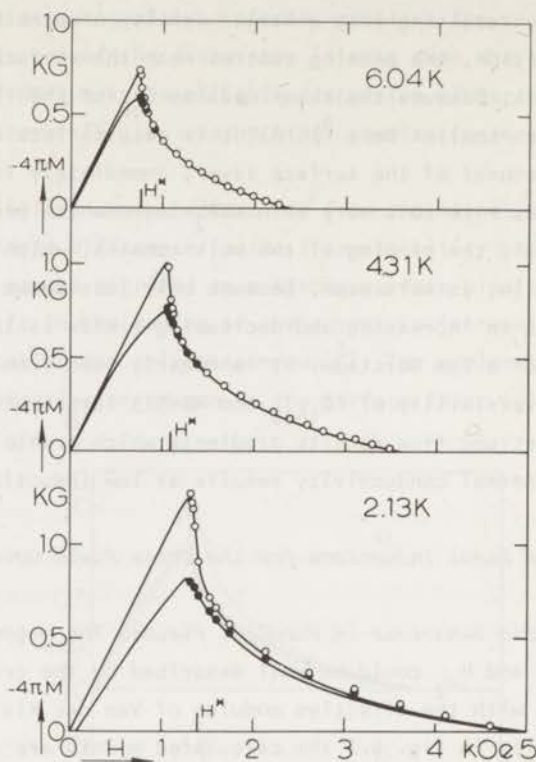


Fig. 6.2 Comparison of the magnetization curves of NO-0 with the theory of Labusch at  $T = 6.04, 4.31,$  and  $2.13$  K. Calculated points: O, field up; ●, field down.

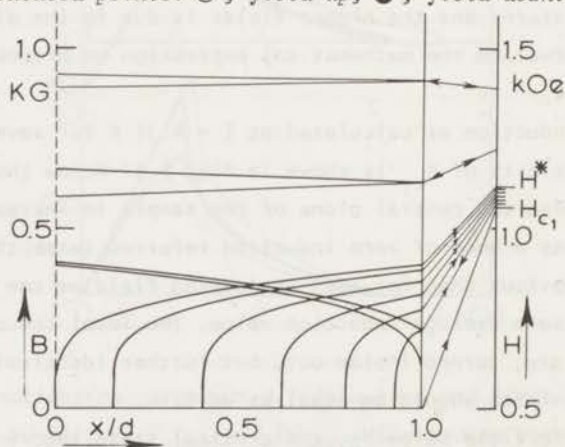


Fig. 6.3 Flux-density distribution for NO-0 at  $T = 4.31$  K in some increasing and decreasing fields near  $H_{c1}$ . The field values are given on the right-hand side;  $2d$  is the thickness of the sample.

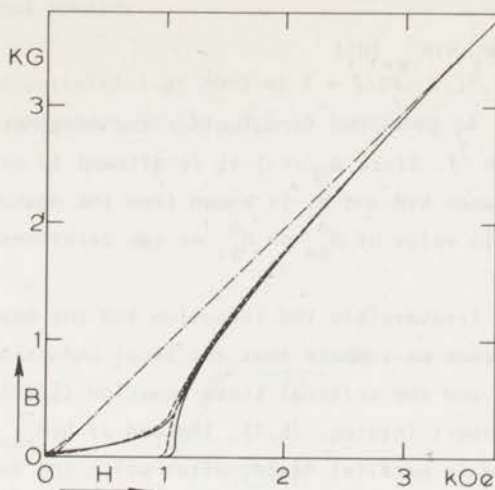


Fig. 6.4 The average magnetic induction plotted versus the applied magnetic field for three orientations. Continuous curves, parallel field; broken curves, transverse field; point-dash curves, perpendicular field.

using the relation  $B = H + 4\pi M$ . An explanation for this effect may be the very large induction gradient at the sample surface which possibly is not stable any more for fields below  $H_{c1}$ , so that the flux leaks from the sample. We believe that this results into a smaller induction over the whole sample, rather than into the formation of a Meissner zone at the surface. At least it is difficult to understand that flux should pass through this zone without being pinned. Perhaps susceptibility measurements in this field region can yield more information about this still unsolved problem.

#### 6.2.2 Determination of the Induction in Transverse and Perpendicular Field.

Since we could not measure magnetization curves in the transverse and perpendicular field orientations, we tried to deduce the induction from the parallel field measurements. We approximated the shape of the sample by an ellipsoid with axes equal to the dimensions of the sample.

In a reversible type-II superconductor the flux is homogeneously distributed over the sample. The homogeneous internal field  $H_i$  and the external field at the surface can be matched along the ellipses for which both fields are parallel:  $H_s^0 = H_i$ . The relation between the applied field  $H_a$  and  $H_s^0$  for a homogeneous magnetization is:

$$H_{sj}^0 = H_a - N_j \cdot 4\pi M_{rev}(H_i) \quad (6.1)$$

where  $j$  stands for  $\parallel$ ,  $=$ , or  $\perp$ . The formulae for the demagnetization coefficients  $N_j$  are given by Osborn<sup>7</sup>). Since  $N_{\parallel} \ll 1$  it is allowed to assume  $H_{s\parallel}^0 = H_a$ , so that the relation between  $4\pi M$  and  $H_i$  is known from the measured Abrikosov curve. Starting from a certain value of  $H_{s=}^0$  or  $H_{s\perp}^0$  we can determine the corresponding value of  $H_a$ .

If the sample is irreversible the induction and the magnetization are not homogeneous. In this case we suppose that the local induction is only determined by the field  $H_s^0$  and the critical state equation (5.24). The simplest solution is then to insert into eq. (6.1), instead of  $4\pi M_{rev}$ , the values of  $4\pi M_{irr}(H_s^0)$  as measured in parallel field, after which the determination of  $H_a(H_{sj}^0)$  is analogous to that for the reversible case. The  $B(H_{\parallel})$  and  $B(H_{\perp})$  curves obtained in this way are also shown in fig. 6.4. The inaccuracy in  $B$  due to a slight irreproducibility of the magnetization measurements is the largest in increasing fields just above  $H_{c1}$  where the curves are very steep.

A fundamental problem, however, arises from the occurrence of a Meissner zone for increasing fields between  $H_{c1}$  and  $H^*$ . In this situation the flux distribution is so inhomogeneous (fig. 6.3) that the question arises whether this configuration can still be described by eq. (6.1). For decreasing fields below  $H_{c1}$  it is most probable that the flux is distributed rather homogeneously, as was discussed in section 6.2.1. Therefore it seems plausible that the inductions determined in this region are more reliable.

In the perpendicular field the problem is the most complicated, because the flux lines enter the sample in a direction perpendicular to that for the parallel or transverse fields. Since the solution of the critical state equation depends among other things on the mutual distance between the sample surfaces parallel to the field direction, it is clear that the irreversible magnetization curves in perpendicular field differ from those in the other field directions. If the sample is nearly reversible, like N0-0, the difference will be negligible well above  $H^*$  as we were able to calculate. But below  $H^*$  it is not allowed to use the measured irreversible magnetization curves in order to calculate the average induction in perpendicular fields. As a rough approximation one can put  $B$  equal to  $H_{\perp}$  as was done by Lowell and Sousa<sup>8</sup>), but we still prefer to apply the method described in this section.

§6.3 Some Experimental Results

The thermal conductivities of NO-O at  $T = 6.04, 4.31,$  and  $2.13$  K and of N-319 at  $T = 2.13$  K are shown in fig. 6.5 as functions of the parallel field.

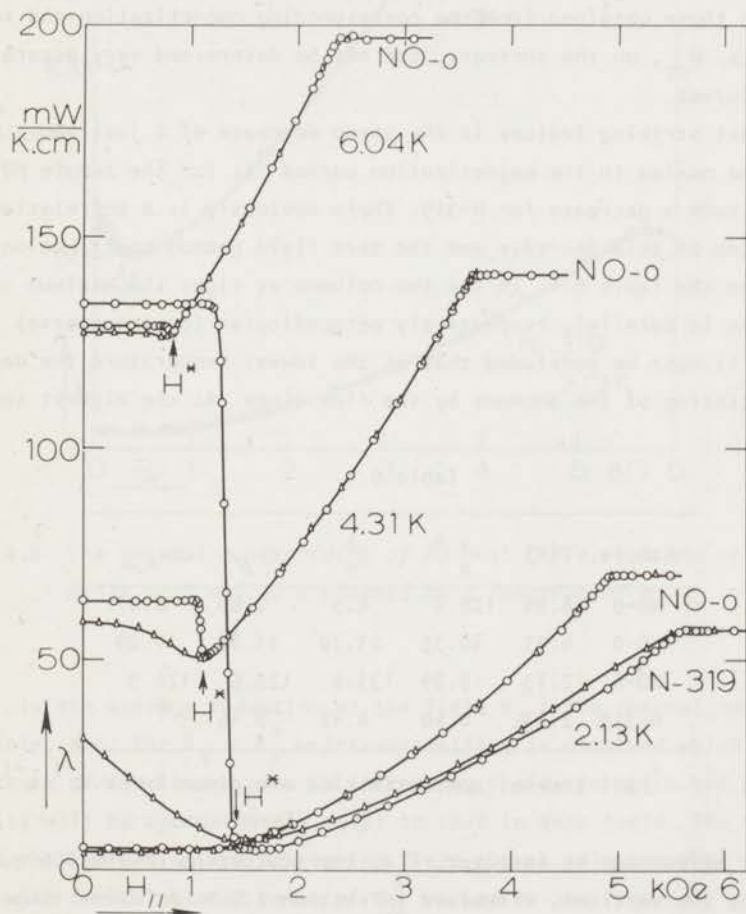


Fig. 6.5 The thermal conductivity of NO-O at  $T = 6.04, 4.31,$  and  $2.13$  K and of N-319 at  $T = 2.13$  K as a function of parallel field.

O, increasing field;  $\Delta$ , decreasing field.

In this figure, and in the following figures, the circles refer to points measured in increasing fields, whereas the triangles denote the measurements in decreasing fields. Although the magnetization curves of N0-0 still show some irreversibility, this can hardly be found back in the thermal conductivity curves, at least, if plotted on this scale. Apparently the thermal conductivity is not very sensitive for small magnetic irreversibilities. However, if these irreversibilities are large, as in N-319, they are detectable indeed. Even the peak effect in the vicinity of  $H_{c2}$  can be observed in fig. 6.5.

The values of  $H_{c2}$  can be read quite precisely from the curves. They coincide nicely with those obtained from the corresponding magnetization and resistance measurements.  $H_{c1}$ , on the contrary, can not be determined very accurately from the  $\lambda(H_{//})$  curves.

The most striking feature is the steep decrease of  $\lambda$  just above  $H_{c1}$  (defined as the maxima in the magnetization curves<sup>3</sup>) for the sample N0-0 and the absence of such a decrease for N-319. There obviously is a correlation between the magnitude of this decrease and the zero field phonon contribution  $\lambda_p^s$ , as follows from the table 6.1. In the two columns at right the maximum values of the decrease in parallel, respectively perpendicular (or transverse) fields are given. It must be concluded that at the lowest temperature the decrease is due to scattering of the phonons by the flux lines. At the highest temperatures

Table 6.1

Sample	T(K)	$\lambda_e^s$ *	$\lambda_p^s$	$\Delta\lambda_{//}$	$\Delta\lambda_{\perp,=}$
N0-0	6.04	120.4	8.5	2.09	6.07
N0-0	4.31	40.35	23.70	13.80	17.29
N0-0	2.13	0.89	133.6	126.6	126.9
N-319	2.13	0.60	4.42	0.45	

\* ) all thermal conductivities are given in  $\text{mW}\cdot\text{K}^{-1}\cdot\text{s}^{-1}$ .

a secondary effect may be involved, i.e. the scattering of the BCS quasi-particles by the vortices, discussed in section 2.5.1. At these temperatures we also observe a dependence of  $\Delta\lambda$  on the field orientations.

Fig. 6.6 shows a plot of  $\lambda$  versus  $B_{//}$ , as derived from the magnetization curves, for N0-0 at 4.31 K and for N-319 at 2.13 K. Clearly the behaviour of N-319 is reversible within the measuring accuracy over the whole field region, even including the peak effect near  $H_{c2}$ . For N0-0 at inductions  $B_{//} > B_{//}^*$

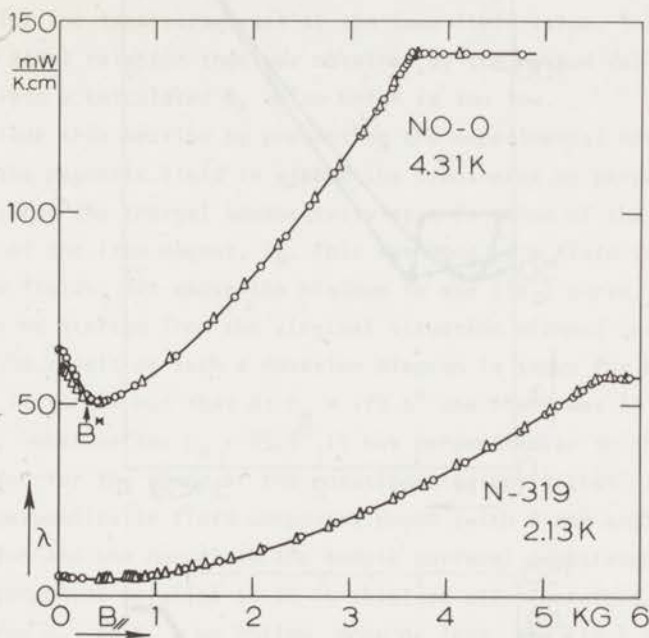
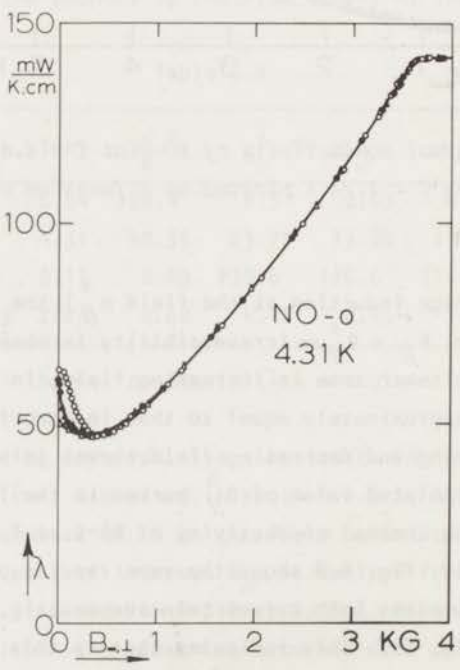
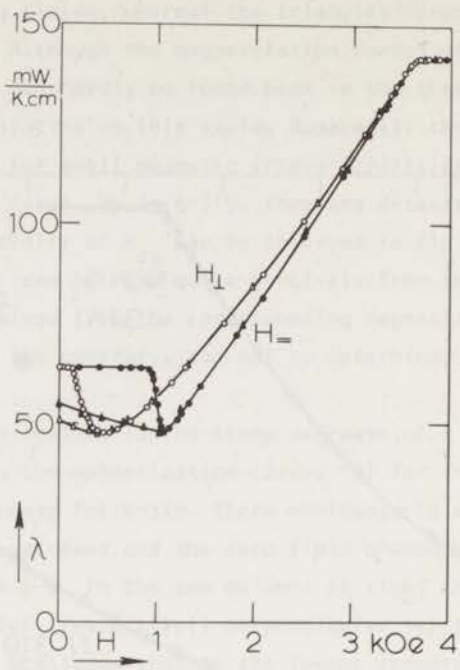


Fig. 6.6 The thermal conductivity of NO-O at  $T = 4.31$  K and of N-319 at  $T = 2.13$  K plotted as a function of  $B_{//}$ .

(where  $B_{//}^*$  is the average induction at the field  $H_{//}^*$ ) the thermal conductivity is reversible, too. For  $B_{//} < B_{//}^*$  an irreversibility is observed which is due to the occurrence of a Meissner zone in increasing field, in which the phonon conductivity will be approximately equal to that in zero field. The value of  $B$  at which the increasing and decreasing field curves join together nearly coincides with the calculated value of  $B_{//}^*$  marked in the figure.

Fig. 6.7 shows the thermal conductivity of NO-O at  $T = 4.31$  K in transverse and perpendicular field. Fig. 6.8 shows the same results plotted versus  $B_{\perp}$  and  $B_{\parallel}$ . At the higher inductions both curves coincide exactly, whereas they are widely different in fig. 6.7. This indicates that in this region the procedure followed in order to obtain  $B_{\perp}$  and  $B_{\parallel}$  gives satisfactory results. For the



smaller inductions a clear difference between the curves in increasing and perpendicular fields is observed. Because for increasing perpendicular fields the Meissner zone is wider than in transverse fields at the same average induction, a larger thermal conductivity in the perpendicular fields results. For small decreasing perpendicular fields much more flux will remain pinned in the sample than for the transverse case at the same field value. This yields a more irreversible  $B(H_{\perp})$  relation than was obtained by the method described before and results into a calculated  $B_{\perp}$  value which is too low.

We conclude this section by presenting the experimental method by which we adjusted the magnetic field in either the transverse or perpendicular direction. We measured the thermal conductivity as a function of the indicated angle on the scale of the iron magnet,  $\theta_M$ . This was done at a field value below  $H_{c1}$  in transverse fields, but above the minimum in the  $\lambda(H_{\perp})$  curve, see fig. 6.7. At each angle we started from the virginal situation without trapped flux in the sample. The result of such a rotation diagram is shown for NO-0 at  $T = 4.31$  K in fig. 6.9. It turned out that at  $\theta_M = 175.5^\circ$  the field was in the transverse position  $\theta_{M=}$ , whereas for  $\theta_M = 85.5^\circ$  it was perpendicular to the sample,  $\theta_{M\perp}$ . The explanation for the shape of the rotation diagram is that, in first approximation, the perpendicular field component  $H\cos\theta$  (with  $\theta$  the angle between the field direction and the normal to the sample surface) penetrates into the sample, whereas the component parallel to it is shielded off. Therefore, by rotating the magnet from  $\theta_{M\perp}$  to  $\theta_{M=}$ , we follow more or less the  $\lambda(H_{\perp})$  curve in a non-linear way. We estimate the accuracy of this method to be better than 0.2 degree.

#### §6.4 Discussion of the Results at Small Inductions

6.4.1 *At Low Temperatures.* The experimental results for NO-0 at small inductions at three temperatures and three field orientations are shown in fig. 6.10. The results at  $T = 2.13$  K can be discussed most conveniently, because the electronic thermal conductivity can completely be ignored at  $B = 0$ , and if Canel's <sup>9)</sup> prediction is true (section 2.5.1), also for inductions of a few hundred Gauss. Then we can restrict the discussion to the behaviour of the

Fig. 6.7 *The thermal conductivity of NO-0 at  $T = 4.31$  K measured as a function of both the transverse and perpendicular field.*

Fig. 6.8 *The thermal conductivity of NO-0 at  $T = 4.31$  K plotted versus  $B_{\perp}$  and  $B_{\parallel}$ , as derived from fig. 6.4.*

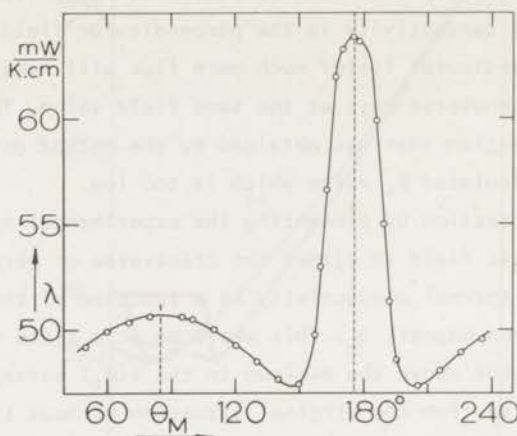


Fig. 6.9 A rotation diagram of the thermal conductivity for NO-O at  $T = 4.31$  K and  $H = 730$  Oe.

phonon conductivity only.

Table 6.2 shows the ratio of  $\lambda_p^s$  and  $\lambda_p^n$  as derived from the data of chapter 4. There we also determined the mean free path of the phonons in the normal state:  $\tilde{\lambda}_p^n \approx 10^4/T \text{ \AA}$ . From this we calculated  $\tilde{\lambda}_p^s$ , which is also given in the table. The mean free path in the superconducting state turns out to be much larger than the flux line distance at say 100 G, where  $a_0 \approx 4800 \text{ \AA}$  according to eq. (2.28). Therefore the conditions are fulfilled (random flux line distribution) under which Vinen et al. <sup>10)</sup> derived equation (2.39):

$$\frac{\lambda_p(0)}{\lambda_p(B)} - 1 = \alpha \frac{B}{H_{c2}} \frac{\lambda_p(0)}{\lambda_p^n}$$

where  $\alpha$  is a constant related to the average scattering diameter  $D$  of a flux line for the phonons:

$$D = \alpha \frac{\phi_0}{H_{c2}} \frac{1}{\tilde{\lambda}_p^n} \quad (6.2)$$

In fig. 6.11 we plotted  $[\lambda(0)/\lambda(B)] - 1$  versus  $B_{//}$ ,  $B_{=}$ , and  $B_{\perp}$ . Although

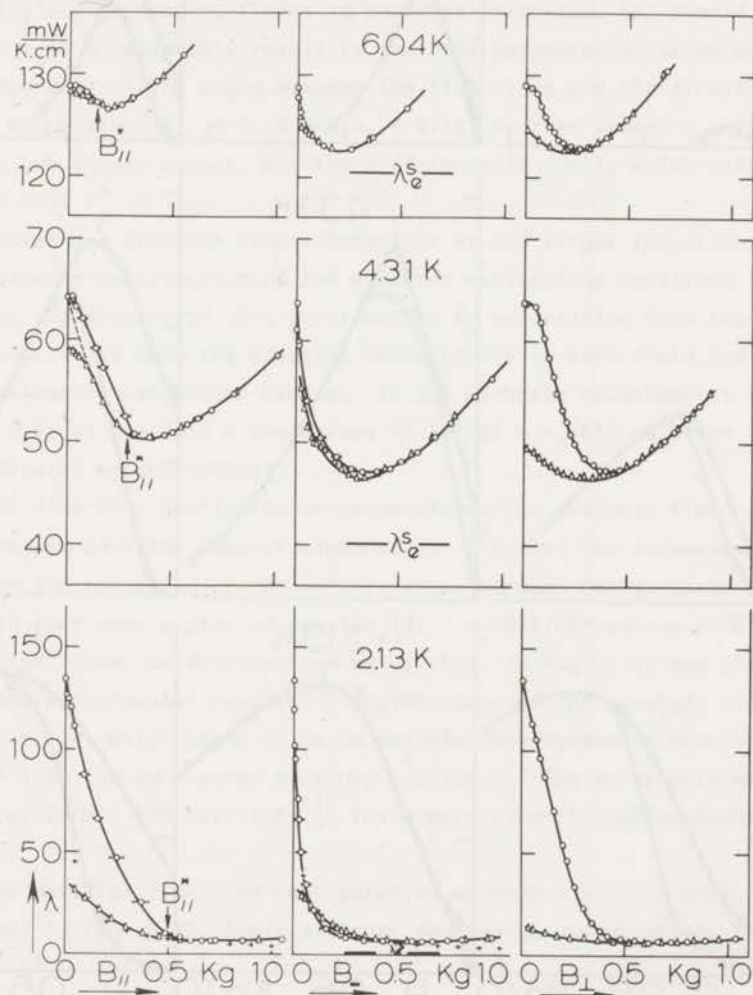


Fig. 6.10 The thermal conductivity of NO-O at  $T = 6.04, 4.31,$  and  $2.13$  K as a function of the magnetic induction below 1000 G for the three field orientations. The crosses in the figures at 2.13 K refer to the calculated values of  $\lambda_e^s + \lambda_p(B)$ .

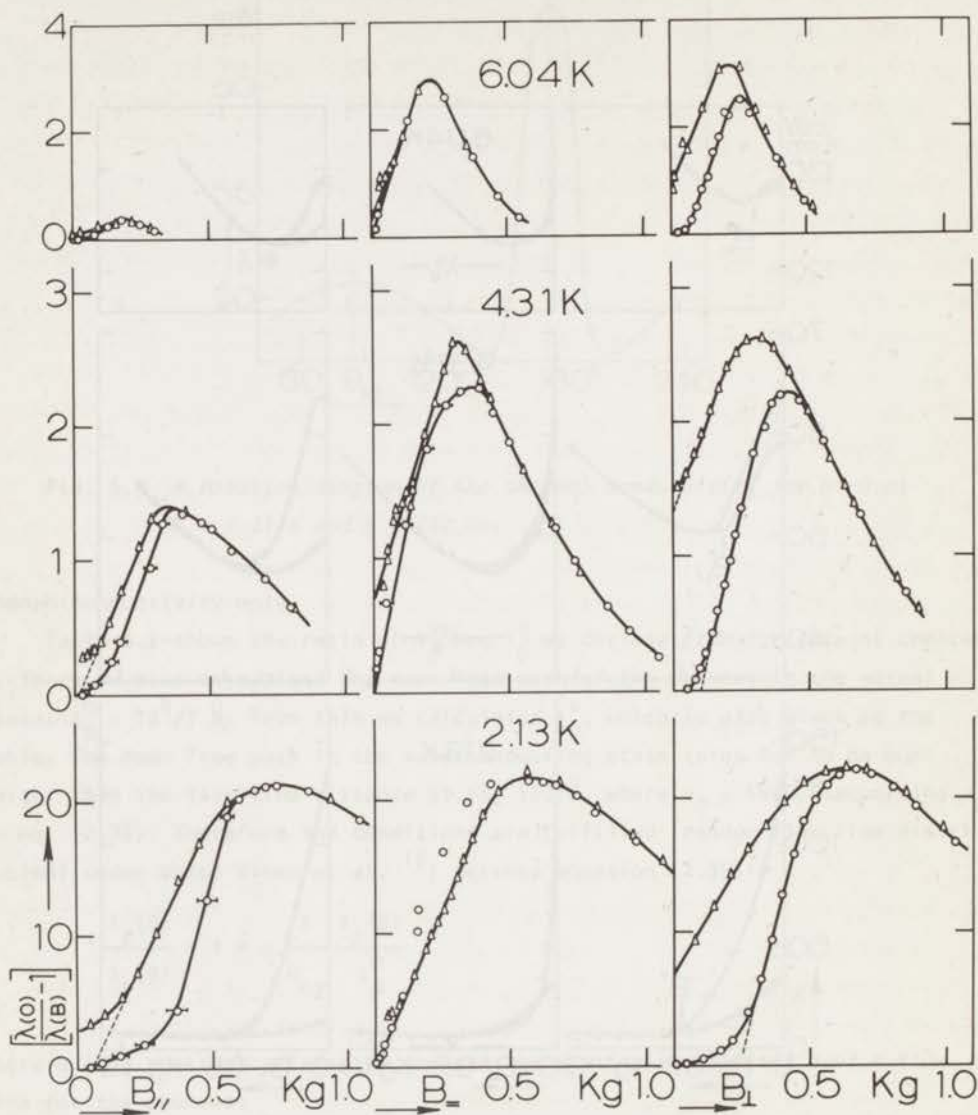


Fig. 6.11 Plot of  $[\lambda(0)/\lambda(B)] - 1$  versus the magnetic induction for the sample NO-0 at  $T = 6.04, 4.31,$  and  $2.13$  K and the three field orientations.

the irreversibility makes a comparison with the theory rather difficult, we believe that we still can estimate  $\alpha$  from the slopes of the straight portions of the lines in decreasing fields for the parallel and transverse orientations. The results for  $T = 2.13$  K are given in the lowest line of table 6.2.

Perhaps the fact that the slope for the transverse inductions is almost equal to the average of the slopes of the linear parts in the curves versus  $B_{\perp}$  in increasing and decreasing fields is somewhat fortuitous ( $\alpha_{\perp}$  should of course be equal to  $\alpha_{\parallel}$ ). A remarkable result is that the parameter  $\alpha$  turned out to be almost independent of the angle between the flux lines and the direction of heat flow. We obtained  $\alpha_{\parallel} = 0.16$  and  $\alpha_{\perp} = 0.19$ , so that indeed  $\alpha_{\parallel}$  is smaller than  $\alpha_{\perp}$ , as one should expect, but the difference is small, which must be due to the fact that  $\tilde{\lambda}_p^5 \gg a_0$ .

The deviations from the linear behaviour at the larger inductions are due to the increasing contribution of the electron excitations localized in the vortex cores. We determined this contribution by subtracting from the measured thermal conductivity both the electron conductivity in zero field and the phonon contribution calculated from eq. (2.39) with the experimental values of  $\alpha$ . In fig. 6.10 at  $T = 2.13$  K the values of  $[\lambda_e(0) + \lambda_p(B)]$  obtained in this way are indicated by the crosses.

For the flux line configuration perpendicular to the heat flow we obtained a good agreement with the idea of Vinen et al.<sup>10)</sup> that the increase in  $\lambda_e$  results from the tunneling of "bound" electrons between the vortices (section 2.5.1.2). In that case a plot of  $\log([\lambda_e(B) - \lambda_e(0)]/\sqrt{B})$  versus  $1/\sqrt{B}$  should give a straight line, as follows from eq. (2.40). In fig. 6.12 the black dots represent the experimental results. From the slope of the straight line we obtained  $\beta_{\perp} = 1.4$ , which seems to be in satisfactory agreement with Vinen's result  $\beta_{\perp} = 1.66$  for much purer niobium,  $\lambda \geq 150 \epsilon_0$ . The value obtained from the theory of Caroli and Matricon<sup>11)</sup> for a pure type-II superconductor is  $\beta_{\perp} = 1.7$ .

For the parallel flux line configuration we made a similar plot, shown by the open dots in fig. 6.12. Again a linear dependence was obtained;  $\beta_{\parallel}$  turned out to be 1.5.

The results are in qualitative agreement with the theory. First of all  $\lambda_e$  for the perpendicular configuration is larger than for the parallel one. Secondly  $\beta_{\parallel}$  is somewhat larger than  $\beta_{\perp}$ . Theoretically this can be explained by the factor  $(\sin \theta)^{-1}$  in front of the argument of the exponent in the electronic wave function of Caroli and Matricon<sup>11)</sup>, in which  $\theta$  is the angle between the direction of propagation of an electron and the flux lines. In the perpen-

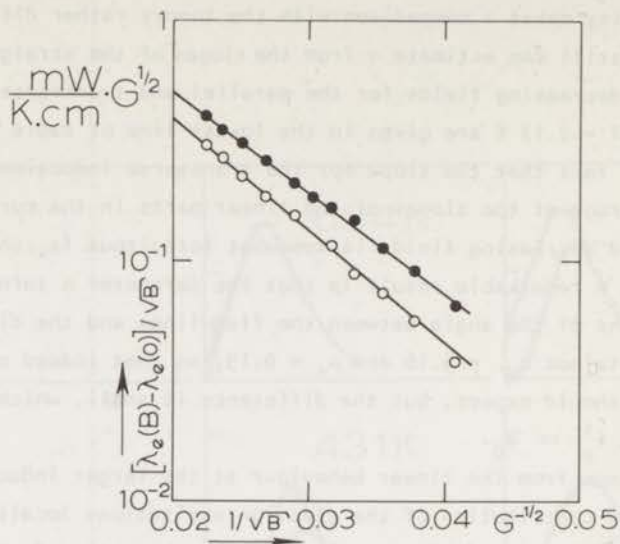


Fig. 6.12 *Semi-logarithmic plot of  $[\lambda_e(B) - \lambda_e(0)]/\sqrt{B}$  versus  $1/\sqrt{B}$  for NO-O at  $T = 2.13$  K for the parallel and transverse field orientations.*

dicular case the largest contribution to the thermal conductivity is expected for  $\sin \theta = 1$ , but in the parallel case this value of  $\sin \theta$  will be smaller, resulting into a larger value of  $\beta$ .

6.4.2 *At High Temperatures.* The results at  $T = 4.31$  K and 6.04 K are also shown in the figs. 6.10 and 6.11. The minima of  $\lambda$  in the parallel configuration are less pronounced than in the perpendicular case. From fig. 6.11 it follows that at the lowest inductions  $[\lambda(0)/\lambda(B)] - 1$  is again a linear function of  $B$ , which can be formally described by eq. (2.39). The deduced  $\alpha$ -values are tabulated in table 6.2. It turns out that at both temperatures  $\alpha_{//}$  is smaller than  $\alpha_{\perp}$ . In addition, an increase in both  $\alpha$ 's is observed with increasing temperature.

From Canel's theory<sup>9)</sup> a small temperature dependence of  $\alpha_{\perp}$  is expected because only the phonons with wavelengths smaller than  $\xi$  are scattered by the vortices, see chapter 2 §5.1.1. At low temperatures this is a more important fraction of the phonons than at high temperatures. Because Canel's criterion is not very exact, it is difficult to give a quantitative prediction for the temperature dependence of  $\alpha_{\perp}$ . However, the ratio of  $\alpha_{\perp}$  at  $T = 2$  K and at 6 K can be estimated to be smaller than a factor of two. With respect to this  $\alpha_{\perp}$

Table 6.2

T (K)	$\lambda_p^s/\lambda_p^n$	$\tilde{\lambda}_p^n$ ( $\mu\text{m}$ )	$\tilde{\lambda}_p^s$ ( $\mu\text{m}$ )	$H_{c2}$ (Oe)	$\alpha_{//}$	$\alpha_{\perp}$	$\alpha_{\perp\text{calc}}$
6.04	9.7	0.16	15	2375	0.4	3.3	0.35
4.31	53	0.22	19	3640	0.33	0.44	0.32
2.13	$12 \times 10^2$	0.44	540	4940	0.16	0.19	

at  $T = 6.04$  K is an order of magnitude too large. This anomaly can only be explained by taking into account the effect of scattering of the normal electrons by the vortex cores, first mentioned by Forgan et al.<sup>12)</sup>, later theoretically calculated by Cleary<sup>13)</sup>, see section 2.5.1.4. It is difficult to separate this effect experimentally from the decrease due to the phonon-vortex scattering, because both effects have the same  $B$  dependence, as follows from eqs. (2.39) and (2.42). Therefore we used eq. (2.42) in order to calculate  $\lambda_e(B)$  and subtracted the results from the measured thermal conductivity. The remaining phonon conductivity was compared again with eq. (2.39). In this way we obtained the reasonable value  $\alpha_{\perp} = 0.35$  at  $T = 6.04$  K, if in eq. (2.42) the value  $\lambda_e = 470 \text{ \AA}$  and  $a_{\perp} = 650 \text{ \AA}$  were substituted, in which  $a_{\perp}$  is the scattering diameter for the BCS quasi-particles by a flux line orientated perpendicular to the heat flow. At  $T = 4.31$  K the change in  $\alpha_{\perp}$  using the same values of  $\lambda_e$  and  $a_{\perp}$  is much smaller, only 15 percent, giving rise to  $\alpha_{\perp} = 0.32$ . The values of  $\alpha_{\perp}$  obtained in this way are given in table 6.2 as  $\alpha_{\perp\text{calc}}$ . Vinen et al.<sup>10)</sup> reported a temperature dependent value for  $a_{\perp}$  varying from  $400 \text{ \AA}$  at 3 K to about  $100 \text{ \AA}$  near  $T_c$ , but the possibility of a two or more times higher value could not be ruled out.

The striking difference between the decreases of the thermal conductivity in the parallel and perpendicular flux line configurations can not satisfactorily be explained by the orientation dependence of the phonon scattering by the vortices. It has to be given in terms of the behaviour of the electrons. There are two possible explanations:

1. The scattering diameter in the parallel configuration  $a_{//}$  is much smaller than  $a_{\perp}$ . Compare Vinen's result: at  $T = 3$  K  $a_{//} = 140 \text{ \AA}$  and  $a_{\perp} = 400 \text{ \AA}$ , near  $T_c$   $a_{//} = 50 \text{ \AA}$  and  $a_{\perp} = 100 \text{ \AA}$ .
2. The contribution of the normal electrons localized in the vortex cores may not be neglected if the heat flow is parallel to the vortices, in contradiction

with Canel's theory.

We are not able to discriminate between these two possibilities. As an example we can calculate the electron contribution as a function of induction inserting into eq. (2.42)  $a_{//} = 230 \text{ \AA}$ , so that our ratio of  $a_{//}/a_{\perp}$  at  $T = 6.04 \text{ K}$  is the same as was experimentally determined by Vinen et al.<sup>10)</sup> We finally obtain for the phonon conductivity a decrease which corresponds with eq. (2.39) but with a value of  $\alpha_{//} = 0.15$ , somewhat smaller than  $\alpha_{//}$  at  $T = 2.13 \text{ K}$ . In view of the poor accuracy with which our  $\alpha$  values could be determined this result seems not impossible, but it does not exclude the second explanation.

Moreover, it is not at all clear how the value of  $\alpha_{//}$  depends on temperature. First of all there is Canel's criterion which leads to a slight increase of  $\alpha_{//}$ , but there also is the influence of the large decrease in the mean free path  $\tilde{\lambda}_p^s$  as the temperature is raised (table 6.2), which must result into a decrease of  $\alpha_{//}$ .

### §6.5 Discussion of the Results near $H_{c2}$

The most interesting quantity of the thermal conductivity in the vicinity of  $H_{c2}$  is the derivative of the electronic contribution with respect to  $H$ . It is in good approximation equal to the derivative of the experimental curve, because the phonon contribution does not vary very much for fields near  $H_{c2}$ . The measured slopes turned out to be finite, which agrees qualitatively with the theory of Caroli and Cyrot<sup>14)</sup> for dirty type-II superconductors in which  $\lambda_e \ll \xi_0$  (eqs. (2.42) - (2.45)). The theory of Maki<sup>15)</sup> for the pure limit ( $\lambda \gg \xi_0$ ) predicts  $\lambda_e \propto (H_{c2} - H)^{\frac{1}{2}}$ , which results into an infinite slope at  $H_{c2}$ . Our experiments do not support the suggestion of Tittmann and Bömmel<sup>16)</sup> leading to a relation  $\lambda_e \propto (H_{c2} - H)^p$  with  $0.5 \leq p \leq 1$  if  $\lambda \sim \xi_0$ .

In fig. 6.13 the experimental results are plotted versus the reduced temperature. If the thermal conductivity curves were irreversible, the slope was determined by averaging the  $H$  values at equal  $\lambda$ . The reason is that the derivative with respect to  $B$  is reversible.

Eq. (2.44) predicts the relation between  $(d\lambda/dH)_{H_{c2}}$  and  $(d4\pi M/dH)_{H_{c2}} = 4\pi\chi_{c2}$  as a function of temperature. The values of  $4\pi\chi_{c2}$  were determined from the magnetization curves taking the average of the slopes in increasing and decreasing fields if  $4\pi M$  was irreversible. At temperatures above about 6 K the accuracy was rather poor because of surface and peak effects. Therefore we calculated  $\kappa_2(T)$  by means of eq. (2.31) and the value  $\kappa_2(T_c) = \kappa$  from Goodman's<sup>17)</sup> relation:

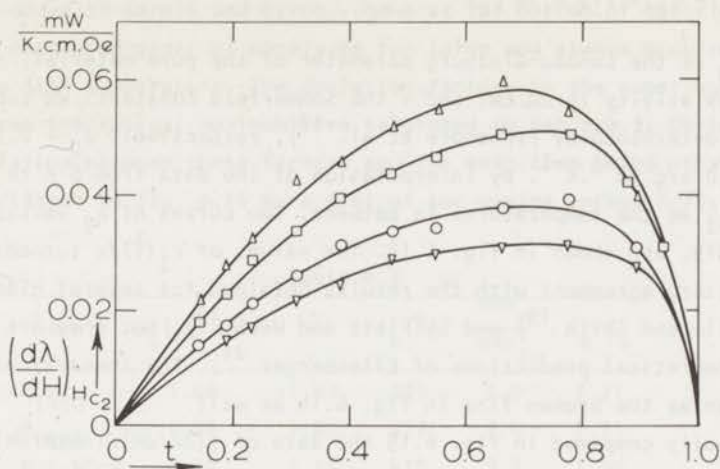


Fig. 6.13 The reversible slopes of the thermal conductivity curves near  $H_{O_2}$  as functions of the reduced temperature for four samples:  $\Delta$ ,  $P_{1600}$ ;  $\square$ ,  $N-0$ ;  $\circ$ ,  $P_{1400}$ ;  $\nabla$ ,  $N-319$ .

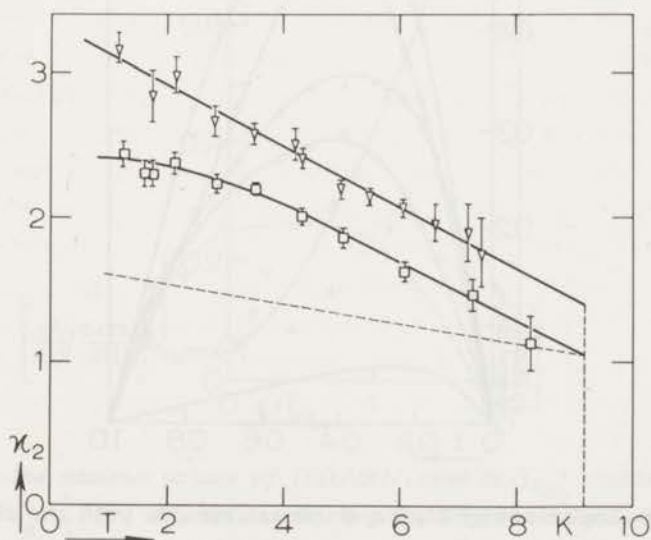


Fig. 6.14 Plot of  $\kappa_2$  versus the temperature;  $\kappa_2$  was determined from the slopes of the magnetization curves near  $H_{O_2}$  for two samples:  $\nabla$ ,  $N-319$ ;  $\square$ ,  $N-0$ . The broken curve represents the values of  $\kappa_2$  for  $N-0$  predicted by the theory<sup>21</sup>).

$$\kappa = \kappa_0 + 7.5 \times 10^3 \rho_0 \gamma^{\frac{1}{2}} \quad (6.3)$$

in which  $\kappa_0$  is the Landau-Ginzburg parameter of the pure material,  $\rho_0$  is the residual resistivity in  $\mu\Omega \cdot \text{cm}$ , and  $\gamma$  the Sommerfeld constant. We substituted the values determined by Finnemore et al. <sup>18)</sup>, respectively  $\kappa_0 = 0.78$  and  $\gamma = 7.3 \times 10^3 \text{erg} \cdot \text{cm}^{-3} \cdot \text{K}^{-2}$ . By interpolation of the data from 6 K to  $T_c$  we could deduce  $4\pi\chi_{c2}$  at the temperatures in between. Two curves of  $\kappa_2$  versus  $T$ , for N-0 and N-319, are shown in fig. 6.14. The values of  $\kappa_2(T)/\kappa$  turned out to be in satisfactory agreement with the results obtained for several niobium samples by McConville and Serin <sup>19)</sup> and by Fietz and Webb <sup>20)</sup>, but they are much larger than the theoretical predictions of Eilenberger <sup>21)</sup>. The theoretical curve for N-0 is given as the broken line in fig. 6.14 as well.

We finally compared in fig. 6.15 the data of  $[(d\lambda/dH)/(d4\pi M/dH)]_{Hc2}$  with

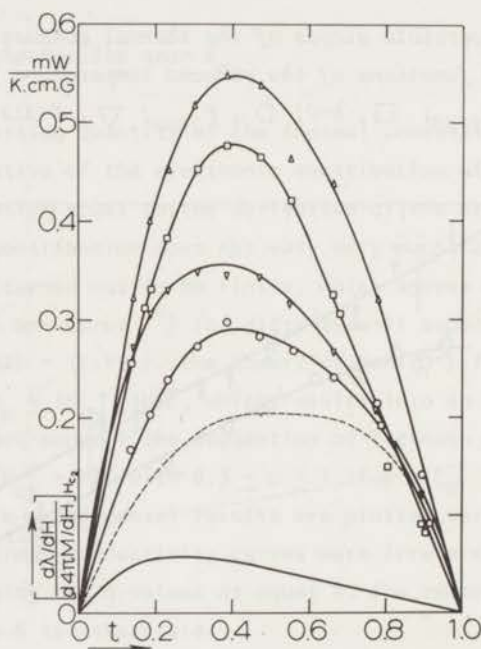


Fig. 6.15 Comparison of the experimental results with the theory of Caroli and Cyrot (lower curve) for four samples:  $\Delta$ ,  $P_{1600}$ ;  $\square$ , N-0;  $\nabla$ , N-319;  $\circ$ ,  $P_{1400}$ . The broken curve represents the calculated values for N-0 using the experimental  $(d\lambda/dH)_{Hc2}$  data and the theoretical  $\kappa_2(T)$  values shown as the broken curve in fig. 6.14.

eq. (2.44). The experimental results deviate in two aspects from the universal theoretical curve of Caroli and Cyrot, shown at the bottom of the figure. The maxima were nearly an order of magnitude too large and always occurred at a somewhat too high temperature. The deviation factors (= the experimental maxima divided by the theoretical maximum) are tabulated in table 6.3. Obviously there exists a relation between these factors and the mean free paths of the electrons. This is elucidated in fig. 6.16 by a plot of the maxima versus  $\lambda_e/\xi_0$ . Similar

Table 6.3

Sample	$\rho_0$ ( $\mu\Omega\cdot\text{cm}$ )	$\kappa$	$\lambda_e$ ( $\text{\AA}$ )	$\frac{\max_e}{\max_t}$	$\lambda_e/\xi_0$
P <sub>1400</sub>	1.08	1.47	305	5.0	0.71
P <sub>1600</sub>	0.68	1.22	520	9.4	1.21
N-0, NO-0	0.74	1.25	470	8.2	1.09
N-319	0.95	1.39	380	6.2	0.88

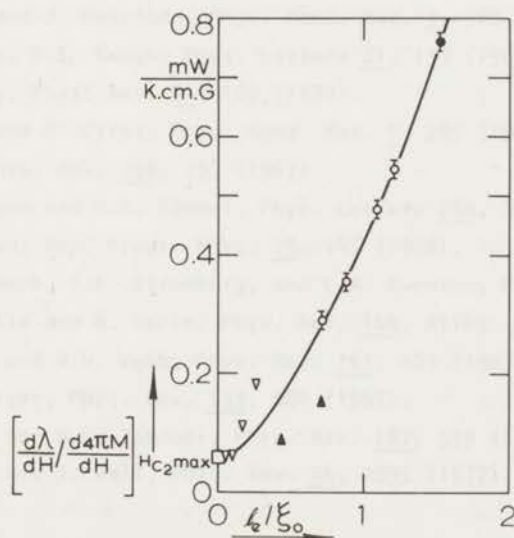


Fig. 6.16 The maximum values of  $[(d\lambda/dH)/(d4\pi M/dH)]_{H_{C_2}^{max}}$  plotted versus  $\lambda_e/\xi_0$ .  $\circ$ , Nb, this work;  $\bullet$ , Nb, Wasim and Zebouni <sup>22</sup>) ( $\lambda_e = 656 \text{ \AA}$  and not  $328 \text{ \AA}$ , as was reported; for  $4\pi\chi_{C_2}$  we took the values of our purest sample);  $\nabla$ ,  $\text{PbIn}_x$  with  $x = 3, 5, 10$ , and  $21$  at%, Gupta and Wolf <sup>23</sup>);  $\blacktriangle$ ,  $\text{Nb}_{1-x}\text{Mo}_x$  with  $x = 2, 15$ , Lowell and Sousa <sup>8</sup>);  $\square$ , the theoretical value for the dirty limit <sup>14</sup>).

deviations have been reported in the literature<sup>8,22,23)</sup> for several type-II superconductors of intermediate purity. These results are also shown in the figure. The curve has been drawn smoothly through the experimental points and extrapolated to the theoretical value in the dirty limit,  $\lambda_e = 0$ .

The reason for the deviation might be the same as for the deviation between the experimental and theoretical data of  $\kappa_2(T)/\kappa$  and therefore we calculated the values of  $[(d\lambda/dH)/(d4\pi M/dH)]_{H_{C2}}$  making use of the experimental data for  $(d\lambda/dH)_{H_{C2}}$  and the theoretical calculations of Eilenberger for  $4\pi\chi_{C2}$ . In fig. 6.15 the result for N=0 is shown as the broken curve. Although the disagreement is smaller than originally, it is clear that the Caroli-Cyrot theory does not provide a satisfactory quantitative description of the thermal conductivity behaviour near  $H_{C2}$  of type-II superconductors of intermediate purity.



## References

1. C.A.M. van der Klein, J.D. Elen, R. Wolf, and D. de Klerk, *Physica* 49, 98 (1970).
2. P.H. Kes, C.A.M. van der Klein, and D. de Klerk, *J. Low Temp. Phys.* 10, 759 (1973).
3. C.A.M. van der Klein, P.H. Kes, H. van Beelen, and D. de Klerk, *J. Low Temp. Phys.*, (in the press).
4. E.J. Kramer and A. Das Gupta, *Phil. Mag.* 26, 769 (1972).
5. C.A.M. van der Klein and G. Hamburg, Memo 73-02 of the Reactor Centrum Nederland.
6. C.A.M. van der Klein, P.H. Kes, and D. de Klerk, *Phil. Mag.*, (in the press).
7. J.A. Osborn, *Phys. Rev.* 67, 351 (1945).
8. J. Lowell and J.B. Sousa, *J. Low Temp. Phys.* 3, 65 (1970).
9. E. Canel, Proc. Bat Sheva Seminar, HaTfa (1968), p. 587.
10. W.F. Vinen, E.M. Forgan, C.E. Gough, and M.J. Hood, *Physica* 55, 94 (1971).
11. C. Caroli and J. Matricon, *Phys. Kond. Mat.* 3, 380 (1965).
12. E.M. Forgan, C.E. Gough, *Phys. Letters* 21, 133 (1966).
13. R.M. Cleary, *Phys. Rev.* B1, 169 (1970).
14. C. Caroli and M. Cyrot, *Phys. Kond. Mat.* 4, 285 (1965).
15. K. Maki, *Phys. Rev.* 158, 397 (1967).
16. B.R. Tittmann and H.E. Bömmel, *Phys. Letters* 28A, 396 (1968).
17. B.B. Goodman, *Rep. Progr. Phys.* 29, 445 (1966).
18. D.H. Finnemore, T.F. Stromberg, and C.A. Swenson, *Phys. Rev.* 149, 231 (1966).
19. T. McConville and B. Serin, *Phys. Rev.* 140, A1169 (1965).
20. W.A. Fietz and W.W. Webb, *Phys. Rev.* 161, 423 (1967).
21. G. Eilenberger, *Phys. Rev.* 153, 584 (1967).
22. S.M. Wasim and N.H. Zebouni, *Phys. Rev.* 187, 539 (1969).
23. A.K. Gupta and S. Wolf, *Phys. Rev.* B6, 2595 (1972).

## S A M E N V A T T I N G

Het gedrag van de warmtegeleiding in een supergeleider wijkt sterk af van hetgeen in een normaal metaal bij lage temperaturen wordt waargenomen. De oorzaak hiervan is het feit dat zowel de elektronen en de fononen, die beide een bijdrage leveren tot het warmtegeleidingsvermogen, de invloed ondergaan van de verboden zone in het energiespectrum van de elektronen rondom de Fermi energie.

De verhouding van de warmtegeleidingscoëfficiënten in de supergeleidende en normale toestand als functie van de temperatuur wordt goed beschreven door de theorie van Bardeen, Rickayzen en Tewordt. De elektronen bijdrage in de supergeleidende fase is altijd kleiner dan in de normale toestand, terwijl voor de fononen bijdrage wordt aangetoond dat deze bijna exponentieel toeneemt voor afnemende temperatuur. Dit gedrag werd door ons gevonden en kon door de genoemde theorieën goed worden beschreven voor de vijf niobium preparaten die wij onderzochten. Deze preparaten, rechthoekig van vorm, verschilden in kristaldefekt structuur ten gevolge van een verschil in warmtebehandeling of door het bestralen met snelle neutronen. Door een nauwgezette analyse van de meetresultaten en door toepassing van de BRT theorie voor de elektronen kon de fononen bijdrage van het totale warmtegeleidingsvermogen worden afgesplitst en in verband gebracht worden met de defekt structuur. Een kwalitatieve overeenstemming met de theorie van Klemens werd gevonden voor de onbestraalde preparaten. Het gevolg van de neutronen bestraling was een vergrote puntdefekt en dislokatie verstrooiings term. De verklaring van het eerste effect was te geven binnen het kader van Klemens' theorie, de herkomst van het tweede effect is nog niet geheel verklaard.

De warmtegeleiding als functie van het magneetveld is door ons onderzocht door metingen te verrichten bij drie verschillende orientaties van het veld ten opzichte van de warmtestroomrichting en het oppervlak van het preparaat. Beneden het eerste en boven het tweede kritische veld,  $H_{c1}$  respectievelijk  $H_{c2}$ , is de warmtegeleiding onafhankelijk van het veld. In de „mengtoestand“, het veldgebied tussen  $H_{c1}$  en  $H_{c2}$ , is vlak boven  $H_{c1}$  bij temperaturen laag ten opzichte van  $T_c$  een zeer duidelijk effect merkbaar van de aanwezigheid van fluxdraden. De fononen worden sterk verstrooid door de normale elektronen, gelokaliseerd in de kern van de vortices, zodat hun bijdrage grotendeels wordt teniet gedaan. Een verrassend neveneffect voor zuivere supergeleiders (d.w.z.

supergeleiders waarvoor de gemiddelde vrije weglengte van de elektronen  $\lambda$  veel groter is dan de coherentie lengte  $\xi_0$ ) is het feit dat de gelokaliseerde normale elektronen zelf nauwelijks bijdragen tot het warmtegeleidingsvermogen. Dit komt, zoals door Canel kwalitatief werd aangetoond, doordat hun effectieve groep-snelheid vrijwel nihil is. Pas wanneer de afstand tussen de vortices afneemt (toenemende inductie), wordt de kans groter dat de gelokaliseerde excitaties zich via een tunneleffect van de ene vortex naar de andere verplaatsen. Bij temperaturen dicht bij  $T_c$ , waar de elektronen de belangrijkste bijdrage leveren, vindt ook een afname plaats van de warmtegeleiding vlak boven  $H_{c1}$ , maar nu door de extra verstrooiing van de niet-gelokaliseerde elektronen aan de fluxdraden. Dit effect, dat voor zuivere supergeleiders een goed meetbare afname tot gevolg heeft, werd beschreven door Cleary.

Een belangrijke voorwaarde om de experimenten te kunnen toetsen aan de theoretische beschouwingen is dat de fluxverdeling, dus de lokale magnetische inductie binnen het preparaat, goed bekend is. Deze volgt uit de meting van de magnetisatie in toe-en afnemend veld. Met behulp van een eenvoudige mathematische uitdrukking voor het reversibele verband tussen inductie en veld en een theoretisch model voor de fluxdraad verankering is het mogelijk het inductiepatroon binnen het preparaat te berekenen voor elk uitwendig veld tussen  $H_{c1}$  en  $H_{c2}$ . Zelfs in ons meest reversibele preparaat was het effect van een inductievrije kern vlak boven  $H_{c1}$  merkbaar in het gedrag van de warmtegeleiding. Desondanks konden we konkluderen dat, ofschoon in dit preparaat  $\lambda \approx \xi_0$ , de theorieën voor de warmtegeleiding in zuivere type-II supergeleiders de experimentele resultaten goed beschrijven.

Voor veldsterkten in de buurt van  $H_{c2}$  vonden we voor alle preparaten een lineair verband tussen warmtegeleiding en inductie. Dit gedrag voldoet kwalitatief aan de theorie van Caroli en Cyrot voor „vuile“ ( $\lambda \ll \xi_0$ ) type-II supergeleiders, maar niet aan Maki's beschrijving voor zuivere type-II supergeleiders bij  $H_{c2}$ , waarvoor een evenredigheid met  $(H_{c2} - H)^{\frac{1}{2}}$  wordt voorspeld. De experimenteel gevonden evenredigheidskonstanten waren een orde groter dan door de theorie was aangegeven; de overeenstemming werd echter beter naarmate de vrije weglengte van de elektronen kleiner was.

Faint, illegible text covering the majority of the page, likely bleed-through from the reverse side.

## Studieoverzicht

Na in juni 1961 het diploma HBS-b te hebben behaald aan het Grotius Lyceum in Den Haag besloot ik wis- en natuurkunde te gaan studeren aan de Rijksuniversiteit te Leiden. Het kandidaatsexamen a' (bijvak sterrenkunde) legde ik af in juni 1964, waarna ik in september van dat jaar mijn werkzaamheden begon op het Kamerlingh Onnes laboratorium in de werkgroep onder leiding van Dr. D. de Klerk. Aanvankelijk assisteerde ik Dr. S.H. Goedemoed bij zijn onderzoek omtrent de verankering van magnetische flux in supergeleidend niobium in de mengtoestand. Vlak voor mijn doctoraalexamen experimentele natuurkunde - afgelegd in juni 1967 met als bijvak klassieke mechanica - werden de eerste metingen verricht aan de warmtegeleiding van een niobium preparaat. Een jaar later werd besloten om de opstelling grondig te verbeteren in verband met de vereiste meetnauwkeurigheid. In de loop van 1970 kon een begin gemaakt worden met de eigenlijke metingen, vermeld in dit proefschrift.

Naast het fysisch onderzoek vervulde ik mijn onderwijstaak als assistent op het praktikum, sedert september 1968 als één der hoofdassistenten van het eerste-jaars praktikum voor hoofdvakstudenten.

Velen hebben hun bijdragen geleverd voor het tot stand komen van dit proefschrift. In de eerste plaats wil ik noemen Drs. J.J. Bosselaar, Drs. J.G.A. Rolfes en de heer J.P.M. van der Veeke voor hun hulp bij de experimenten en de uitwerking der meetresultaten.

De samenwerking met Drs. C.A.M. van der Klein heb ik bijzonder op prijs gesteld. Een groot deel van de magnetisatie experimenten werden door hem - en ook door de heer G.P. van der Mey - verricht. Tevens verzorgde hij het contact met Drs. J.D. Elen van de afdeling „materiaalkunde" van het R.C.N. te Petten, waar de preparaten werden vervaardigd.

De heer T.P.M. van der Burg zorgde voor het technische gedeelte van de opstelling. De hoogvacuumpomp en het overige glaswerk werden verzorgd door de heren C.J. van Klink en L. van As. De temperatuurstabilisator werd vervaardigd door de heer J. van der Zeeuw.

De vlotte afwerking van dit proefschrift is te danken aan het efficiënte typewerk van mevrouw E. de Haas-Walraven en de ijver van de heren W.J. Brokaar en W.F. Tegelaar die de tekeningen en de foto's maakten.



